How Can Modern 1D Simulation Techniques Be Used to Optimise the Performance of a Bentley Blower Engine?

School of Digital, Technology, Innovation & Business

University of Staffordshire

Word Count: 13,566

Name: Spencer Marc Potts

Student Number: 22014285

Module Leader: Andrew Cash

Module Code: ENGG61010

Supervisor: Andrew Cash

Submission Date: 01/05/2026

Abstract

Historically, optimising the performance of vintage racing engines, such as the 1920's supercharged 4.399 litre Bentley Blower, relies on traditional, high-risk, expensive, and potentially destructive physical trial-and-error based tuning principles. Rapid expansion of the historic motorsport sector has created a critical need to leverage modern technology to enhance performance, while simultaneously safeguarding these irreplaceable cultural artifacts. This project therefore investigates and applies One-Dimensional Computational Fluid Dynamics (1D CFD) to systematically optimise the gas dynamic performance of the Bentley Blower engine – without necessary physical intervention.

Utilising Ricardo WAVE, a faithful digital-twin of the engine was developed and rigorously calibrated against actual engine dynamometer data, achieving a Mean Absolute Error (MAE) of only 2.06%. A sequential prototyping methodology was employed to execute a comprehensive parametric study across intake and cylinder geometries, camshaft kinematics, port flow coefficients, and compression ratios. The project culminated with a single Pareto optimal configuration which features a 66mm intake length reduction and new 135mm diameter; camshaft timing optimisation with a 1.28× exhaust lift multiplier; polished ports, and a safe static compression ratio of 7.5:1.

This optimal configuration yields a 16.8% increase in peak brake power (275.61 brake horsepower (BHP) at 4000 revolutions per minute (RPM)) as well as a transformative 26.2% increase in mid-range torque delivery (441.69 Nm at 3000 RPM). Critically, these optimisations improve thermodynamic efficiency and shifts the torque delivery to align with the Bentley's gearing requirements. The study conclusively validates this modern, industry-standard method of virtual prototyping as a highly effective, sustainable tool for unlocking the performance of mechanically governed vintage powertrains while fundamentally safeguarding their historical integrity.

Acknowledgements

I would like to express my sincere thanks to my project supervisor, Andrew Cash, for his invaluable guidance, technical expertise, and continuous support from start to finish of this final year project at the University of Staffordshire.

I am deeply grateful to Bentley Motors (Mulliner), having had the great privilege of completing a portion of my industrial placement year within their talented engineering team, as well as being immersed within the Donnington Historic and Le Mans Classic events held in 2025. Witnessing the Bentley Blower within its natural environment provided invaluable insight and inspiration for this project. Their continued support and technical insights significantly elevated the historical accuracy and engineering depth of this project's research and shaping of the methodology.

Finally, I extend my appreciation to Vintage Bentley for kindly inviting me to a guided tour of their Works in West Sussex.

Contents

List of Figures

List of Tables

List of Equations

List Of Abbreviations

Abbreviation	Full Term
1D	One-Dimensional
3D	Three-Dimensional
CFD	Computational Fluid Dynamics
MAE	Mean Absolute Error
BHP	Brake Horsepower
RPM	Revolutions Per Minute
Nm	Newton Metres
BSFC	Brake Specific Fuel Consumption
ICE	Internal Combustion Engine
NA	Naturally Aspirated
SOHC	Single Overhead Camshaft
CD	Constant Depression
psi	Pounds per Square Inch
SI	Spark Ignition
FMEP	Friction Mean Effective Pressure
CHT	Conjugate Heat Transfer
FEA	Finite Element Analysis
ECU	Electronic Control Unit
CNC	Computer Numerical Control
IVC	Intake Valve Closing
IVO	Intake Valve Opening
EVC	Exhaust Valve Closing
FIA	Fédération Internationale de l'Automobile
NASA	National Aeronautics and Space Administration
UN	United Nations
SDG	Sustainable Development Goals
ASME	American Society of Mechanical Engineers
ISO	International Organization for Standardization

Nomenclature (Symbols)

Symbol	Full Term	SI Unit
η_t	Thermal Efficiency	-
η_v	Volumetric Efficiency	-
$\eta_{v(abs)}$	Absolute Volumetric Efficiency	-
n_R	Revolutions per Power Stroke	-
V_d	Displacement Volume	m^3
N	Engine Speed	RPM
$\dot{m}_{air}$	Mass Flow Rate of Air	kg/s
ρ	Density	kg/m^3
$\rho_{(amb)}$	Ambient Air Density	kg/m^3
P_{ratio}	Pressure Ratio	-
T_{ratio}	Temperature Ratio	-
P_b	Brake Power	W
P_{me}	Mean Effective Pressure	N/m^2
L	Stroke Length	m
A	Cross-Sectional Area	m^2
z	Number of Cylinders	-
L_{Ac}	Acoustic Length	m
v_s	Speed of Sound	m/s
n	Harmonic Order	-
t	Time	s
u	Velocity	m/s
x	Distance	m
ρA	Mass per Unit Length	kg/m
$\rho u A$	Mass Flow/ Momentum	kg/s
$\rho u^2 A$	Connective Momentum Flux	N
p	Pressure	Pa
pA	Pressure Acting on Fluid Face	N
$p\frac{dA}{dx}$	Pressure Force Exerted	N/m
f	Friction Force	N
e_o	Total Specific Energy	J/kg
h_o	Total Specific Enthalpy	J/kg
q	Heat Transfer Rate	W
x_b	Mass Fraction Burned	-
θ_0	Crank Angle	rad
$\Delta\theta$	Total Combustion Duration	rad
a	Efficiency Form Factor	-
m	Shape Form Factor	-
$P_{(amb)}$	Ambient Pressure	Pa
$P_{(man)}$	Manifold Pressure	Pa
$P_{(boost)}$	Boost Pressure	Pa
$T_{(amb)}$	Ambient Temperature	K
$T_{(man)}$	Manifold Temperature	K
$\eta_{v(base)}$	Base Volumetric Efficiency	-
T	Peak Torque	Nm

G	Gear Ratio	-
η	Drivetrain Efficiency	-
r	Radius	m

1.0 Introduction

1.1 Background

"The embodiment of daring engineering and vintage racing spirit"

Known universally as the “Blower”, the 4.399L Supercharged Bentley stands as one of the most significant and enduring icons of pre-war motorsport. As detailed by Kurczewski (2007) in ‘One for the Boys; 1930s Blower Bentley’, the car was the brainchild of Sir Henry “Tim” Birkin who defied Walter Owen (W.O.) Bentley’s preference for larger engine displacement through the utilisation of a Roots-Type supercharger attached to the pre-existing engine. This engineering divergence cumulated in a machine of legendary status, giving Sir Tim Birkin the title as one of the original “Bentley Boys”. This status was not only cemented by its heroic duel with the Mercedes SSK at the 1930 Le Mans 24 Hours (Bentley Motors, 2019), but also according to the 1930 Autocar review, the fifty road going versions of the Bentley Blower had, “The Appeal of Immense Power, Linked with Great Docility,” (Bentley Motors, 2025). Therefore, it can be said that the Bentley Blower holds significant historical, engineering, and cultural importance as a racing and road-going vehicle, representing the pinnacle of Pre-War British luxury performance.

Figure 1 - Chassis 'UU 5782' and 'GH 6951' at the Mille Miglia (Bentley Motors, 2025)

The relevance of this project extends far beyond the engineering specifics of one vehicle; it is framed by the exponential growth of the historic motorsport sector. More than a niche hobby, the preservation and use of historic vehicles has evolved into a significant global industry with the Fédération Internationale de l'Automobile (FIA, 2023), reporting that the historic vehicle engineering sector contributes an estimated circa €5.1 billion annually to the European economy alone. Events such as the Goodwood Revival, Le Mans Classic, and Donnington Historic attract hundreds of thousands of spectators, creating demand which proves these vehicles are not just static museum pieces but active, high-performing racing machines with fierce competition between constructors.

However, this boom creates a paradox. According to the FIA, historic vehicles like the Bentley Blower are not merely machines but “living testimonies,” of the technical evolution within the 20th century (FIA, 2023). As such they are recognised as “cultural artifacts,” and preserving the operational integrity of these vehicles is critical. As regulations tighten and parts become scarcer, the FIA emphasises the need to, “secure the future of our motoring heritage,” through innovation. A solution is therefore required to allow engineers to explore performance limits, whilst critically ensuring that these artifacts of history are preserved for future generations.

1.2 Problem Statement

"You simply cannot try 50 different camshafts on a 100-year-old engine without ruining it or spending a fortune"

The fundamental problem facing the historic racing industry then is the inherent risk of traditional physical methods of 'trial-and-error' tuning. Destructive testing, combined with component scarcity and the extreme cost of replacing such components, make it difficult for engineers to push the limits of performance.

1.2.1 Break Down

- **The Core Issue –** The process of optimising a mechanically governed engine and relying on physical hardware has long been identified as a critical inefficiency. As stated by the National Aeronautics and Space Administration (NASA) within their technical report 'Reducing the Time and Cost of Testing Engines,' reliance on physical prototypes means, "high development time and cost," which makes it difficult to enhance the engine design (NASA, 2004).

- **Historic Example –** Indeed the core issue is not a theoretical risk, it is intertwined into the history of the Bentely Blower itself. During its original development, Tim Birkin's reliance on physical tuning to increase the supercharger boost pressure resulted in several catastrophic failures, including his infamous retirement from the 1930 Le Mans 24-hour race due to engine failure (Frankel, 2021).

Figure 2 - Tim Birkins No.9 Bentley Blower on 22nd June 1930 Le Mans 24 Hours

- **The Modern-Day Consequence –** If destructive tests of this nature were to occur today, the consequences are severe. The 4.399 litre engine features a monobloc design (Hucknall, 2024). This means that an error made during tuning, such as increasing compression ratio, can cause detonation which often scraps the entire primary casing. Therefore, Hucknall, (2024) explains that the traditional method of 'tune it until it breaks, then back off,' is no longer an ethical or economically viable option for these cultural artifacts of time.

1.3 Proposed Solution

"Virtual prototyping is the non-destructive solution"

To overcome the previously discussed risks associated with traditional tuning, this project proposes a non-destructive testing solution through the implementation of one-dimensional (1D) Computational Fluid Dynamics (CFD). Realis software called Riccardo WAVE enables the creation of a high-fidelity digital-twin to be used as a virtual prototype. This advanced 1D simulation platform allows engineers to accurately model complex transient gas dynamics, in-cylinder combustion processes, and thermal flows across the entire engine system without the need for any physical testing (Realis, 2025). This process of translating the engine to a computational environment means that hundreds of component permutations, such as valve timing, re-boring, increase in compression ratio, camshaft lobe profiles, and manifold geometry, can be evaluated simultaneously and most importantly safely.

A virtual prototyping solution carries significant sustainability benefits, aligning directly with the United Nations (UN) Sustainable Development Goals (SDG's) (UN, 2015). It champions SDG 12 (Responsible Consumption and Production) by eliminating material waste and reducing energy consumption as the scrapping of physical prototypes is no longer necessitated. It additionally supports SDG 11 (Sustainable Cities and Communities), specifically target 11.4 to Protect the Worlds Cultural and Natural Heritage, by providing a modern, non-destructive framework to safeguard and study upon an internationally recognised engine of cultural and industrial heritage.

2.0 Aim

'Provide quantifiable, evidence-based data on the performance gains achievable in the 4.399L Supercharged Bentley Blower engine by creating a validated 1D CFD model, utilising a systematic optimisation methodology to maximise its transient fluid dynamic properties.'

2.1 Scope and Limitations

This project is bounded in its entirety to the evaluation and optimisation of the transient gas dynamic effects of the Bentley 4.399L Blower engine. As such the in-scope, out-of-scope, and limitations are detailed below:

1. **In-Scope –** The study will firstly focus upon the development of a 1D CFD model using Ricardo WAVE. This sequentially enables the simulation of steady-state, full-load performance curves such as brake power and torque across the operational RPM range. The optimisation parameters are confined to mechanical gas dynamic variables.

   This includes:
   a) Intake geometry optimisation
   b) Bore increase
   c) compression ratio increase
   d) Optimisation of camshaft
   e) Optimisation of gas flow ports

2. **Out-of-Scope –** The project does not explore the structural integrity, mechanical stress, or thermal fatigue placed upon the engine block and its moving components. As such finite element analysis (FEA) is excluded from the project scope. Furthermore, additional factors affecting performance including vehicle dynamics, gearbox, fuelling, tyres, brakes, weight reduction, and whole vehicle aerodynamics are omitted from the study.

3. **Limitations –** By employing the streamlined Ricardo WAVE 1D CFD software, the simulation relies on spatial averaging to assume the complex three-dimensional (3D) in-cylinder flow (tumble and swirl) and detailed Conjugate Heat Transfer (CHT) (Millo *et al*,. 2020). This detailed source goes on to explain that this characterises 1D systems to have limited predictive capabilities regarding the combustion process itself. The complex flow phenomena is captured using built-in, established 1D sub-models such as the Wiebe combustion model.

3.0 Objectives

"Performance shaped by the objectives that guide it"

1. Conduct a comprehensive literature review which encompasses internal combustion engine (ICE) optimisation techniques considering historical, non-electrical tuning principles, the Bentley Blower Engine, as well as the function and suitability of utilising the 1D CFD Ricardo WAVE tool.

2. Identify and extract concrete physical measurements of all the Bentley Blower engines' major components.

3. Develop a baseline 1D transient fluid dynamic model of the Bentley Blower engine within the Ricardo WAVE environment.

4. Validate the predictive capability of the developed model by calibrating it to satisfy real world engine dynamometer data, to ensure high fidelity and accuracy within an acceptable error margin.

5. Perform a systematic optimisation study based on the findings of the literature review, utilising a parametric study, to determine the optimal configuration which maximises brake power.

6. Assess and quantify the results of the optimisation study detailing the predicted maximum gain in brake power and torque over the desired operational RPM range.

4.0 Literature Review

4.1 Background of Internal Combustion Engine Optimisation

"Refining the explosion through the art of doing more with less"

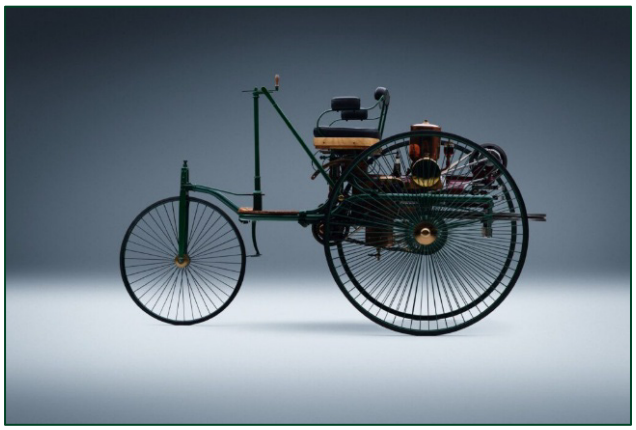

Figure 3 - Benz Patent-Motorwagen - The World's First Petrol-Powered Automobile (Nathan, 2026)

Since the creation of the first petrol-powered motorcar in the late 19th century, automotive engineers have been fundamentally driven by the pursuit of maximising efficiency and power output from internal combustion engines (Nathan, 2026) (Martins *et al.*, 2018). While the core principles of combustion have remained largely consistent, the methods in which the performance is extracted has evolved drastically over the last 140 years. According to Dahham *et al.* (2022), contemporary spark-ignition (SI) engines achieve high thermodynamic efficiency, generally between 30 and 36%, while meeting stringent emission standards first introduced by the European Union in 1992 (RAC, 2025). This is achieved through innovations such as the integration of advanced electronic control units (ECU's), direct fuel injection (DI), and variable geometry systems (Hubmann *et al.*, 2012).

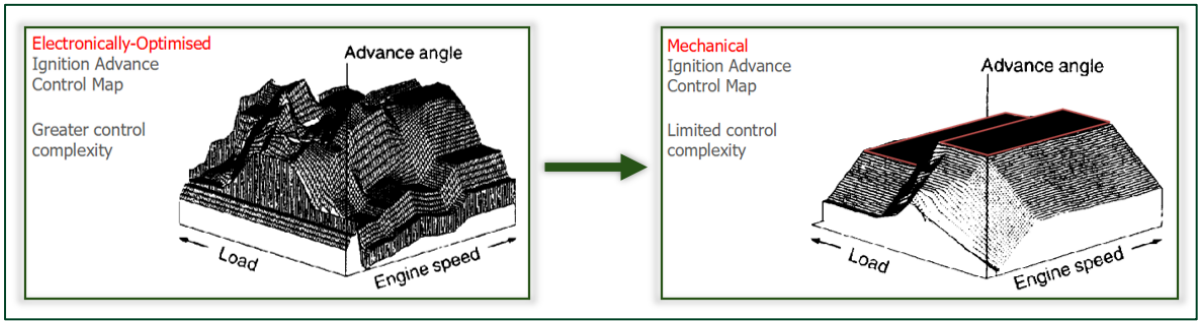

Figure 4 - Annotated Visual Representation of the Limitations of Mechanical Tuning (Bosch, 2011)

However, vintage power units, such as the 4.399 litre Bentley Blower, present a highly juxtaposed engineering challenge. Lacking the electronic intervention of modern powertrains, the performance of such engines are dictated strictly by the mechanical architecture and fluid dynamic principles. As is widely historically documented, extracting additional power from these engines is attained through the meticulous, physical tuning of gas exchange components (Irving and Clymer, 2015), with a visual representation provided above on the limitations of injection tuning by Bosch (2011).

As early 20th century engineers developed a deepened understanding of power production, there was a notable paradigm shift toward, “obtaining increased performance from engines of more moderate cubic capacity,” (Irving and Clymer, 2015, p.2). This historical trend captures and contextualises the adoption of forced induction to elevate power without simply increasing engine displacement. Irving and Clymer (2015), as also supported by Baugan (2025), concludes that performance tuning relies heavily on mastering gas flow dynamics, refining carburation, reducing frictional losses, and manipulating valve timing to optimise the volumetric efficiency.

Achieving these mechanical optimisations historically required a tuning methodology which was highly iterative, costly, and slow, as noted in the technical assessments of NASA’s engine development (NASA, 2004). This relied heavily on physical prototype creation, extensive dynamometer (dyno) testing, followed by a trial-and-error approach. Consequently, transitioning from physical dyno iterations to modern virtual prototyping offers profound advantages which replaces destructive and expensive testing loops with highly efficient, simulation-driven development. (To be discussed in detail later in this report).

4.2 The Bentley 4.399L Blower Engine

"A tale of endurance and aggressive evolution"

One of the core objectives and key deliverables of this investigation relies upon the comprehensive understanding of the original 4.399L Bentley Blower powertrain. Developed in the late 1920's by Sir Henry 'Tim' Birkin and engineer Amherst Villiers, the Blower was an aggressive evolution of W.O Bentley's naturally aspirated (NA) 4.5 litre in-line-four engine.

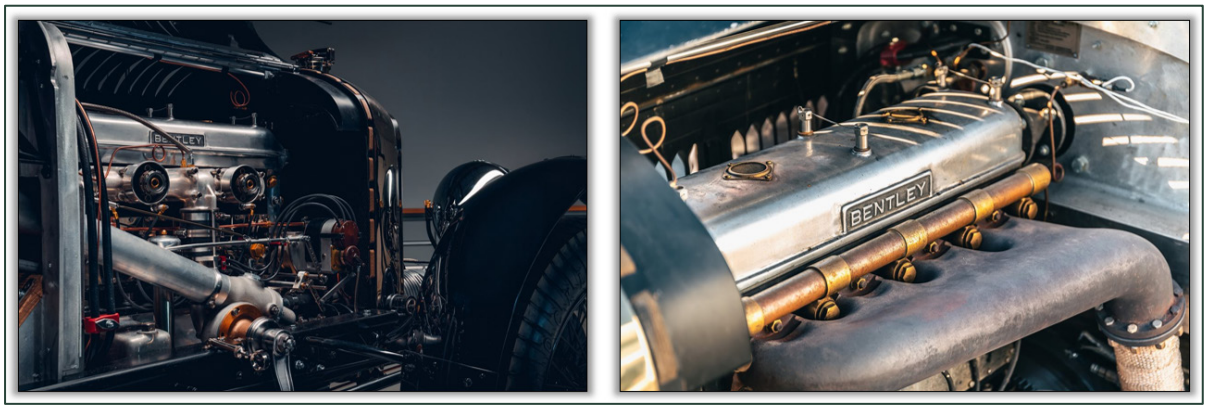

Figure 5 - Bentley Blower Engine Intake Side and Exhaust Side (Source: www.bentleymedia.com)

This 4.399 litre unit was a reworked version of the three-litre engine which founded Bentley Motors in 1919. The design itself was a, "somewhat hybrid between the earlier four-cylinder 3-litre and the six-cylinder 6 ½ litre," (Brown and Wagstaff, 2017). Motor Sport Magazine (1927) added, "the new engine will really consist of 4 cylinders of the 6-cylinder Bentley engine, which has the same bore and stroke."

While W.O. Bentley famously believed that increasing engine displacement was the only reliable method for achieving greater power, Birkin sought to overcome the physical packaging limits of the chassis by implementing forced induction (Kurczewski, 2007).

4.2.1 Internal Engine Architecture Explained

Engine Block

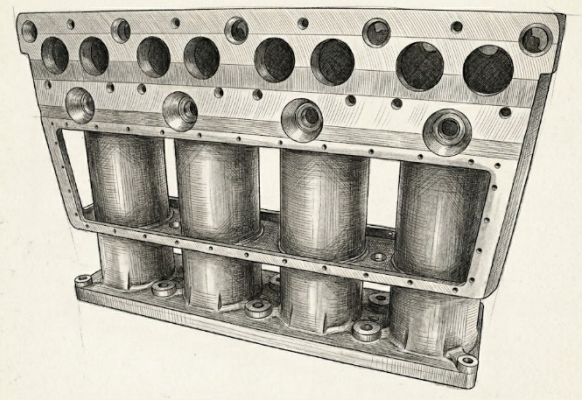

Figure 6 - Sketched Image of the Engine Block

The underpinning foundation of the Bentley Blower is a 4,398 cm^3 in-line four-cylinder, highly undersquare engine featuring a bore of 100mm and a 140mm stroke length. A defining architectural feature of this era of Bentley's high-performance powertrains is the fixed-head monobloc casting, where the engine block and cylinder head are cast as a single, indivisible iron unit. This design eliminates the need for a head gasket, significantly improving the structural rigidity and the engines' ability to withstand the high cylinder pressures (Brown and Wagstaff, 2017).

Valvetrain

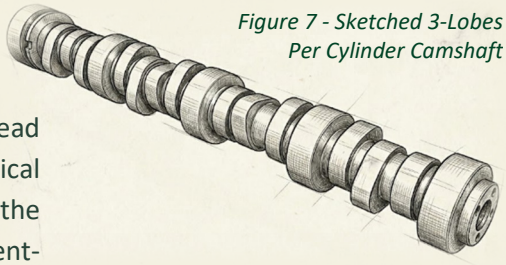

Figure 7 - Sketched 3-Lobes Per Cylinder Camshaft

The valvetrain features a sophisticated single overhead camshaft (SOHC) configuration. This is driven by a vertical bevel gear shaft at the front of the engine. Unlike much of the competition in this era, the Bentley Blower features a pent-roof combustion chamber with four valves per cylinder inclined at an angle: two for intake, and two for exhaust. This configuration of a multi-valve layout was considered highly advanced for the 1920s, heavily promoting superior volumetric efficiency; a crucial prerequisite for effective supercharging (Irving and Clymer, 2015). There are three cam lobes per cylinder, with two operating the exhaust valves via a pair of rockers, and one lobe for the two inlet valves operated via a single forked rocker (Brown and Wagstaff, 2017).

4.2.3 Component Flow Path

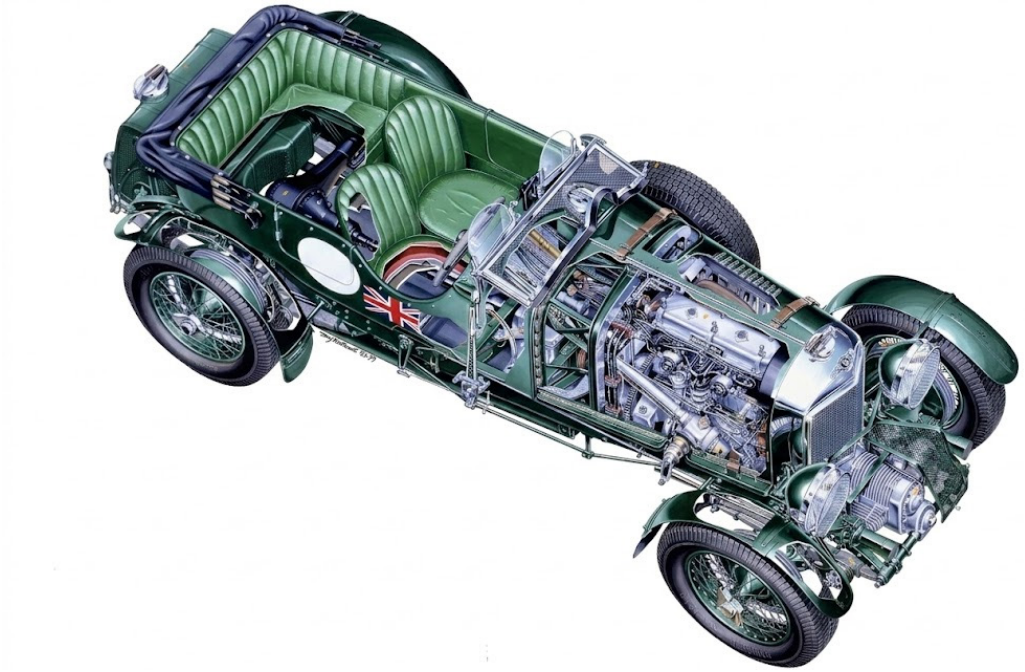

Figure 8 - Bentley Blower Cutaway Image (Source: Bentley 4 1/2 Litre Owners Workshop Manual by Haynes (Brown and Wagstaff, 2017))

To successfully model the gas dynamics within Ricardo WAVE, the precise physical sequence of the gas exchange components must be uncovered. The Bentley Blower utilises a draw-through forced induction system, which dictates the specific component order which is fundamentally different from modern blow-though systems. Below explains the principle of this system as detailed in the Haynes Owners' Workshop Manual (Brown and Wagstaff, 2017) and with special acknowledgement to Bentley Mulliner:

Phase One: Carburetion

Ambient air enters through a pair of SU HVG5 carburettors mounted at the very front of the vehicle. These twin units are uniquely suited to the Bentley Blower because of their constant depression (CD) design meaning that the venturi system is variable. This allows the carburettor to automatically adjust the fuel metering and airflow to match the high, fluctuating demands of the supercharger. This along with large 1⅝ inch bore flow, provides more than a sufficient intake area for the engine to reach its full potential without a restriction (Knight, 2020).

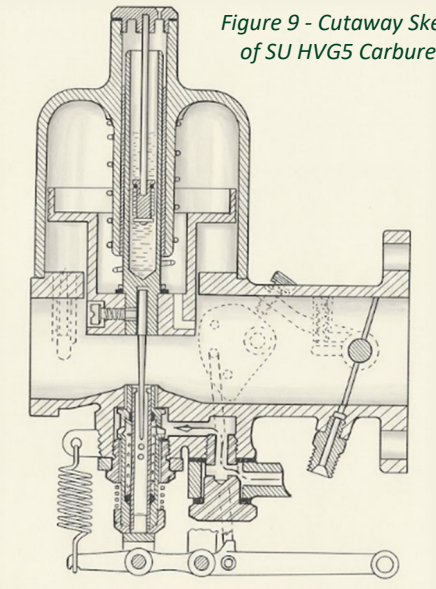

Figure 9 - Cutaway Sketch of SU HVG5 Carburettor

Phase Two: Supercharging

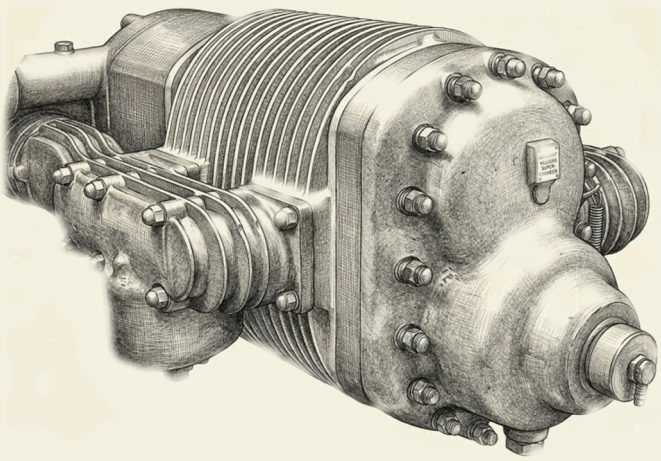

Figure 10 - Amherst Villiers Supercharger Sketch

Next, the combustible fuel-air mixture is drawn directly into the Amherst Villiers Mk IV Roots-type supercharger. Housed within a 650mm aluminium casing, the unit is driven by a short spindle connected to the front of the crankshaft. This drive assembly utilises fabric 'rag' joints (flexible discs made of reinforced, heavy-duty layers) which act as a coupling to accommodate chassis flex and dampen engine vibrations (Professor Low, 1930).

The supercharger employs a twin-lobe rotor design. As these rotors spin, they capture the fuel-air mixture between the lobes and the outer housing, carrying the charge around the perimeter of the casing toward the discharge port creating 12 pounds per square inch (psi) boost (Pomeroy, 1955).

Phase Three: Intake Ducting

The heated, compressed charge exits the supercharger through a 90° bend where it is forced down a heavily finned 70mm cast-aluminium intake duct running up to the engine. This leads to a further 90° bend where the flow is split from 1 to 4 in the intake manifold before entering the combustion chamber via the two valves.

Phase Four: Exhaust

After combustion, the gases are expelled through the dual exhaust valves into a 4 to 1 branched manifold. A large bore exhaust pipe (3-inches in diameter) then runs prominently along the exterior of the vehicle.

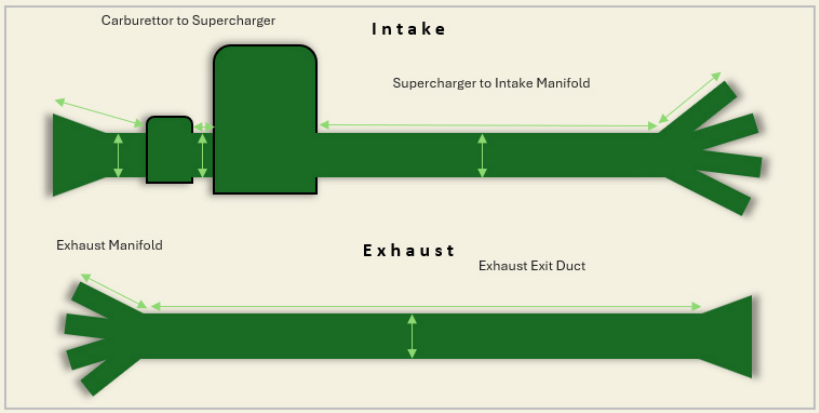

Figure 11 - Intake and Exhaust Diagram (Extract from Engine Technical Specification Sheet)

4.2.4 Technical Specification for Model Inputs

Translating the mechanical architecture into a digital 1D CFD environment requires a great number of specific engineering numerical inputs. These critical dimensions, such as precise valve lift profiles, intake/exhaust manifold dimensions, and compression ratio to name a few have been meticulously sourced from the Haynes Owners Workshop Manual (Brown and Wagstaff, 2017), supporting period literature, and with acknowledgement to Bentley Mulliner.

To provide a non-negotiable, structured guide for the subsequent WAVE simulation setup, these extracted dimensions and operating parameters have been synthesised into a comprehensive technical specification sheet. This will serve as the geometric blueprint for the 1D CFD model and is provided in appendix section A.

4.3 Fundamentals of Internal Combustion Engines

"Defining the source of horsepower"

Like all conventional spark ignition (SI) engines, the thermodynamic foundation of the Bentley Blower is the four-stroke Otto cycle operating sequence (Heywood, 2018). The theoretical thermal efficiency (η_t) of this cycle is principally governed by the engine's expansion ratio; typically, equal to the compression ratio. In historic supercharged applications however, this ratio is mechanically restricted to approximately 6.5:1 to mitigate the onset of destructive engine knock given the low-octane fuels of the 1920's and 30's era (Sir Riccardo, 1931).

Because thermal efficiency is geometrically constrained by the threat of detonation then, the alternative, equally significant primary mechanism for increasing brake power lies in maximising the volumetric efficiency (η_v). This metric is defined as the ratio of the actual mass of air into the cylinder compared to the theoretical mass that it could fill under the static manifold conditions (Heywood, 2018). The Amherst Villiers Roots-type supercharger increases the charge density prior to cylinder entry allowing the Bentley Blower to achieve a volumetric efficiency (η_v) that far exceeds 100%. This is best explained via the absolute volumetric efficiency formula below:

$$\eta_{v(\mathrm{abs})} = \frac{\dot{m}_{air} \times n_R}{V_d \times N \times \rho_{(amb)}}$$

Where:

- $\eta_{v(\mathrm{abs})}$ = Absolute Volumetric Efficiency
- $\dot{m}_{air}$ = Actual mass flow rate of air ingested
- n_R = Number of revolutions per power stroke (2 for a 4-stroke engine)
- V_d = Displacement volume
- N = Engine speed (RPM)
- $\rho_{(amb)}$ = Ambient air density (inlet conditions outside the supercharger)

Equation 1 - Volumetric Efficiency Formula

Within this equation, the mass flow rate ($\dot{m}_{air}$) is the critical variable effected by the supercharger which compresses the charge with a boost pressure of plus 12 psi. This subsequently increases the air density (ρ) within the intake manifold significantly above the ambient density ($\rho_{(amb)}$). According to Heywood (1988), while NA engines are limited by atmospheric pressure and gas flow friction, forced induction allows for a "trapped mass" which exceeds the physical volume of the cylinder. Even though the Bentley Blower lacked intercooling, which lead to a temperature-induced density penalty as described by Sir Harry Riccardo (1931), the pressure ratio provided by the constant-displacement Roots supercharger is sufficient to overcome these losses ($P_{ratio} > T_{ratio}$).

Performance figures, cited from Bentley Motors (2019), validates this theory. The leap from 110 bhp (from the NA engine) to approximately 240 bhp (from the race trim car) represents a power increase of over 118%. This jump in output serves as empirical evidence that the engine's absolute volumetric efficiency allowed the 4.399L displacement to move the air mass of a much larger power unit. Refer to additional formulae and sample calculations in appendix section B.

Even with the Bentley Blower's forced induction system artificially increasing intake air density, there are still some outstanding factors which limit power output. This includes the fluid dynamic losses throughout the engine system, mechanical friction, and pumping losses – collectively measured as Friction Mean Effective Pressure (FMEP) (Stone, 2012).

Furthermore, it is important to note that the Bentley Blower is not a high-revving modern engine rather a large displacement, long 140mm stroke, overhead-cam engine designed to drive the 1.9 tonne vehicle out of Tertre Rouge up to 120 mph on the Mulsanne Straight in only four gears. It is a heavy engine made from primarily steel components designed for endurance. Therefore, a target peak RPM of 3500 is a technically and historically accurate window for peak performance (Hay, 1990). With a stroke of 140mm, 3500 RPM equates to a mean piston speed of 16.33 metres-per-second (m/s), which represents a safe structural limit for the forged steel components of the era (Fayette Taylor, 1985).

Other factors which attribute to this target include the Amherst Villiers Supercharger providing nearly constant boost relative to engine speed, making it optimised for mid-range volumetric efficiency. Also, the gear and final drive ratios fundamentally justifies 3500 RPM as the ideal shift point. Gillespie (1992) explains that by reverse engineering the gearing ratios, a sawtooth analysis shows that a shift at 3500 RPM results in a recovery engine speed of 2520 RPM which is where the onset of the engines peak volumetric efficiency and torque surge occurs. This therefore maximises the tractive effort, ensuring consistent forward thrust throughout the acceleration phase. Detailed analysis and explanation available within appendix section C.

Ultimately, optimising the power output of the engine requires minimising these flow restrictions and exploiting the transient pressure waves within the intake tracts to induce scavenging and ram effects (Smith and Morrison, 1971). Identifying the specific mechanical parameters to most effectively manipulate these gas dynamics forms the basis of the parametric study.

4.4 Parametric Study Options

"Optimising combustion whilst respecting the limits"

Based upon the fundamental principles of volumetric and thermal efficiency established, numerous physical parameters can be altered to optimise the Bentley Blower's power output. It is important that proposed modifications must be evaluated based not only on the theoretical performance benefit but also metrics such as financial, ethical, and practical implications. The following options represent the primary pathways in which this rare, century old ICE can be optimised:

4.4.1 Bore Increase

Increasing the cylinder bore directly increases the total engine displacement, allowing a greater mass of air and fuel to be inducted per cycle. The foundational formula for brake power (P_b) in a four-stroke engine is:

$$P_b = \frac{P_{me} \times L \times A \times N \times z}{2 \times 60}$$

Where:

- P_{me} = Mean Effective Pressure
- L = Stroke Length
- A = Piston Area ($\frac{\pi \times Bore^2}{4}$)
- N = Engine Speed (RPM)
- z = Number of Cylinders

Equation 2 - Brake Power in a Four-Stroke Engine

In theory, assuming a constant mean effective pressure (P_{me}) and engine speed (n), the brake power is directly proportional to the piston area (A). As A is a function of the bore squared, the theoretical power increase can be derived and expressed as a ratio of the bore change ($P_b \propto Bore^2$) (Heywood, 1988). This means that the anticipated result in the Bentley Blower's case would be a 10.25% increase in brake power when the bore is increased to 105mm from 100mm. Increasing bore yields an increase in torque and power from helping to unshroud the valves which allows the engine to move air more efficiently (Stone, 2012); potential for higher peak RPM as the engine becomes more oversquare (Gillogly, 2020), as well as incrementally increasing the compression ratio.

However, it must be noted reboring the Bentley's fixed-head monobloc would require machining which comes at a high cost both financially and ethically. The original component would undergo irreversible changes, or a new non-original head would need to be manufactured; custom oversized pistons would need to be sourced – making this modification undesirable for heritage preservation.

4.4.2 Intake Geometry Optimisation

Altering the length and diameter of intake runners and primary exhaust pipes exploits acoustic wave tuning. Through the timing of the arrival of high-pressure waves at the intake valve slightly before it closes, the Helmholtz ram effect forces additional mass into the cylinder. This can be similarly applied to tuning exhaust lengths to enhance cylinder scavenging (Heywood, 2018).

Specifically, the quarter-wave resonance formula can be utilised to calculate the ideal acoustic intake runner length for a specific engine speed and harmonic order (Smith and Morrison, 1971):

$$L_{Ac} = \frac{15 \times v_s}{N \times n}$$

Where:

- L_{Ac} = Acoustic length of the runner (metres)
- v_s = Speed of sound in the intake runner ($331.3\sqrt{1 + \frac{Temp_{Celsius}}{273.15}}$)
- N = Target engine speed (RPM)
- n = Harmonic order
  ** $n=2$ for 2nd harmonic (Strong pressure boost, ideally suited for the low revving, high torque Bentley engine)*

Equation 3 - Quater-Wave Resonance (Intake Side)

With speed of sound (v_s) being the most critical variable in acoustic tuning, as it dictates how fast the pressure pulses travel, the value used must be adjusted in-line with the 110°C temperature within the manifold after the supercharger. This means that, using the standard thermodynamic relationship formula, the speed of sound increases by 14% from 343 m/s (at room temperature) to 392.4 m/s. When substituting the temperature adjusted v_s value and a target engine speed (N) of 3500 RPM, the ideal acoustic length is calculated as 841mm. When comparing this to the current intake runner dimensions totalling 920mm (after the supercharger) (refer to appendix section A), a 79mm reduction is required to shift the resonance peak to 3500 RPM using the 2nd order harmonic relationship. The findings from the theory shows that the current 920mm setup is tuned for approximately 3200 RPM.

Furthermore, the low real-world cost and high feasibility make this an attractive optimisation option. Fabricating bespoke intake runners or exhaust headers is standard practice in motorsport (Sharma *et al.,* 2017). Crucially, it is a completely reversible modification option which requires no destructive modification to the original engine architecture.

4.4.3 Optimisation of Camshaft

Altering valve timing, such as changing Intake Valve Closing (IVC) and valve overlap, is critical for harnessing dynamic fluid inertia; enhancing performance by improving volumetric efficiency and gas flow (Blair, 1999). Increasing valve lift and duration allows a larger volume of the supercharged fuel-air mixture into the cylinders, which can increase power output. Also, timing adjustments can be used to shift the power band ensuring the engine breathes optimally at the targeted peak RPM as well as potentially broadening the power curve. According to Shaun (2025), advancing the cam generally increases low-end torque and responsiveness while retarding the cam typically increases higher RPM power. Finally, increasing exhaust duration facilitates cylinder purging as the engine has longer to expel the spent exhaust gasses – ensuring cylinder pressure is maintained and allowing for a fresh intake charge to enter (LeBarron, 2025).

While a moderate cost is associated with Computer Numerical Controlled (CNC) machining a custom billet camshaft, it is a highly feasible and straightforward modification (Kaufman, 2012). The original historic camshaft can be stored, while a new optimised camshaft can be swapped into its place, making the optimisation entirely non-destructive and fully reversible.

4.4.4 Optimisation of Gas Flow Ports

This type of optimisation involves the enlarging or smoothing of the internal surfaces of the intake and exhaust ports to reduce fluid friction and boundary layer separation, directly reducing pumping losses and FMEP (Heywood, 2018). The specific process known as ‘porting’ is the process of removing material from and smoothing out the port surfaces. According to Aaron (2026), the benefit of porting is that it increases the volumetric efficiency and leads to a more complete combustion by enhancing the swirl and distribution of the air-fuel mixture which can boost brake power and torque output. Furthermore, porting can support the optimal function of the Amherst Villiers Supercharger as well as other upgrades as previously discussed.

However, the cost of ‘porting’ from a time, financial cost, and ethical perspective is high. As the process involves the removal of material from the original parts and the castings, which is timely and expensive in itself, it permanently effects the geometry and risks damaging the engine, such as breaching the century old water jacket for example.

4.4.5 Compression Ratio Increase

As discussed within section 4.3, raising the static compression ratio directly improves the thermal efficiency (η_t) by extracting more mechanical work from the same mass of inducted fuel-air mixture (Heywood, 2018).

However, increasing compression ratio comes at a high cost and risk. Increasing compression in the Bentley engine requires manufacturing custom domed pistons. As discussed previously, this is a risky modification which can result in fundamental damage to the engine internals as detonation or knock can lead to catastrophic, uncontrolled pre-ignition. Further, as higher compression increases the mechanical stress, components such as the crankshaft, rod bearings, and piston rings can be detrimentally affected (Irving and Clymer, 2015).

4.4.6 Weighted Ranking

To objectively determine which of these parameters are the best modifications overall, the below weighted decision matrix evaluates the options based on their performance benefit, financial cost, practical feasibility, and ethical complications:

Parametric Study Options - Weighted Ranking

Optimisation	Performance Benefit (Effectiveness of increasing BHP)		Financial Cost (Cost vs effectiveness)		Practical Feasibility (Time taken, difficulty to execute)		Ethical Implication (Risk of causing irreversible change)		Total
	Ranking	Weight	Ranking	Weight	Ranking	Weight	Ranking	Weight	
Bore Increase	5	10	3	4	4	6	1	6	92
Intake Geometry	2	10	4	4	3	6	4	6	78
Camshaft Tuning	4	10	2	4	5	6	5	6	108
Gas Flow Ports	1	10	5	4	2	6	3	6	60
Compression Ratio Increase	3	10	1	4	1	6	2	6	52

Table 1 - Weighted Ranking of Parametric Study Options

In summary, camshaft tuning represents the clear favourable option. Even though its cost effectiveness is lower, with a ranking of 2, it scores 5s in both feasibility and ethical implications. This is closely followed by bore increase which is predicted to result in the largest performance gain.

The clear loser is compression ratio increase. Even though it is predicted to achieve moderate gains in performance, the potential of ethical implications and low feasibility score (such as needing to redesign and manufacture new pistons) makes it the high risk, low reward option.

4.5 The Role of Computational Fluid Dynamics

"The high efficiency logic of a single digital dimension"

It is widely acknowledged within the automotive industry that shifting engine calibration and optimisation efforts from traditional physical testing, as was used during the era of the Bentley Blower, to virtual computational models is a method which, "reduces the cost of engine development," (Yu *et al.,* 2022).

4.5.1 Defining 1D CFD and Governing Equations

One-Diamentional Computational Fluid Dynamics is defined as the use of applied mathematics, physics, and computational software to visualise how a gas or liquid flows (Schoegl *et al.,* 2010). In the context of internal combustion engines and Riccardo WAVE, 1D CFD simplifies the complex 3D physical architecture of the engine into a topological network of one-dimensional pipes, ducts, and junctions. According to Realis (2025), the software rigorously solves the fundamental Navier-Stokes equations which govern fluid dynamics:

1. **Conservation of Mass**
   This equation ensures that the rate change of mass within a pipe element is balanced by the mass flux across its boundaries.

$$\frac{\partial(\rho A)}{\partial t} + \frac{\partial(\rho u A)}{\partial x} = 0$$

Where:

- ρ = Density of fluid (kg/m^3)
- A = Cross-sectional area of pipe (m2)
- t = Time (s)
- u = Velocity of fluid (m/s)
- x = Distance along the pipe axis (m)
- ρA = Mass per unit length
- $\rho u A$ = Mass flow rate/ flux

Equation 4 - Conservation of Mass within a Pipe

2. Conservation of Momentum

The equation representing Newton's Second Law which ensures pressure forces, wall friction, and changes in pipe geometry are accounted for.

$$\frac{\partial(\rho u A)}{\partial t} + \frac{\partial(\rho u^2 A + pA)}{\partial x} = p\frac{dA}{dx} - f$$

Where:

- ρuA = Momentum per unit length
- $\rho u^2 A$ = Connective momentum flux
- p = Static pressure (N/m2)
- pA = Pressure force acting on the fluid face
- $p\frac{dA}{dx}$ = Pressure force exerted by a tapered section of pipe walls
- f = Friction force per unit length

Equation 5 - Conservation of Momentum within a Pipe

3. Conservation of Energy

The equation which tracks total energy of the fluid, important for calculating the actual adjusted speed of sound and the resultant timing of pressure waves.

$$\frac{\partial(\rho e_o A)}{\partial t} + \frac{\partial(\rho u h_o A)}{\partial x} = q$$

Where:

- e_o = Total specific energy (static internal energy + kinetic energy) (J/kg)
- h_o = Total specific enthalpy representing energy transported by the flow (J/kg)
- q = Heat transfer rate per unit length (W/m)

Equation 6 - Conservation of Energy within a Pipe

These governing equations are discretised using a finite volume method and solved across a staggered spatial grid at discrete time steps (Aspley, 2020). The above numerical framework explains the foundation which allows the software to accurately capture the highly transient, compressible gas dynamics as well as the propagation of acoustic pressure waves through duct work of the engine.

4.5.2 Advantage of 1D Over 3D (for this case)

With 3D CFD being unparalleled for resolving highly detailed spatial flow conditions, it is computationally very demanding (Esposito *et al.,* 2020). This includes precise tumble and swirl motion of combustion gasses inside a cylinder or even boundary layer separation inside of a manifold. As such, running a multi-cylinder engine within a transient simulation across a wide RPM sweep would require potentially weeks of computer processing time. On the other hand, 1D CFD relies on empirical sub-models, such as the Wiebe function for combustion, to approximate 3D flow phenomena (Realis, 2025). This allows a full engine system simulation to solve an RPM sweep in a matter of minutes. This much enhanced computational efficiency is what makes 1D CFD the 'industry standard' for the whole system performance predictions and the feasible choice for executing this nature of parametric optimisation.

4.6 Summary and Knowledge Gap

"Identifying the digital void in the mechanical masterpiece"

Exponential growth within the historic motorsport sector provides compelling justification for this engineering methodology. This is evidenced through the significant growth of premier events such as Le Mans Classic. Transitioning to an annual schedule starting in 2026, the event has seen competitor vehicle entries rise by approximately 170%; a near 700% surge in spectator numbers in 2025 since its inception in 2002 (Le Mans Classic, 2025). When coupled with other fixtures such as the Goodwood Revival, Monaco, Nürburgring, and Donnington Historic, the rise in popularity is a direct catalyst for growth within the historic vehicle sector – with a value £7.3 billion in the UK alone (Federation of British Historic Vehicle Clubs, 2025). The fierce competition between rivals incentivises the application of modern technology to optimise vintage performance machinery (Lawson, 2021).

However, a distinct knowledge gap remains. While 1D CFD simulation is the definitive standard in modern powertrain development, its application to systematically optimise historic, mechanically-governed engines like the Bentley Blower is largely undocumented within academic literature and the public domain. Therefore, this project aims to address a significant gap in the market by applying the proven, modern methodology of 1D CFD engine optimisation via Riccardo WAVE to an historically significant classic engine. The study aims to quantify the performance gains achievable through simulation-led, data driven tuning. The outcome should not only secure the vehicles competitive viability but also preserve its cultural status as an artifact of history.

5.0 Methodology

The specific engineering methodology executed within this project is structured to follow a sequential prototyping workflow. This is a process defined by Gurav (2021) as a way of working which ensures tasks are completed in a highly prescribed, step-by-step order. This means each critical step within the project must be concluded and verified before the next key sequential phase is permitted to begin. In the wide context of modern engineering, utilising this methodology within a digital environment enables engineers to robustly simulate and refine designs long before physical manufacture. Importantly, this significantly mitigates development time and prototyping costs (Wang, 2002).

For this project, virtual prototyping of the 4.399L Bentley Blower engine is divided into three primary sequential phases. The linear progression of each task is set out visually within the below critical path flowchart:

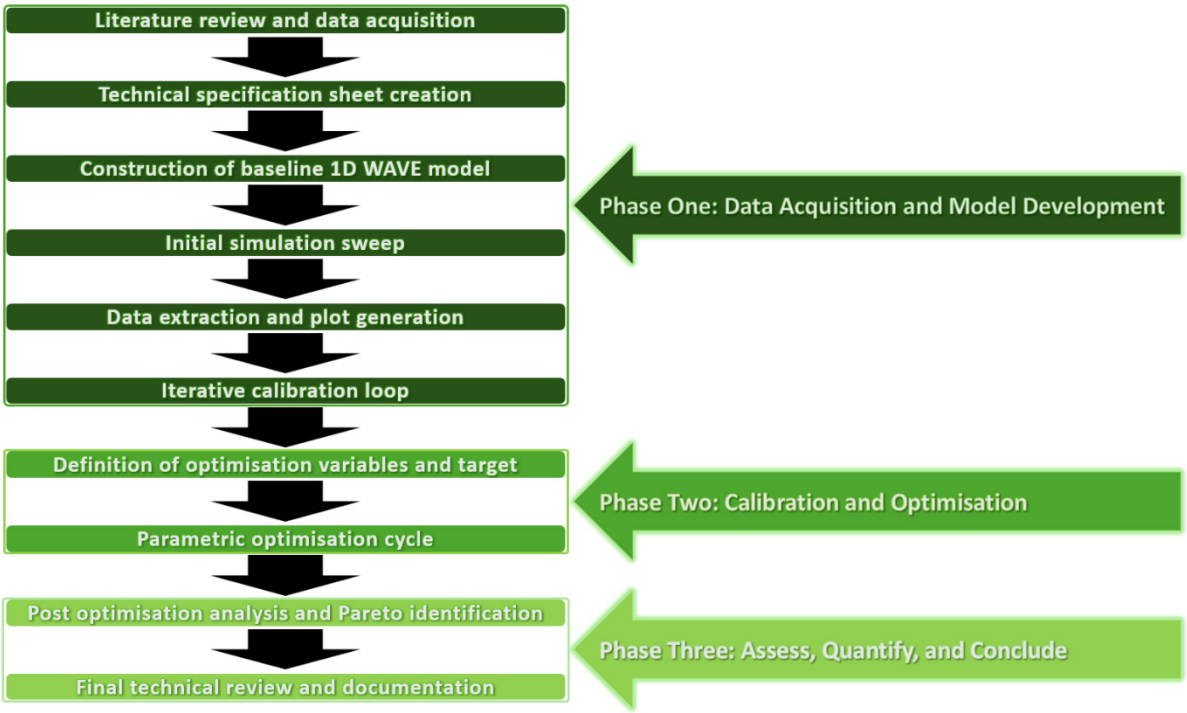

Figure 12 - Sequential Virtual Prototyping Critical Path for Project

5.1 Phase One: Data Acquisition and Model Development

"Quality preparation paving the path to performance"

Initially the project starts with an informational phase to lay the geometric foundation required to build an accurate, faithful digital-twin. This leverages on the historical documentation and performance data previously collated into a comprehensive, synthesised technical specification sheet (available in appendix section A). This sheet provides precise mathematical inputs for the Riccardo WAVE environment, including accurate geometric data, volumetric variables, and fluid flow characteristics. Thus, allowing the baseline computational model to be constructed using the software's 1D flow element library. This involves digitally assembling the engine's architecture using interconnected ducts, pipes, and plenums. Further, other metrics such as the supercharger map and fuel flow characteristics are defined as an input.

The essential combination of quality research and precise inputs at this stage is critical to ensure the digital-twin created is as representative as possible. This means it must closely reflect the original engines architecture as well as ensure the model conforms to the mechanical constraints which are relied upon for period engine tuning during the optimisation process.

5.2 Phase Two: Calibration and Optimisation

"The core engineering challenge"

As described by Lopez *et al.* (2023), the scientific credibility of any CFD simulation relies wholly upon its proven ability to accurately reflect real-world behaviours. Consequently, before any form of optimisation can occur, the baseline model created in phase one must undergo a rigorous, iterative calibration loop:

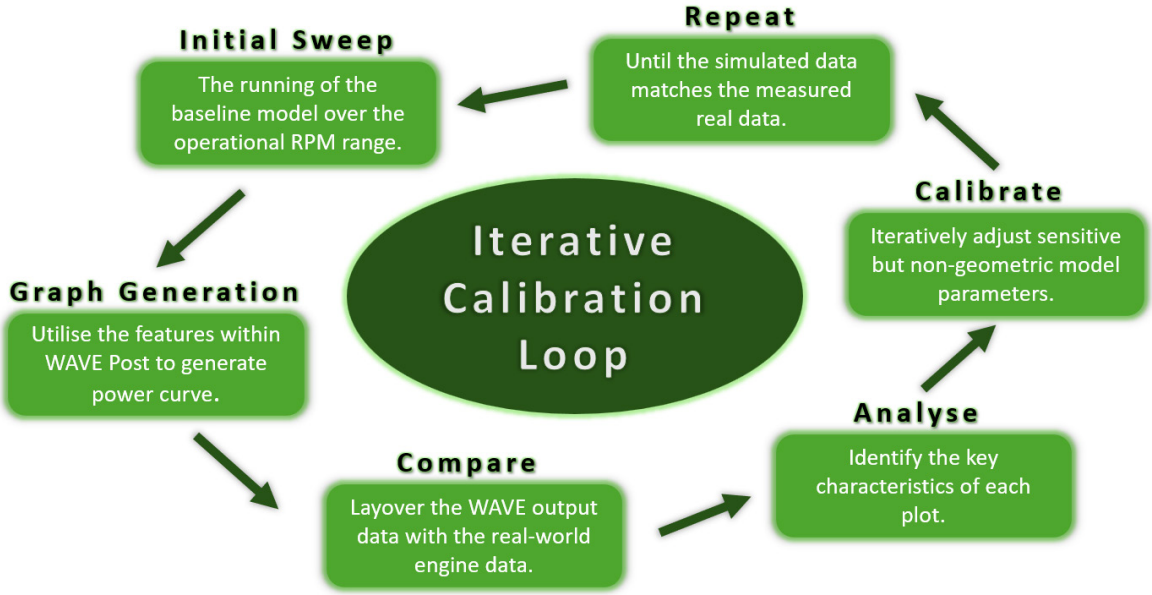

Figure 13 - Iterative Calibration Loop for Project

As illustrated in the above iterative calibration loop, the process begins with an initial simulation sweep across the operational power band. The simulated brake power against RPM data will be extracted via WAVE Post and graphically overlaid to compare directly against the real engine dyno performance output. Discrepancies between the computational model's output and real-world data can then be analysed which sequentially prompts the iterative tuning of sensitive, non-mechanical variables. This includes adjustments to the Weibe combustion and heat transfer sub-models. The iterative calibration loop repeats until the virtual model's power output satisfies an acceptable engineering tolerance within ± 5% range of the dyno data.

5.2.1 Executing the Parametric Study within Ricardo WAVE

Upon establishing a fully validated stock baseline model, the sequential workflow transitions into the virtual optimisation stage of phase two. It is important to understand how the physical changes, as detailed in section 4.4, are enacted within the Ricardo WAVE digital environment. WAVE Build utilises a parametric architecture whereby a centralised constants table can be used to define a sweeping number of variables for each simulation, such as an RPM sweep or even a series of duct length changes (Realis, 2025). Guided by research completed within section 4.4 of the literature review, specific mechanical variables will be chosen to run within the parametric optimisation study:

1. **Bore Increase –** Investigating the effect of up to a 5% increase in cylinder diameter.

   With bore being a simple scalar input, the geometric property can be manipulated within the engine's primary properties. Further, the constants table can be utilised to explore the effects of changing bore to target a specific RPM range.

2. **Intake Geometry –** Adjusting the length and diameter of the primary intake duct.

   Rather than manually replacing ducts of differing lengths within the system, the lengths and diameters of the primary runner length can be assigned a parameter name within the constants table. Starting with length followed by diameter change guided by theory, the value can then be varied within one sweep targeting a specific RPM range.

3. **Camshaft Optimisation –** Sequentially changing intake and exhaust timing as well as duration and lift profile of the cam lobes.

   Simulating new camshaft profiles and altering timing within WAVE Build is a highly efficient process. Rather than importing many different kinematic data arrays for every cam variation, WAVE allows for the single baseline lift profile to be manipulated using anchors and multipliers. For example, to advance or retard the Intake Valve Opening (IVO) or Exhaust Valve Closing (EVC), anchor points are shifted relative to the current crank angle degree. Or to simulate a higher lift profile cam lobe, a multiplier is applied to mathematically scale the whole lift curve uniformly.

4. **Gas Flow Ports Optimisation –** Enhancing fluid flow within the engine ducts.

   Porting and polishing within Ricardo WAVE can be numerically simulated by adjusting factors which effect wall friction within the ducts. This can once again be controlled via the utilisation of the constants table by assigning one value to all the key ducts.

5. **Increasing Compression Ratio -** Incrementally increasing cylinder compression.

   Compression ratio is dictated by adjusting the cylinder's defined clearance volume within the constants table, forcing the solver to recalculate the thermodynamic expansion ratios. A specific RPM range can be targeted to achieve the optimal output.

5.3 Phase Three: Assess, Quantify, and Conclude

"Through the lens of analysis, the Pareto optimal approach emerges"

The final phase of the project transitions away from simulation execution to critical data analysis. To improve efficiency, for most optimisation options, a specific RPM will be targeted to analyse the effect the geometric change has within a single sweep.

Then the optimal Ricardo WAVE Post output, including power and torque sweeps across the entire usable RPM range, will be mapped out graphically and compared to the stock baseline model. From this, the data will then be filtered through to identify the Pareto optimal engine state. According to Cope (2025), this is the configuration which represents the absolute best compromise to maximise peak brake power and torque within the required RPM range without adversely affecting other variables such as brake specific fuel consumption (BSFC) – which will also be analysed.

Finally, the project will conclude by defining the predicted effect each individual upgrade will have and, importantly, how the geometric and timing alterations combine to achieve the Pareto optimal engine. A recommendation will be made to assess which upgrade is expected to achieve the greatest gain, definitively quantifying the predicted percentage increase in performance relative the validated stock baseline.

6.0 Simulation Setup (Engine Build)

"Historical truth becomes the bedrock of a digital-twin"

Construction of the 1D CFD model within Ricardo WAVE is executed as a systematic and iterative process. Starting with a generic four-cylinder engine model and then slowly assembling complex elements of the powertrain allows for isolation and troubleshooting of individual fluid dynamic errors.

6.1 Version One: Fundamental Elements

The foundational ingredients of the model are the core geometric dimensions complimented by the elements which define the Bentley Blower. Some internal engine architecture, such as the 100mm bore and 140mm stroke, are extracted from literature (Brown and Wagstaff, 2017). However, highly specific geometry, including cam-lobe profiles, valve timing, valve diameters, fuel flow rate, and compression ratio are from primary and secondary sources with particular acknowledgement of Mulliner – (available within appendix section A).

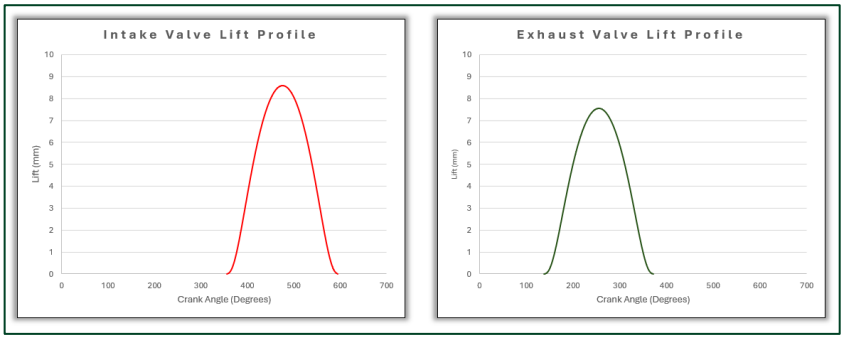

Figure 14 - Cam-Lobe Lift Profiles

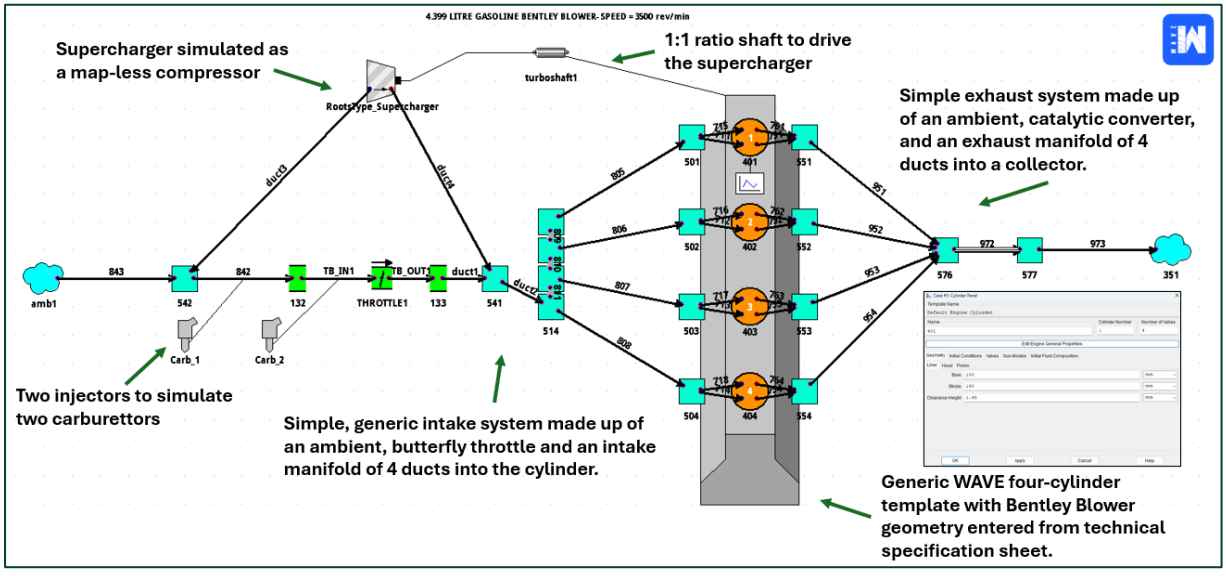

Figure 15 - Engine Build Version One

6.2 Version Two and Three: Troubleshooting

The below engine model represents a more simplified design than previous in attempt to identify any potential sources of error causing the engine output to be abnormal. Figure 16 shows the supercharger removed and an increase in overall ambient conditions to reflect the 12-psi boost provided to investigate if the previous map was a cause of ineffective simulation.

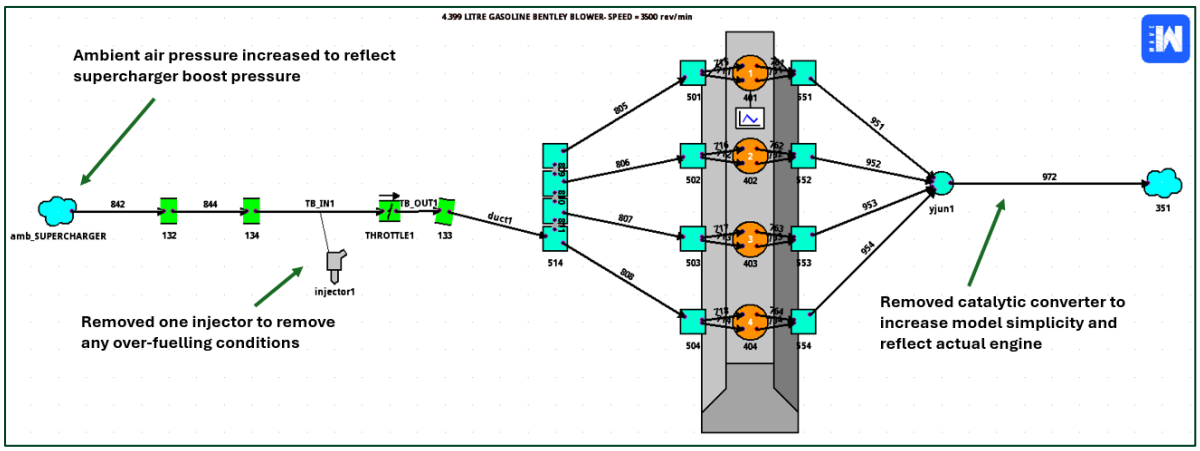

Figure 16 - Engine Build: Version Two

The carburettors were changed to a single injector, which simulates the function of two carburettors. These were added to the correct position within the intake system. The supercharger is also added back to the model simulated again with a map-less compressor.

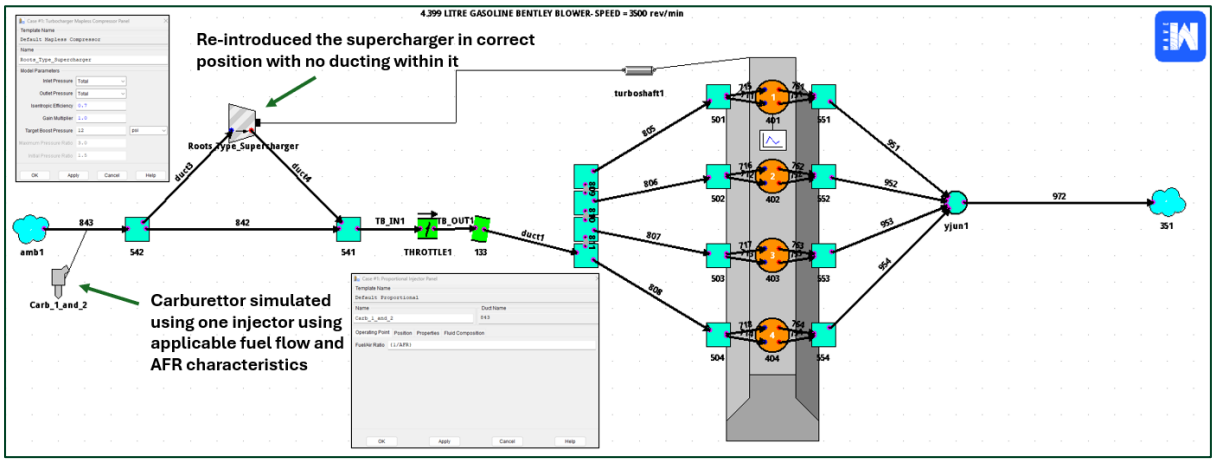

Figure 17 - Engine Build: Version Three (Detailing Supercharger and Carburettor Changes

6.2.1 Supercharger Modelling Strategy

A defining mechanical feature of the Bentley Blower is the front-mounted Amherst Villiers Roots-Type supercharger. As the Blower utilises a mechanically driven 1:1 ratio, positive-displacement pump, the design is inherently capable of delivering its boost pressure almost immediately from idle engine speed. Therefore, to authentically replicate the low RPM delivery of supercharger boost pressure, it is modelled as a map-less compressor set to 12 psi.

6.3 Version Four: Detailed Geometric Inputs

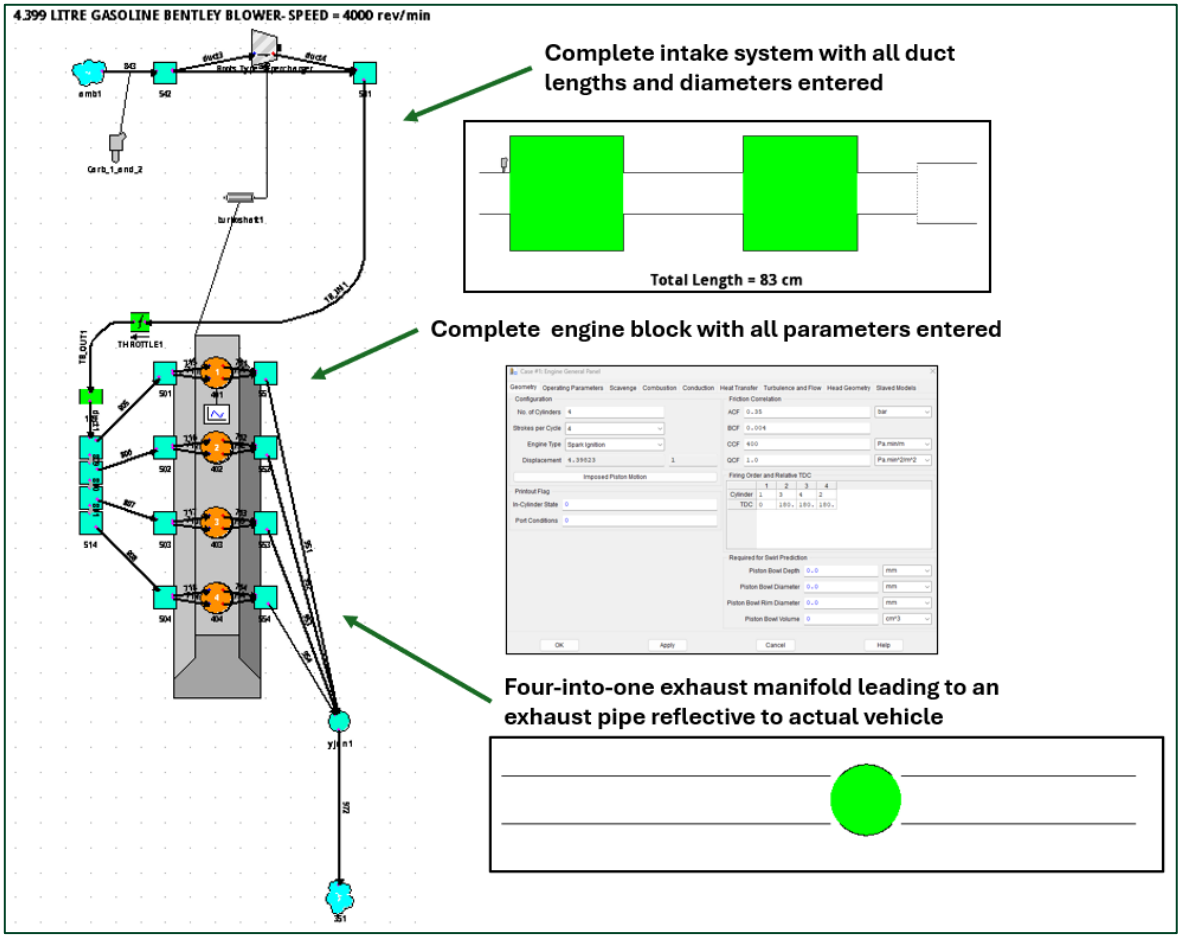

Figure 18 - Engine Build: Version Four (Completed)

Figure 18 shows the completed engine build with all mechanical data entered to reflect the actual 4.399L Bentley Blower engine. All components are placed in the correct order and troubleshooting to resolve any fundamental WAVE Post errors has been completed. At this stage the engine is ready for validation.

6.3.1 Primary Research for Duct Geometry

To enable the accurate capture of critical volumetric data required for wave tuning analysis, some physical measurements are taken directly from chassis UU 5782 (the original Tim Birkin Bentely Blower located at Bentley Motors' CW1 House in Crewe, Cheshire). This primary, hands-on research facilitates the accurate modelling of the intake runner lengths, plenum volumes, and exhaust manifold dimensions – which are generally undocumented within literature.

Figure 19 - Pictures of Chassis UU 5872 taken at CW1 House

6.4.1 Sub-Models

Because 1D CFD simplifies spatial flow, it relies on mathematical sub-models to approximate complex and turbulent 3D phenomena, according to Realis (2025). This includes the in-cylinder combustion process and mechanical friction. During the engine model build up to this point, these sub-models are populated with empirical estimates to provide a base which allows the engine to operate and will be validated at a later stage.

1. Combustion Sub-Model (Wiebe Function)

Rather than calculating complex chemical kinetics, Ricardo WAVE predicts the rate of heat release using the industry standard Weibe function. Explained by Heywood (2018), this mathematical model calculates the Mass Fraction Burned (x_b) of the air-to-fuel mixture as a function of the engines crank angle (θ):

$$x_b(\theta) = 1 - exp\left[-a\left(\frac{\theta - \theta_0}{\Delta\theta}\right)^{m+1}\right]$$

Where:

- θ_0 = Crank angle at the start of combustion
- $\Delta\theta$ = Total combustion duration
- a and m = Adjustable form factors for efficiency and shape

Equation 7 - Mathematical Model for Mass Fraction Burned

By utilising this function, the simulation effectively predicts in-cylinder pressure rise without the need of high computational demands (Heywood, 2018).

2. Friction Sub-Model (Chen-Flynn Correlation)

Gross power generated by the combustion model must be accurately reduced to account for parasitic mechanical losses. This is calculated using a Friction Mean Effective Pressure (FMEP) sub-model – the Chen-Flynn correlation. According to Tadros, (2025), this calculates friction as a function of peak cylinder pressure and mean piston speed.

It is crucial to note that because historical sub-model data of the Bentley Blower engine are unknown quantities, the initial sub-model values inputted serve only as a starting baseline. These will then be leveraged as a variable to adjust during the subsequent iterative calibration phase to match the dyno data.

7.0 Validation

7.1 Initial Model Verification

"Confidence in results begin with confidence in the model"

Before commencing any rigorous iterative calibration, it is imperative to establish that the baseline 1D CFD model is computationally stable and exhibits expected fluid dynamic behaviour:

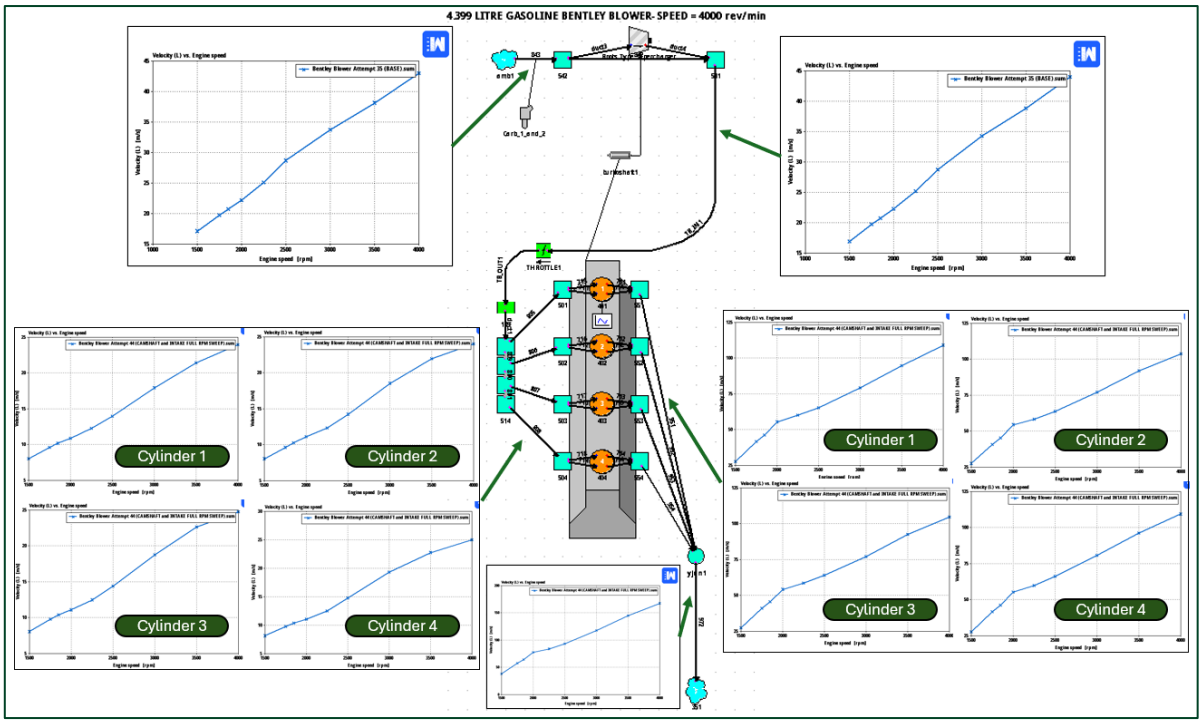

Figure 20 - Flow Velocity Diagrams Across All Major Engine Ducts

Figure 20 illustrates the completed engine model accompanied by an analysis of all major intake and exhaust ducts. The data, which shows fluid flow velocity (m/s) as a function of engine speed (RPM), confirms that components including carburettors, map-less supercharger, intake manifold, valve kinematics, and exhaust are successfully integrated and working as expected. Importantly, as anticipated by fluid dynamic principles, the duct flow velocities scale proportionally with engine speed throughout the system. Further, reflective of the era's design, the inefficiency of flow into and out of the cylinders varies with the distance travelled to and from the collector.

The successful generation of these logical flow velocity graphs initially validates the geometric and operational integrity of the model, providing a foundation for the following iterative calibration phase.

7.2 Calibration Process

"Iterative calibration to transform approximation into accuracy"

With the initial kinematic function of the model verified, the next sequential step is to calibrate to ensure its chemical and thermal properties align with real-world performance. To achieve this an iterative calibration loop systematically targeting these variables must be carried out. A strict engineering tolerance of ±5% is targeted – as set out by The American Society of Mechanical Engineers (ASME) (Schwer, 2009) also specified by Gumbie, (2024). A complete numerical dataset charting the calibration process, including all Mean Absolute Error (MAE) values, is provided in appendix section D.

7.2.1 Establishing the Baseline

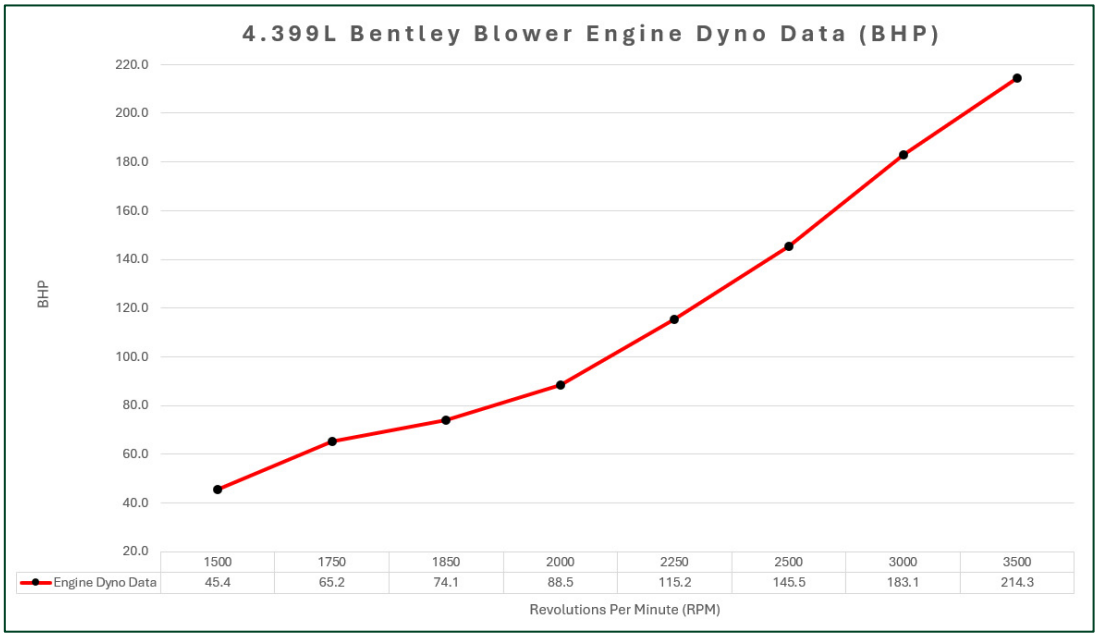

Figure 21 - 4.399L Bentley Blower Baseline Dyno Data

According to the International Organization for Standardization (ISO) (2017), the key to a successful calibration relies on having a definitive target which remains consistent throughout the process. The above graph plots the historical, real-world dyno data for the race specification 4.399L Bentley Blower, displaying BHP as a function of engine speed (1500-3500 RPM). This precise run taken from a calibrated engine dyno serves as the absolute truth for simulation. As such, all subsequent iterations will be assessed on their ability to replicate this specific performance characteristic.

7.2.2 Validation Overview

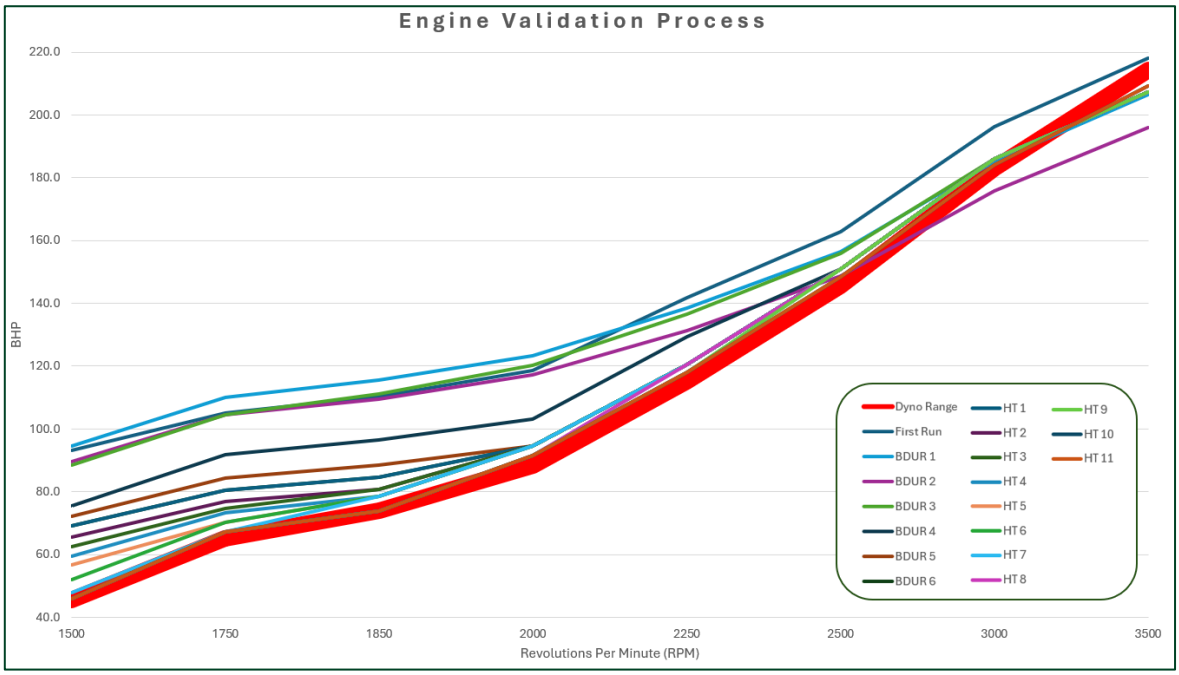

Figure 22 - Complete Validation Process Overlaid with ±5% Engineering Tolerance Range

The above graph visualises the progressive tightening of the simulations accuracy by providing a complete overview of the engine's calibration journey. It overlays the ±5% target range derived from the dyno data; the uncalibrated initial run; the intermediate sub-model adjustments, and the final calibrated output.

7.2.3 First Run (Uncalibrated)

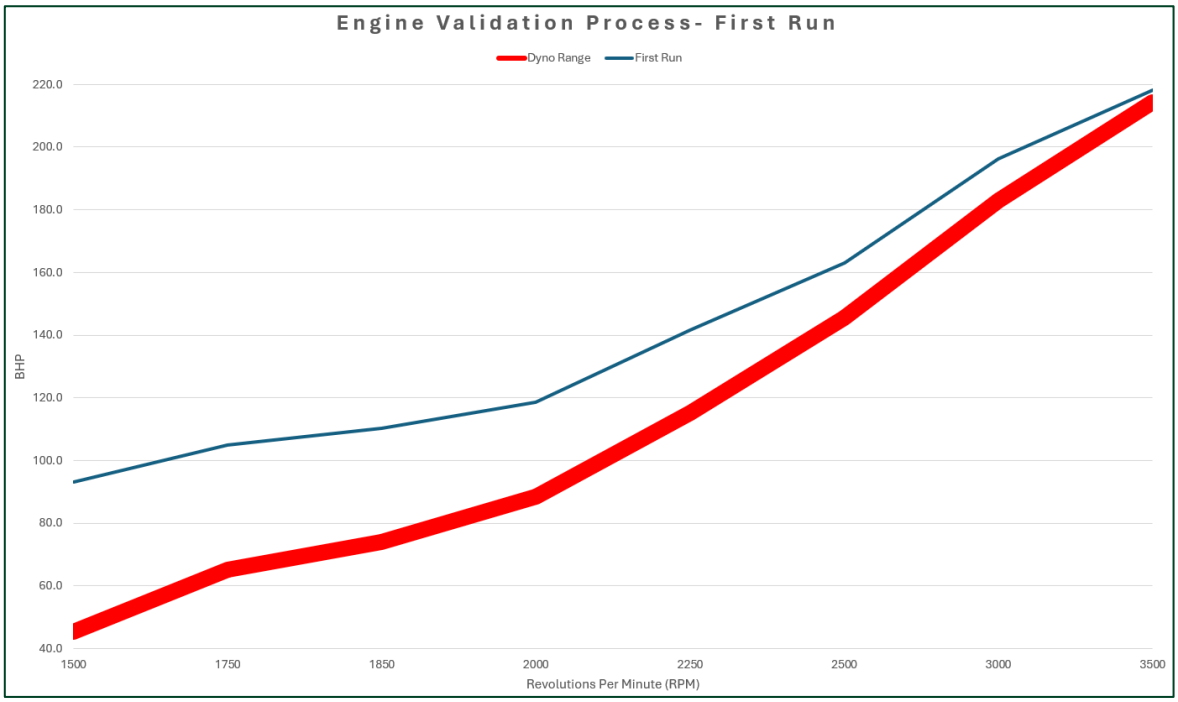

Figure 23 - First Run vs Baseline Dyno Data Range

Figure 23 isolates the initial simulation run. It highlights a drastic overprediction of initial engine performance as a result of using generic, modern interpretations of the Weibe and heat transfer sub-models. Even though the overall MAE of the model was a respectable 12.32%, the model exhibited a specific 52.02% error at 1500 RPM. This highlights that whilst the fluid dynamics and geometry is correct, the assumption of modern combustion efficiency fundamentally flaws the 1920s powertrain.

7.2.4 Combustion Sub-Model Calibration

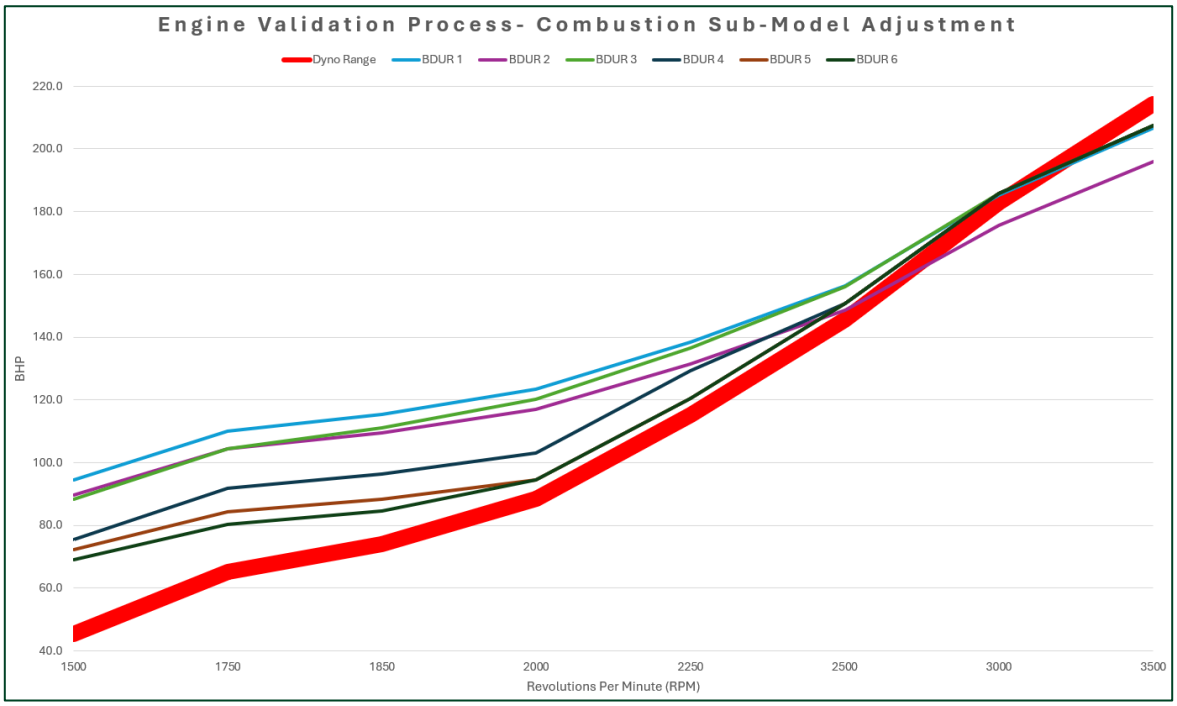

Figure 24 - Combustion Sub-Model Adjustment Process vs Baseline Dyno Data Range

To address the severe low-RPM overprediction, the Wiebe combustion sub-model requires historical contextualisation. By changing the burn duration at within the lower RPM range, the slow combustion effected by low compression ratios and unrefined fuel of the era is effectively simulated. Furthermore, according to Acosta (2020), the Bentley utilises Scintilla magnetos driven directly by the engine which means that they generate a weaker spark at low-RPMs. So, by extending the burn duration specifically at lower engine speeds, the engine model is forced to replicate this mechanical and chemical inefficiency. The above graph shows that this calibration method drastically improved accuracy, reducing the 1500 RPM error from 52.02% down to 5.41%, lowering the overall MAE to 4.21%.

7.2.5 Heat Transfer Sub-Model Calibration

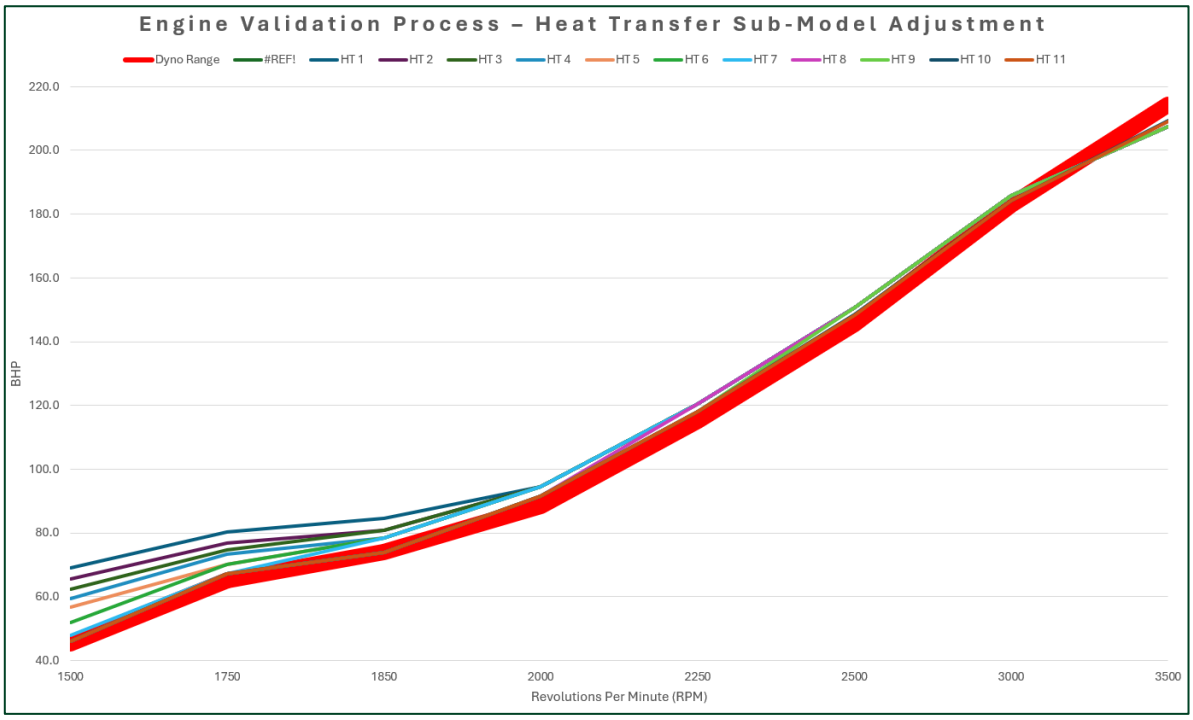

Figure 25 - Heat Transfer Calibration Process vs Baseline Dyno Data Range

Even though the combustion adjustment corrected the low-end delta to a degree, the model still required fine-tuning to sit comfortably within the ±5% tolerance. This can be explained by how the Bentley Blowers' engine architecture manages its thermal losses. According to Brown and Wagstaff (2017), the Bentley features a fixed-head monobloc cast-iron engine with a primitive water jacket cooling system which retains and rejects heat vastly differently from how modern engine blocks made from modern alloy materials do. By utilising a modified Woschni heat transfer model, which changes the in-cylinder heat transfer coefficient, the simulation accurately accounts for these historical performance losses. The graph illustrates how the adjustment pulls the whole performance curve into alignment, achieving a highly accurate final MAE of 2.06%.

7.2.6 Calibration Summary

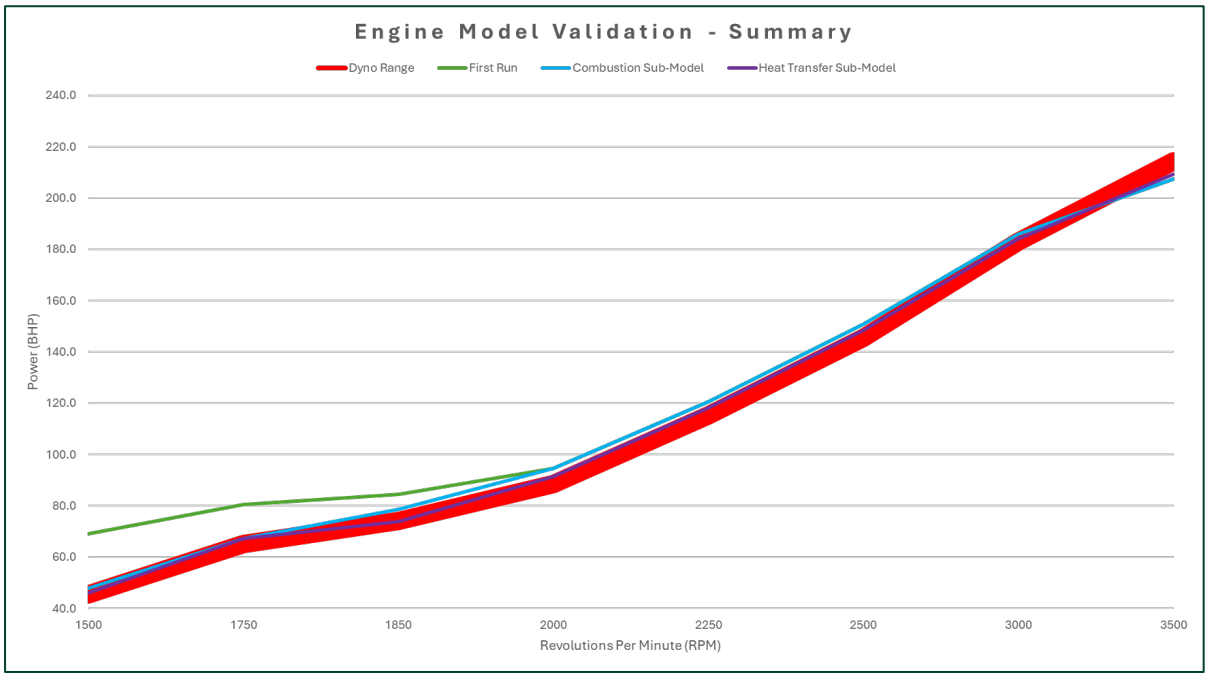

Figure 26 - Engine Calibration Summary Graph

The final calibration graph summarises the delta between the initial model and the fully calibrated digital-twin. It shows the process of taking modern 1D CFD sub-models and turning them into historically accurate versions, such as accounting for magneto inefficiencies and thermodynamic properties of cast-iron, iteratively brings the power curve into the correct position. Refer to appendix section E to see how the constants table changes throughout this process.

With a final model validated within a MAE of 2.06%, the project phase can transition to the next key phase – the parametric optimisation study.

8.0 Results of Parametric Study

8.1 Bore Increase

"More capacity creating more opportunity for power"

8.1.1 Isolating Target RPM

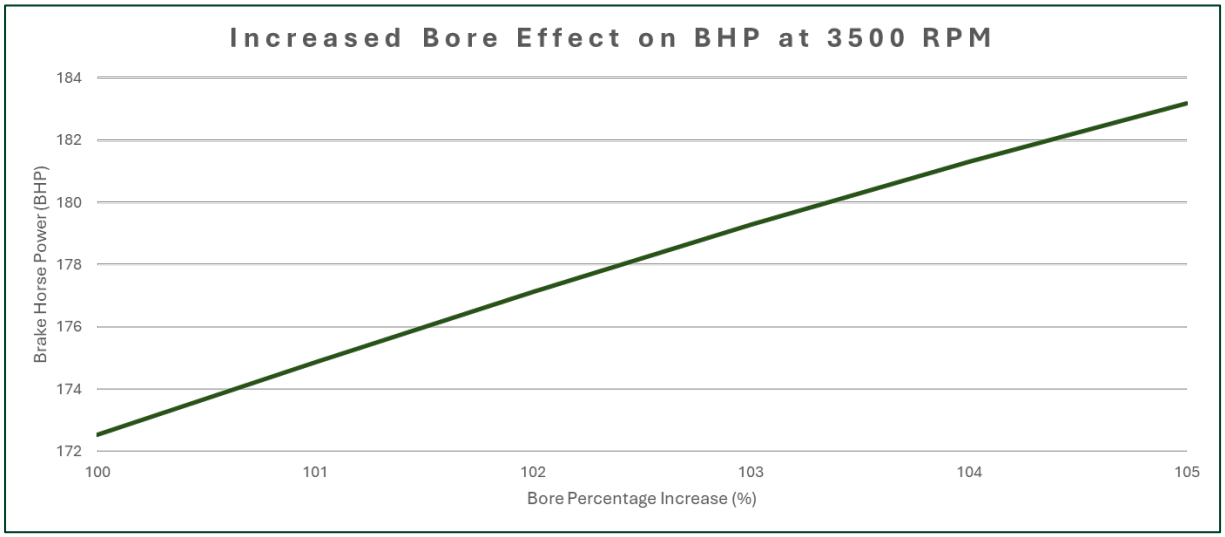

Figure 27 - Line Graph Showing Effect of Increasing Bore at 3500 RPM

When firstly isolating at 3500 RPM, a linear relationship can be identified when analysing the effect of increasing bore on BHP. Isolating a specific RPM is done within Ricardo WAVE by utilising the constants table and ticking the 're-initialise at each step' toggle within simulation settings. It visually and mathematically demonstrates that as combustion chamber volume incrementally expands, the engines capacity to ingest air, burn fuel, and generate useful work increases at a directly proportional rate – with a gain of approximately 2.14 BHP per 1% of increase in bore size.

8.1.2 Brake Power Result

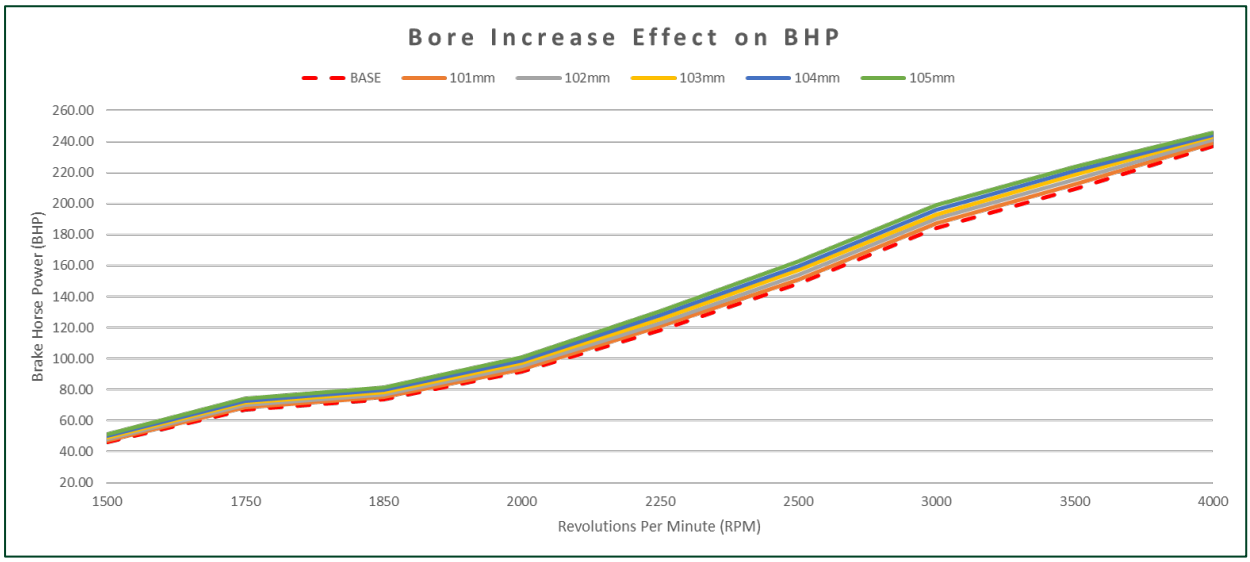

Figure 28 - Line Graph Demonstrating the Effect of Increasing Bore throughout the Operating Range

Figure 28 illustrates the effect of increasing engine bore in 1mm increments throughout the whole engine's operating range. The graph shows a uniform trend, stacked increase as the result of each 1mm expansion in bore increases cylinder displacement, allowing the engine to burn more fuel within each combustion cycle.

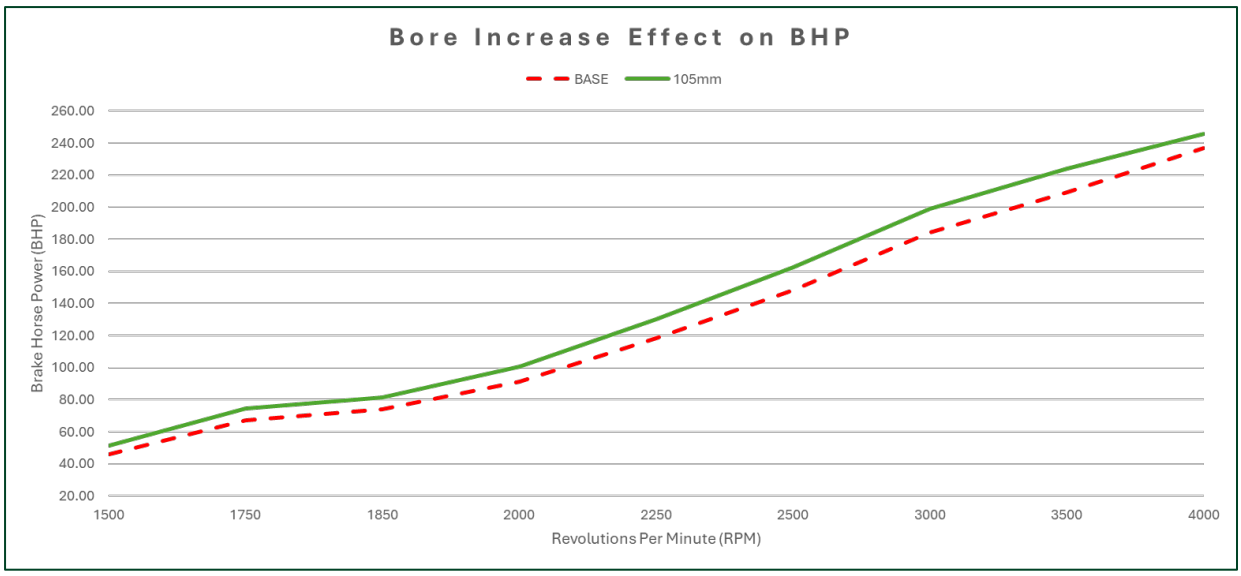

Figure 29 - Line Graph Isolating Optimal Bore vs Base Engine BHP Output

Focusing on a 105mm cylinder bore as the optimal configuration facilitates the analysis of theoretical versus actual power gains. As researched in section 4.4.1, according to the formula from Heywood (1988), the anticipated gain in BHP was 10.25% (refer to Equation 2, section 4.4.1). Within the midrange of the sweep (2500 RPM), this theory aligns almost perfectly as the base BHP was 145 and the 105mm bore BHP is 160 – an increase of 10.3%.

As RPM increases beyond 3000 though, a tapering effect can be observed with a mere 2.9% increase in brake power by 4000 RPM. The reasons for this result are best explained when analysing torque, which will be completed next.

8.1.3 Torque Result

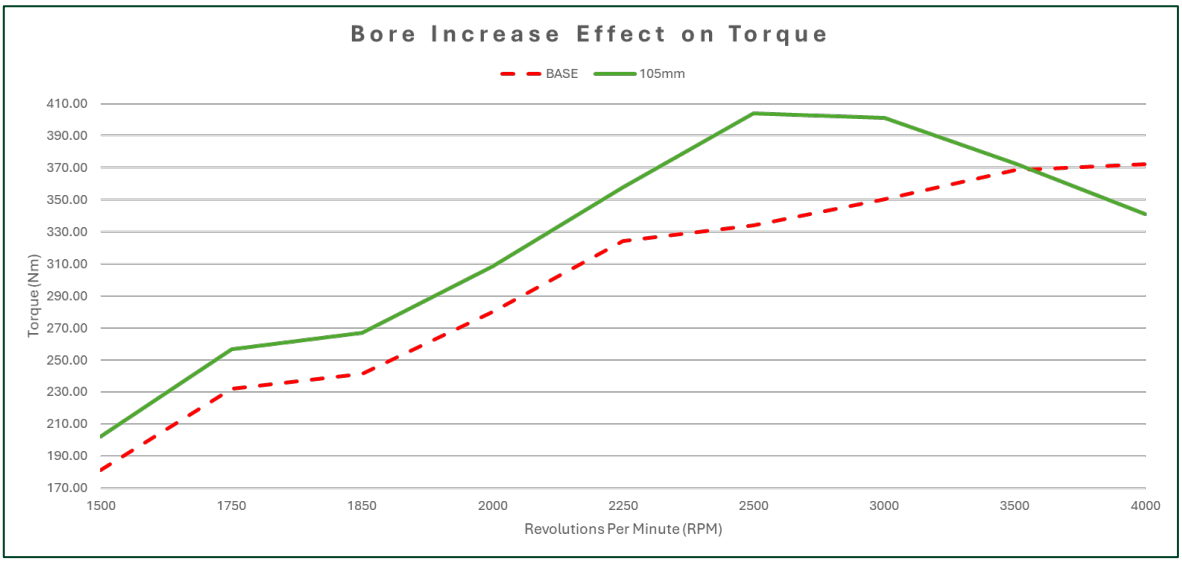

Figure 30 - Line Graph Illustrating Optimal Bore Increase Effect on Torque

The above torque graph facilitates critical analysis of the direct force generated by combustion. It shows that between 1500 and 2500 RPM, the 105mm bore produces a mathematically proportional torque increase. At this stage, the piston speed is relatively slow giving the cylinder enough time to fill with fuel/air mixture effectively.

A peak occurs at 2500 RPM followed by a precipitous drop, eventually dropping below the stock output at approximately 3600 RPM. According to Blair (1999), this is an effect of choked flow. He noted that when air velocity though the intake valve exceeds a Mach index of approximately 0.60, the stock intake ports, valves, and camshaft design acts as a restrictor. This means the cylinder becomes starved of air, pumping losses increase, and volumetric efficiency plummets. Therefore, to allow the effects of increasing bore to be maximised, further optimisations must be applied in addition to relieve the engine of the choking issues.

8.1.4 Brake Specific Fuel Consumption

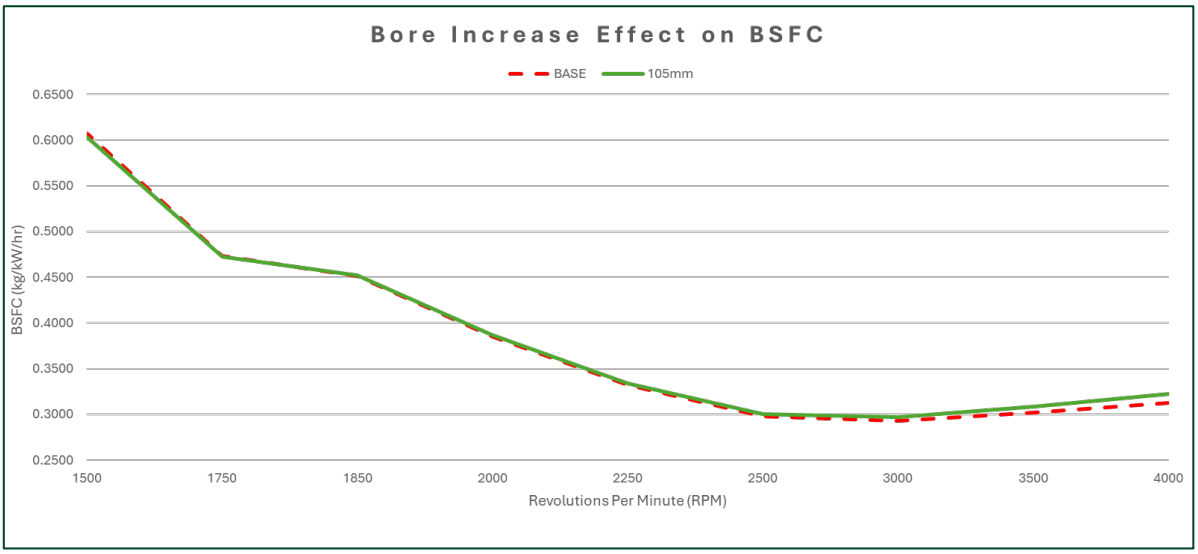

Figure 31 - Line Graph Showing the Effect Increasing Bore has on BSFC

The above BSFC line graph confirms that increasing bore to 105mm does not cause catastrophic loss of engine efficiency. Throughout the low to mid-range, the modified bore curve almost perfectly mirrors the base curve perfectly. Beyond 3000 RPM, the 105mm curve starts to drift slightly above, indicating an expected slightly worse fuel efficiency. Because the engine is experiencing the chocking effect, it must consume proportionally more fuel for the power it generates.

8.2 Intake Geometry Optimisation

"Airflow governing what capacity alone cannot deliver"

8.2.1 Single RPM Sweeps

Firstly, focusing on a specific RPM threshold of 3500, the objective of this specific study is to exploit acoustic wave tuning, as researched in section 4.4.4, and reduce the fluid flow restrictions.

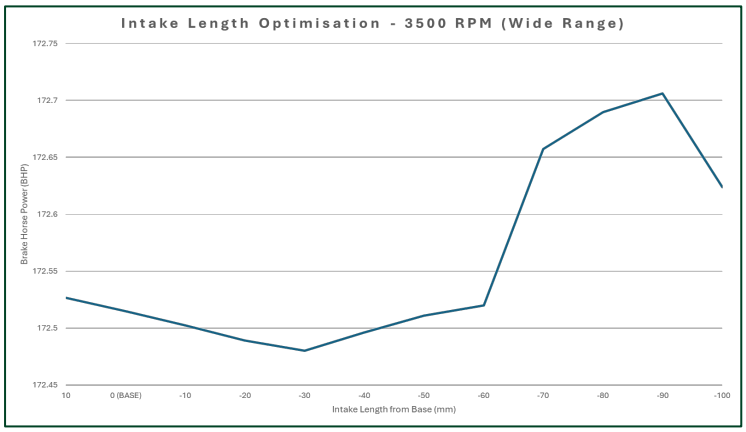

Figure 32 - Line Graph Presenting a Wide Range of Primary Intake Lengths Effect on BHP

The initial sweep varied the primary intake runner length over a broad range, from +10mm to -100mm relative to the baseline. Brake Power exhibits a district non-linear response to length variations. Critically, within the -70 to -90mm range, a spike in power is observed. This power surge aligns with theory provided by Smith and Morrison, (1971), whose formula predicted a 79mm reduction would optimally time the arrival of high-pressure acoustic waves.

To pinpoint the optimal length, a secondary, higher resolution sweep was conducted across a narrower range. While the theoretical quarter-wave equation predicted a 79mm reduction as the best (equation 3 section 4.4.2), it assumes, idealised, frictionless conditions. As the 1D CFD simulation accounts for complex boundary layer friction and pressure distributions, the high-resolution graph reveals that the peak BHP at 3500 RPM is a 66 mm reduction as compared to the base model.

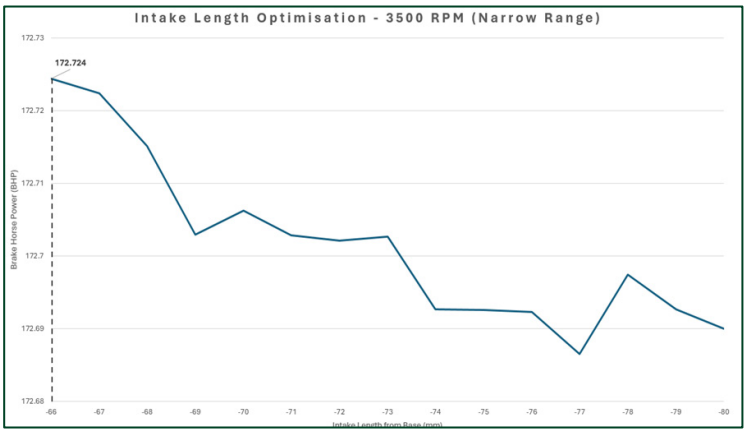

Figure 33 - High-Definition Line Graph Showing a Narrow Range of Primary Intake Lengths Effect on BHP

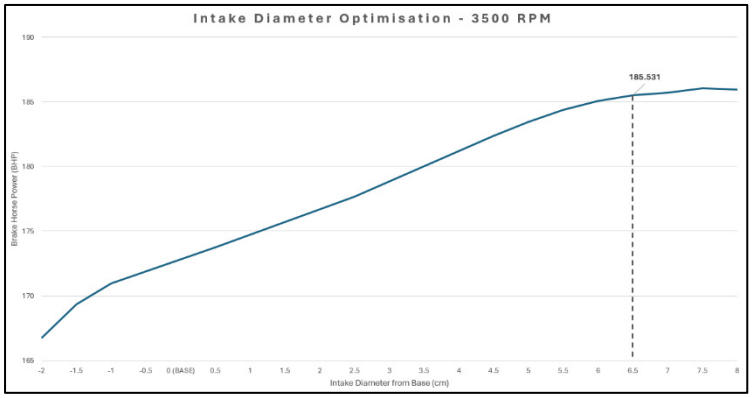

Figure 34 - Line Graph Showing Effect of Adjusting Primary Intake Diameter

Further to length tuning, the primary intake diameter was subjected to a sweep to evaluate the effects of reducing flow restriction. The base engine has an intake diameter of 70mm. This graph varies the diameter within a -20mm to a +80mm range. The data shows a rapid, near-linear increase in brake power as diameter is incrementally expanded, with the linear section of graph showing a gain of approximately 2.2 BHP per cm of intake diameter increase. Beyond +65mm, the curve begins to flatten out, indicating diminishing returns. This means the intake port is no longer acting as a restrictive bottleneck in the system. Therefore, the optimal primary intake duct diameter is definitively defined as 135mm (70mm base + 65mm increase).

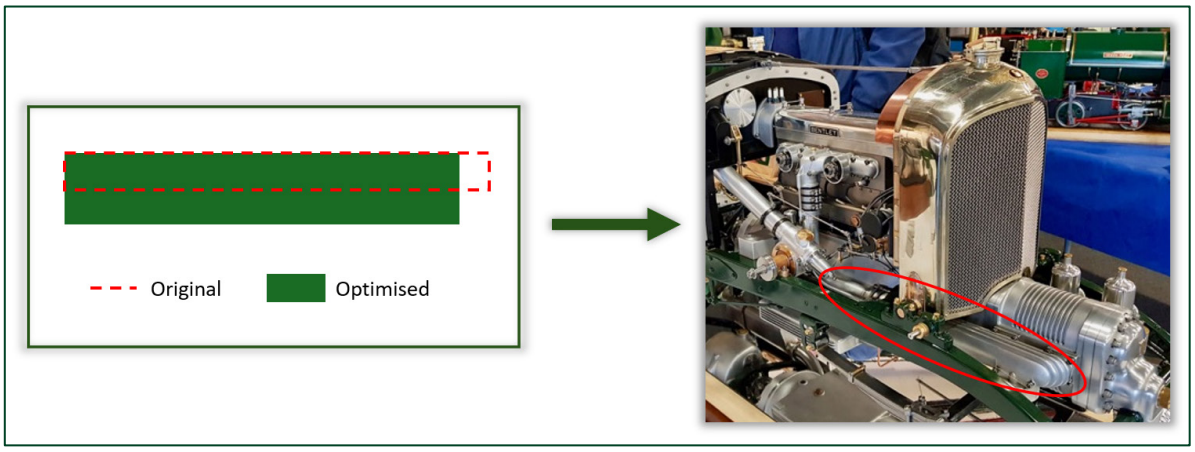

Figure 35 - Scale Diagram Overlaying Original vs Optimised Intake Duct and Annotated Bentley Blower Intake System

8.2.2 Brake Power Result

Now the optimal primary intake geometry has been identified (66mm length reduction and a new 135mm diameter), a full RPM sweep must be conducted to assess the full impact of these combined changes.

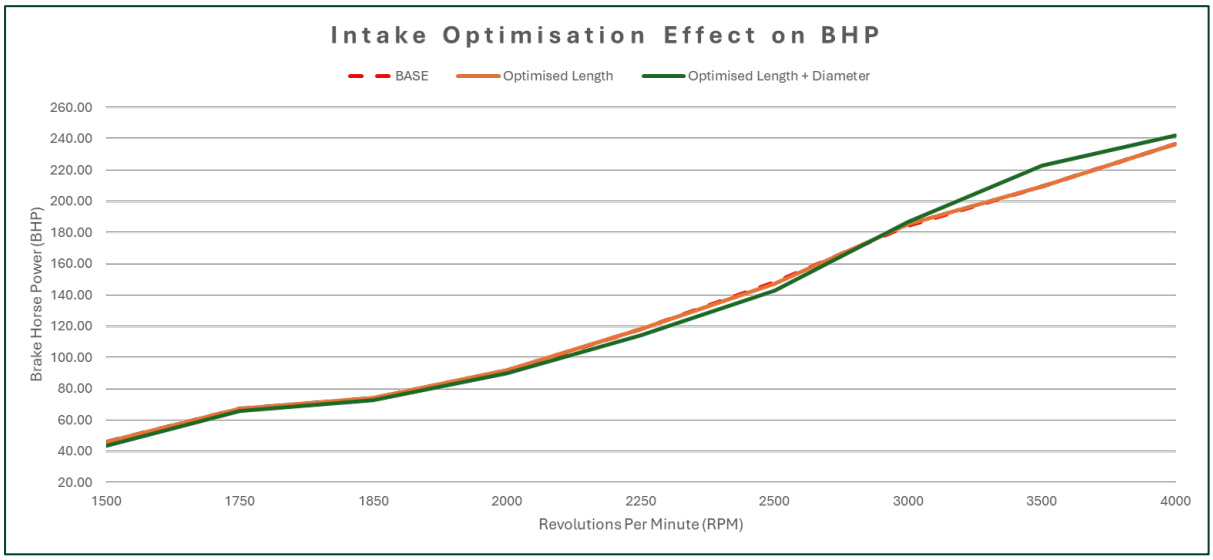

Figure 36 - Line Graph Showing Effect of Intake Optimisation on BHP

The above BHP sweep illustrates the thermodynamic contributions of both variables. It shows that a modification to intake length yields marginal top-end improvements over the baseline. However, when combined with a diameter increase, a more significant higher RPM breathing capability is unlocked. This can be explained by the reduction of fluid friction which delays the onset of choking the flow. This results in a peak power increase of approximately 2.5%.

8.2.3 Torque Result

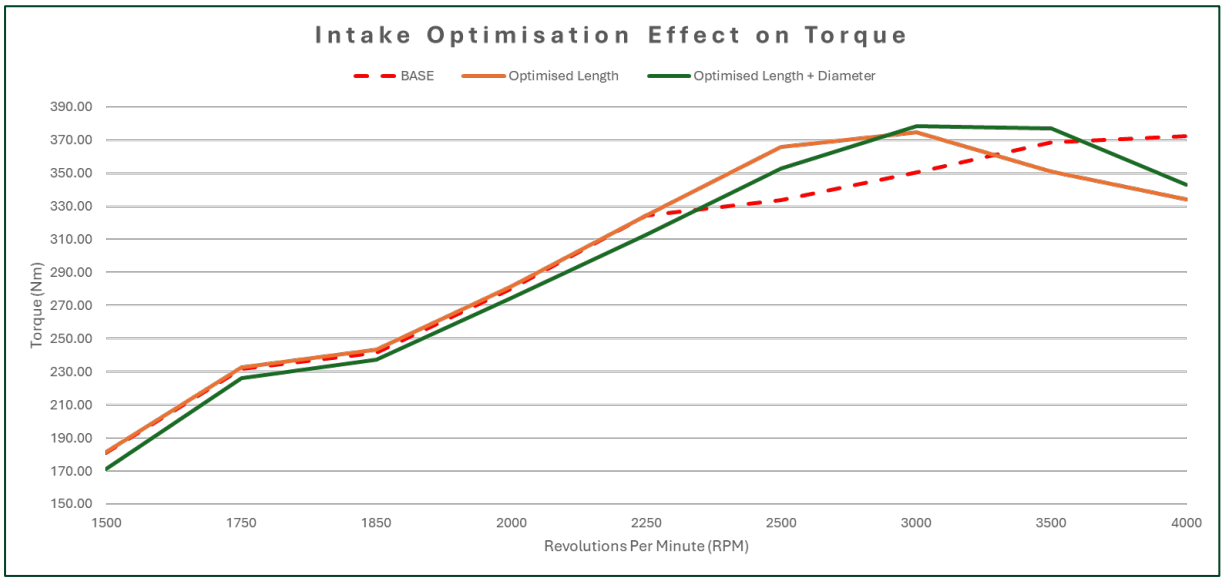

Figure 37 - Line Graph Showing the Effect of Intake Optimisation on Torque

The above torque graph reveals the profound mechanical effect from intake length and diameter optimisation. Firstly, by applying the 66mm reduction, the resonance peak is shifted to 3000 RPM – utilising 2nd order quarter-wave resonance acoustics (Smith and Morrison, 1971) (refer to Equation 3, section 4.4.2). The combination of this and the diameter increase achieves not only a slightly higher peak torque value but, more importantly, the peak torque window shifts to a later point for longer – between 3000 and 3500 RPM. Specifically, at 3000 RPM, where the torque surge now begins to peak, the engine produces approximately 8% more torque than the baseline model.

8.3 Camshaft Tuning

"Dictating the rhythm of horsepower"

As the two variables are so closely linked, the previously optimised intake geometry will be carried forward into this section where the kinematic parameters of the single overhead camshaft will be explored. This process involves the systematic adjustment of the camshaft anchor points for timing, multipliers for duration, and lift profiles – targeting a primary optimal BHP at 3500 RPM.

8.3.1 Intake and Exhaust Timing

Changing the intake anchor involves altering the phasing of the intake lobe relative to the crank angle. This variable is adjusted first as the IVC point is an important valve event in a four-stroke engine. According to Heywood (1988), it dictates the dynamic compression ratio and influences where the engine makes its peak torque.

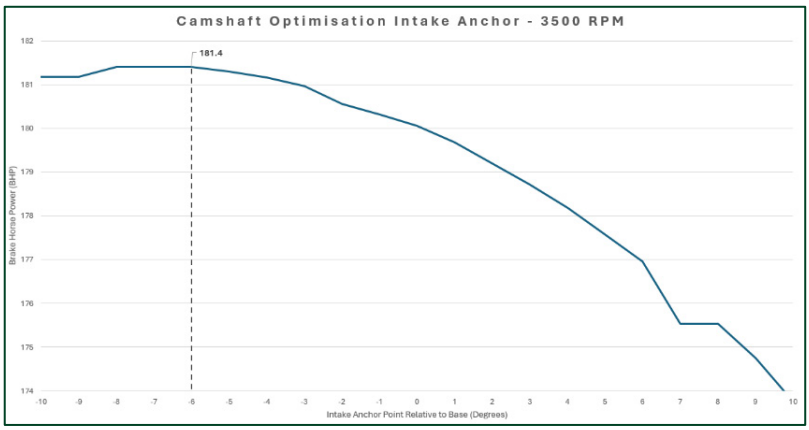

Figure 38 - Line Graph Showing Intake Anchor Optimisation at 3500 RPM

The 3500 RPM sweep for intake anchor reveals a definitive performance peak when the timing is advanced by 6 degrees from the baseline. As previously mentioned, this change synergises with the shorter intake runner length by effectively trapping the incoming, high-pressure acoustic waves generated by the 'ram effect', maximising the dynamic compression ratio.

Conversely, the exhaust anchor point 3500 RPM sweep demonstrates a peak at a retardation point of +7 degrees. As this adjustment fundamentally alters the valve overlap period, retarding the EVC event allows the engine to exploit the momentum of exiting exhaust gasses to create a stronger scavenging effect (Jan Siczek, 2016). This means that the engine is assisted by pulling a fresh, pressurised intake charge into the cylinder more effectively.

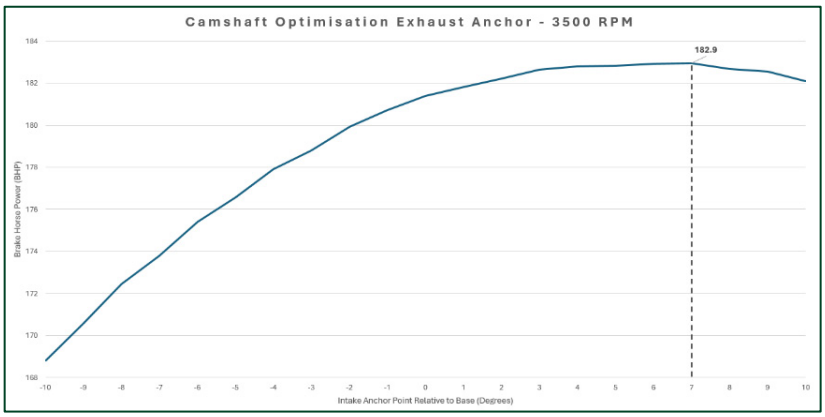

Figure 39 - Line Graph Showing Exhaust Anchor Optimisation at 3500 RPM

8.3.2 Intake Duration and Lift

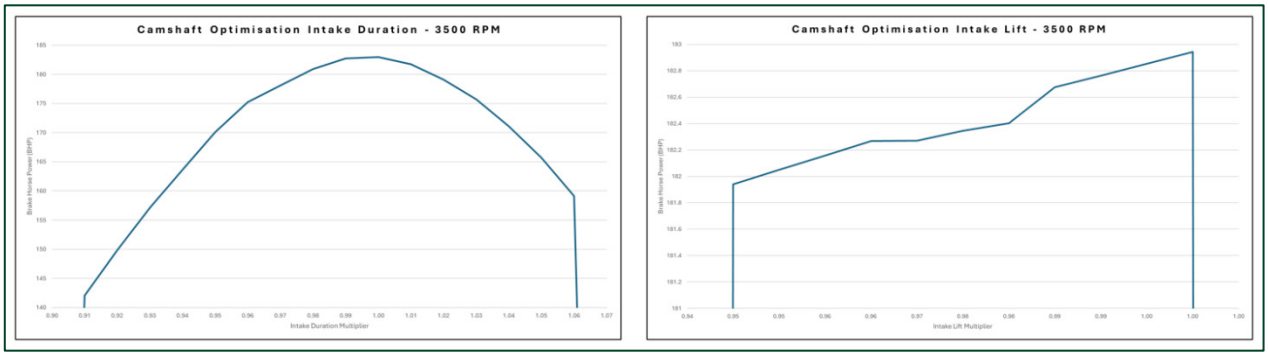

Figure 40 - Line Graphs for Intake Duration and Lift Profiles at 3500 RPM

Interestingly, the 3500 RPM sweep analysing intake duration reveals that the original lobe profile is already at the optimal point with performance subsiding when applying a positive or negative multiplier. This means that the breathing characteristics of the intake lobe is already ideal for the engine and any change to the gas exchange process results in a brake power reduction.

Similarly, the intake valve lift optimisation curve confirms that the baseline multiplier of 1.00 remains ideal. This indicates that the baseline intake lift value (approximately 8.6mm) already provides sufficient time for the incoming pressurised air into the cylinder; meaning that any flow restriction is lying elsewhere within the system.

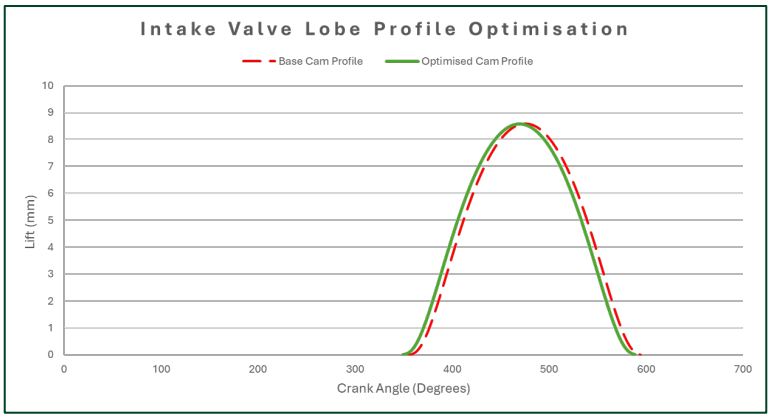

To illustrate the mechanical timing adjustment, this graph plots the baseline intake lobe profile against the newly optimised profile. It shows the subtle -6 degree timing advancement meaning that the IVO event has shifted earlier in the crank cycle whilst maintaining original maximum lift.

Figure 41 - Line Graph Comparing Intake Cam Lobe Changes

8.3.3 Exhaust Duration and Lift

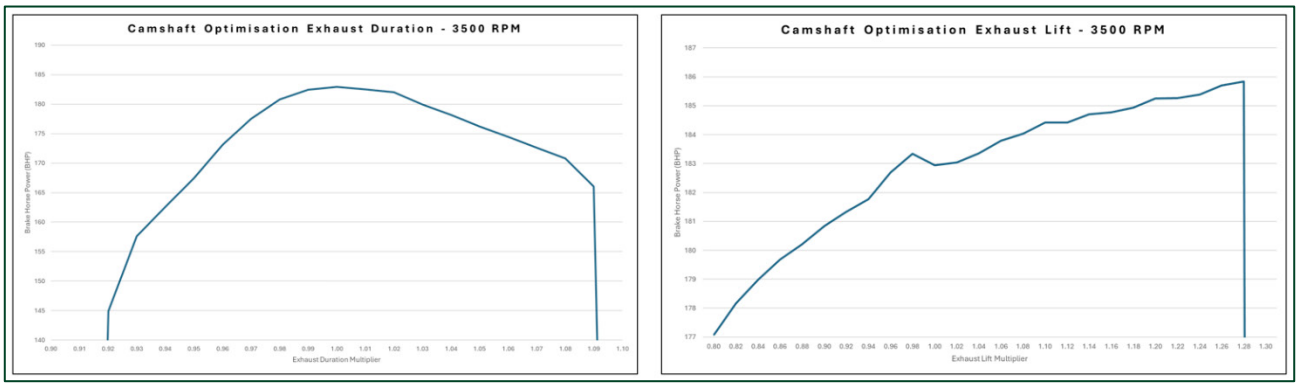

Figure 42 - Line Graphs for Exhaust Duration and Lift Profiles at 3500 RPM

Even though the shape of the curve is different to intake, the exhaust duration sweep reveals the same results. Once again, the original base multiplier of 1.00 remains as the optimal profile to suit the engines breathing characteristics. Any change to this value in a positive or negative direction results in a reduction of brake power.

Unlike the other dimensional parameters, the exhaust valve lift sweep at 3500 RPM reveals an opportunity to increase performance. From the base lift value, a steady and substantial climb in performance as the exhaust lift increases can be observed – finally plateauing at a 1.28 multiplier.

The adjacent graph visualises the final optimised exhaust cam lobe profile. It demonstrates an aggressive design change with amplification of the peak lift increasing to 28% to 9.6mm and the profile shifting 7 degrees forwards to optimise valve overlap.

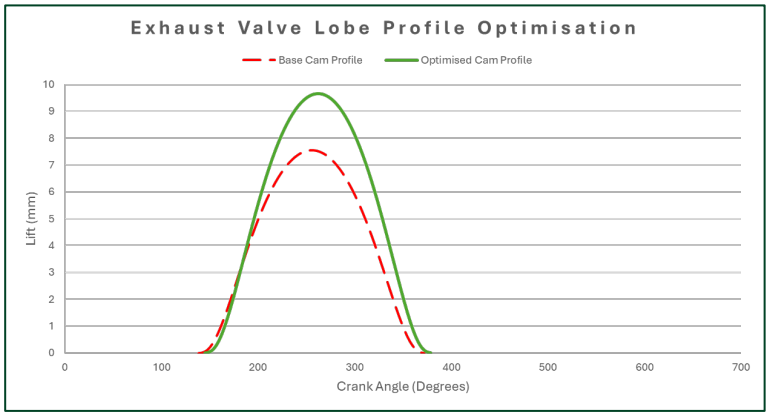

Figure 43 - Line Graph Comparing Exhaust Cam Lobe Profile Changes

8.3.4 Brake Power Result

To assess the cumulative effect of optimising the intake and the camshaft, a full RPM sweep must be executed.

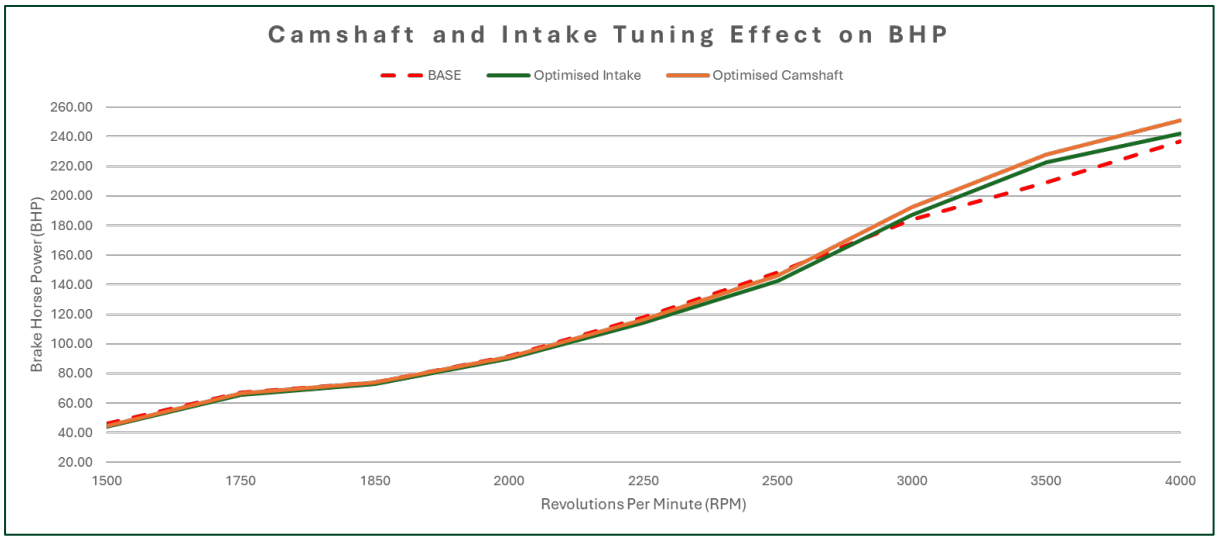

Figure 44 - Line Graph Analysing Optimised Intake and Camshaft vs Baseline

The above BHP sweep demonstrates the compounding benefits of the pair of optimisations. While both upgrades clearly break away from the baseline beyond 3000 RPM, the combined setup goes further resulting in a peak brake power increase of approximately 6.8%. This is done through syncing the improved gas flow capacity provided by the intake along with an improved scavenging effect created by the new exhaust lobe. The absolute increase of 16 BHP validates the harmonic relationship between the intake tuning and valve events.

8.3.5 Torque Result

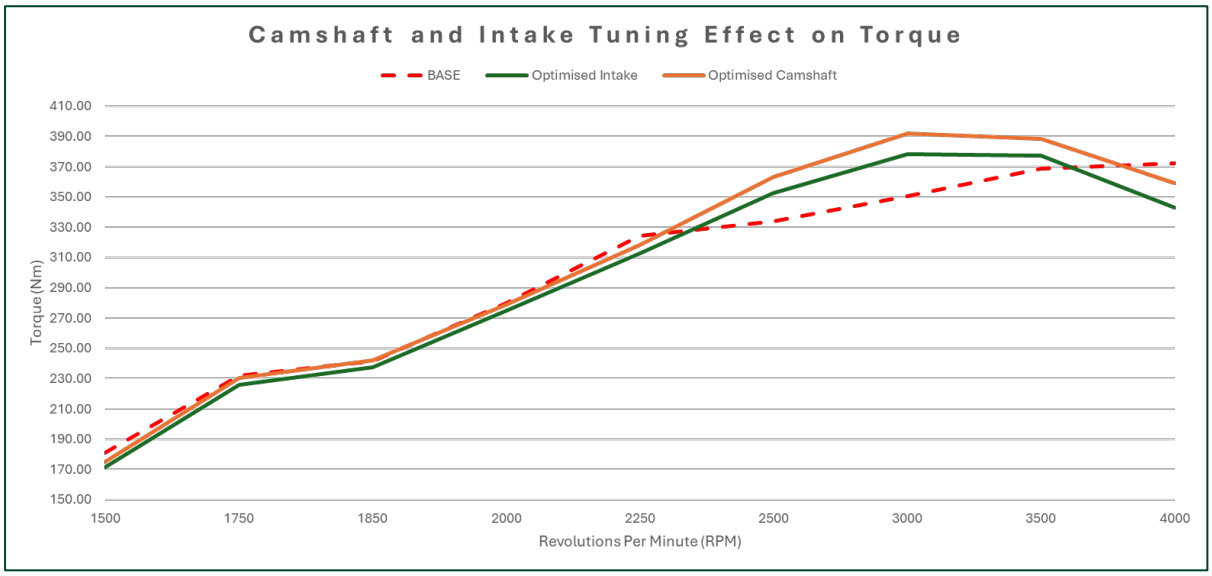

Figure 45 - Line Graph Comparing the Impact on Torque from Optimised Intake and Camshaft

The above torque graph showcases significant vehicle drivability and performance improvements. With the new intake shifting the peak torque to a more favourable RPM range, introducing the optimal camshaft further amplifies this new peak. At 3000 RPM, torque is now increased by 42Nm representing an approximate 16% increase when compared with the baseline model. This substantial increase in mid-range tractive effort effectively transforms the engines dynamic profile, ensuring favourable acceleration capability when the driver upshifts.

8.3.6 Brake Specific Fuel Consumption

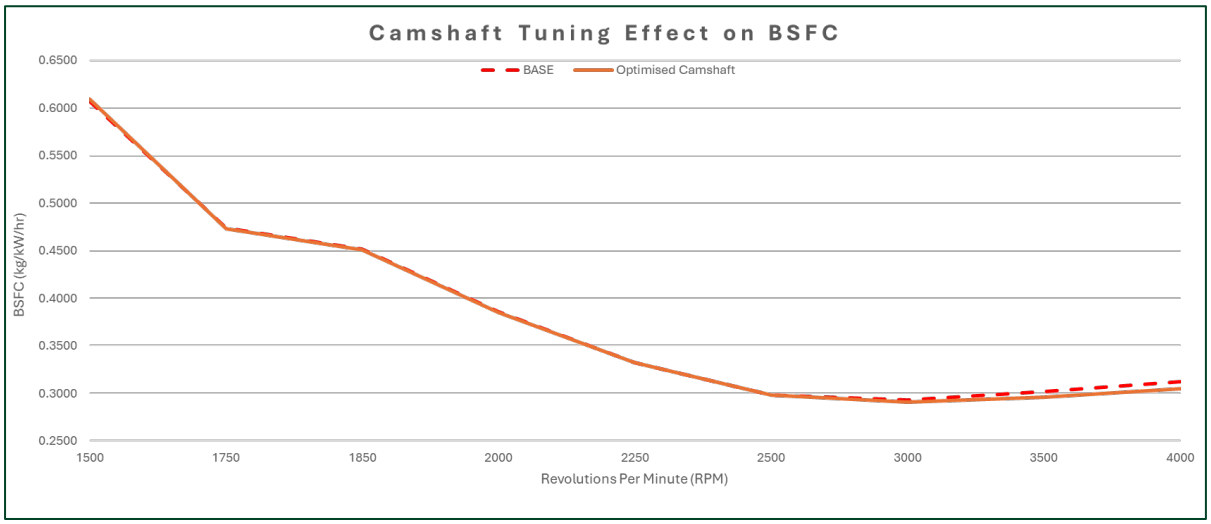

Figure 46 - Line Graph Showing Effect of Camshaft Optimisation on BSFC

To further validate the effectiveness of the improvements, the optimisation study confirms that, from 2500 RPM onwards, the optimised engine runs more efficiently. This is evidence that the two modifications have successfully reduced pumping losses and improved volumetric cylinder filling – meaning the engine can extract more useful mechanical work from the same amount of air/fuel mixture.

8.4 Engine Porting

"Smoother flow for stronger performance"

8.4.1 Simulation Method

Simulating the effects of intake porting and polishing within a 1D CFD environment presents a unique set of challenges. While 3D simulation methods can accurately model flow separation and specific changes in turbulence, a 1D code relies upon empirical coefficients and combined parameter model changes.

The primary challenge lies in the fact that engine porting garners multi-dimensional results involving minor geometry, surface finish, and thermal characteristic changes (Aaron, 2026). For example, in Ricardo WAVE, reducing the wall friction is mathematically distinct from improving the discharge coefficient or altering heat transfer. Therefore, the first step to achieve reliable simulation results is to find the most representative variables, within the available options WAVE has to offer, to capture the synergised benefits realised from porting a physical engine.

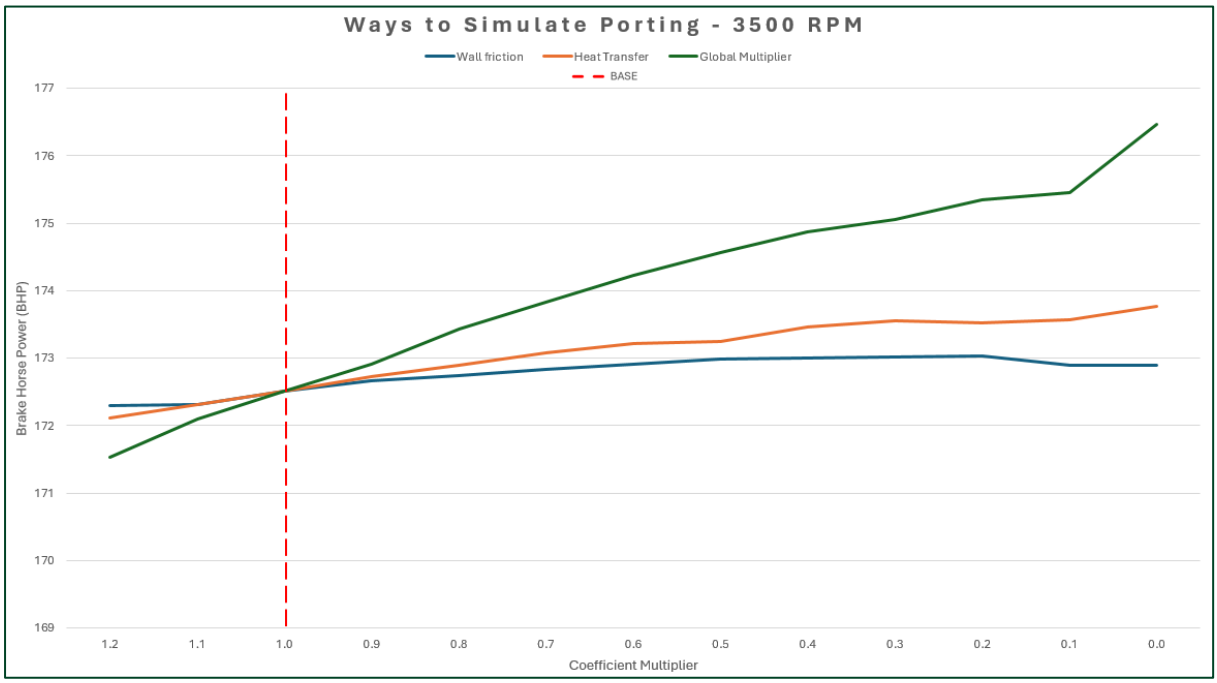

Figure 47 - Line Graph Comparing Different Methods of Simulating Engine Porting at 3500 RPM

The 3500 RPM simulated performance sweep (figure 47) demonstrates the clear limitations of isolated variable adjustment. When only the wall friction coefficient is adjusted, the simulation shows a rapid plateau effect. This means that surface finish alone is not the dominant restrictive bottleneck, with only a negligible gain in brake power. Conversely, when heat transfer is adjusted, a more consistent upward trend can be observed. By reducing this variable, the simulation maintains a higher air density meaning that a higher fuel/air mass is available for combustion – yielding a steady brake power gain. Finally, by combining the effects in the form of a global multiplier, all variables effected by engine porting are adjusted in tandem. This results in an ideal, accurate simulation where wall friction reduction compliments the improved thermal efficiency.

The secondary task is to now determine which WAVE multiplier value correlates with the expected gains from a professional engine porting job. According to Aaron (2026), a "high quality," job yields a brake power increase of 2-5% with most of the gain higher in the RPM range. Therefore, at the tested sweep point of 3500 RPM, a realistic gain is approximately 1-1.5% - aligning well with the global multiplier being set to 0.4 (a 1.4% gain from the baseline).

It is also crucial to note that while WAVE simulation allows the global multiplier to reach a value of 0.0, this is a mathematical abstraction and would be physically impossible. Indeed, diminishing returns begin to be observed when adjusting the multiplier below 0.4 as any smoother surface finish provides no measurable increase in mass flow. Rather the airflow becomes entirely governed by the port's cross-sectional area and the valves' dynamic profile – summarised in the below table:

Engine Porting Multiplier Summary Table		
Coefficient	Physical Equivilant	Power Gain Expected
1.0	Sand Cast Baseline Engine with significant peaks and valleys within the duct walls	N/A
0.6 to 0.8	A de-burred, cleaned finish smoothing all major bumps	0.5 - 1%
0.4	Full professional porting job with all port surfaces smoothed out	2-5%
0.2 to 0.3	Acheivable only from material changes such as specialised ceramic or teflon internals	5% +
0.0	Physically impossible to achieve	N/A

Table 2 - Engine Multiplier Summary Table

8.4.2 Brake Power Result

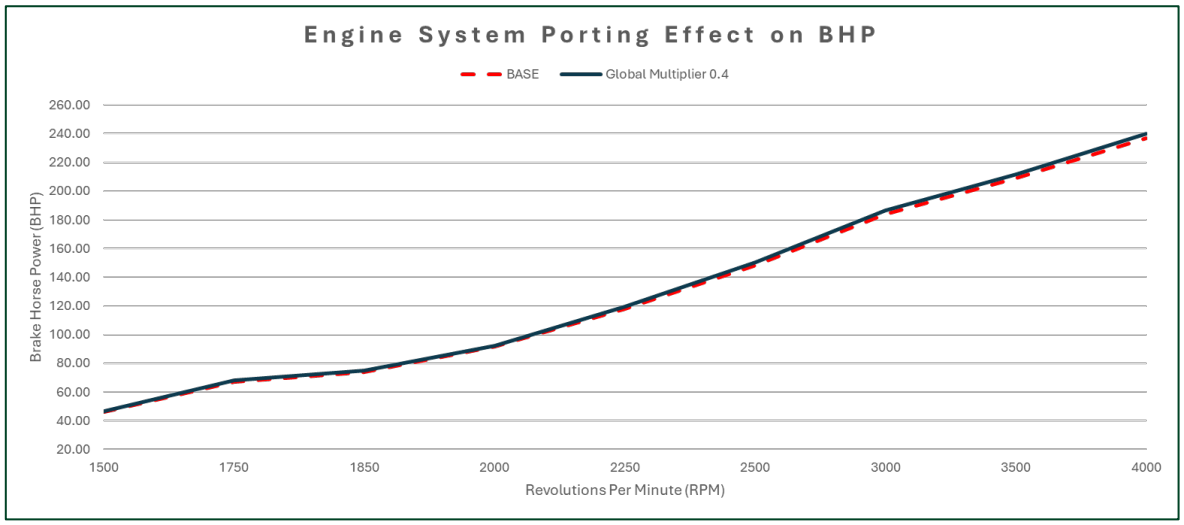

Figure 48 - Line Graph Showing Engine Porting Effect on BHP

The comparative analysis between the base engine model and the 0.4 global multiplier, simulating the combined synergy of reduced wall friction and heat transfer, indicates a consistent and incremental improvement in brake power output. As RPM increases, the gap from the baseline model widens, with a peak gain of 6 BHP at the maximum difference. The average gain throughout the range is approximately 2.5% making the change highly realistic when compared with the expected increase.

8.4.3 Torque Result

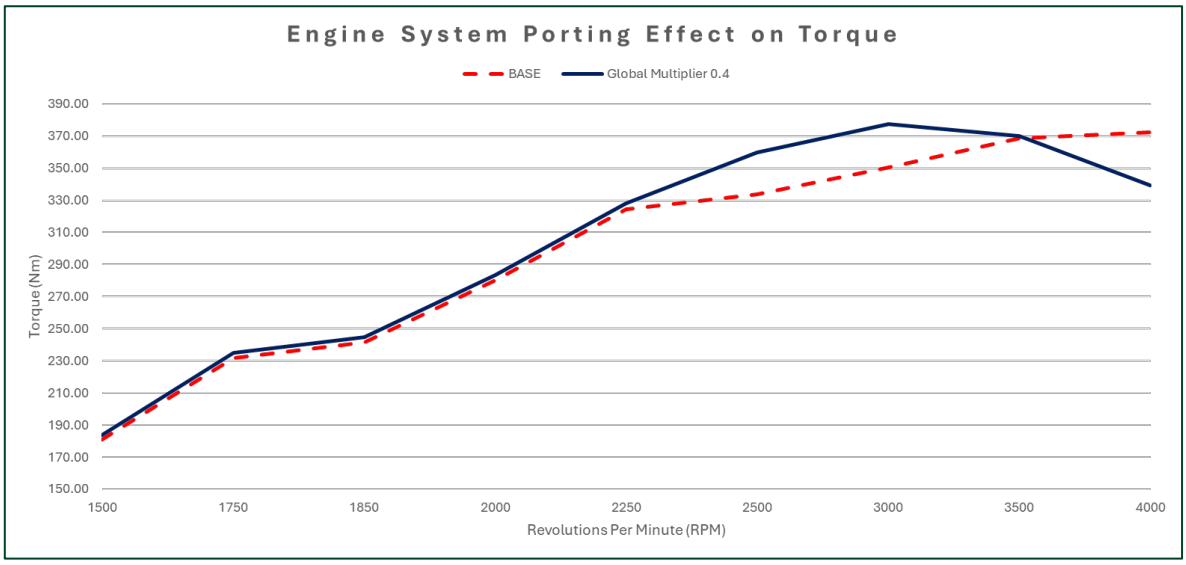

Figure 49 - Line Graph Analysing Torque Increase from Engine Porting vs Base Model

The full RPM range sweep shows a characteristic shift in the torque curve. The combined reduction of wall friction and heat transfer has shifted the resonant frequency of the intake air – yielding a peak performance increase of approximately 11% at 3000 RPM. Even though the change has resulted in a crossover point at 3400 RPM, as discussed within section 4.3, centring the torque peak within the 3000 – 3500 RPM range maximises the tractive effort within the key acceleration phase of the vehicle.

8.5 Increasing Compression Ratio

"Efficiency rises where risk is carefully managed"

Returning to the baseline engine model, an independent range of compression ratios will be tested to analyse the thermodynamic effects and resultant performance gains.

8.5.1 Single RPM Sweep

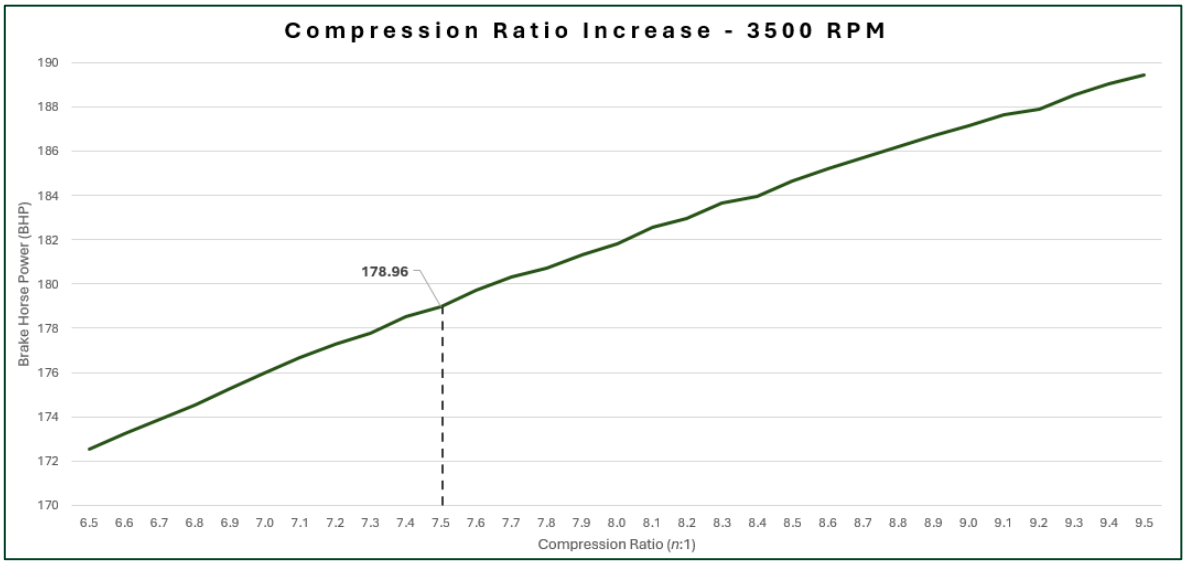

Figure 50 - Line Graph to Analyse the Impact of Increasing Compression Ratio on BHP at 3500 RPM

The above graph plots how compression ratio effects brake power output at 3500 RPM, ascending incrementally from the base 6.5:1 up to 9.5:1. The sweep confirms the fundamental principle of the Otto four-stroke cycle, as discussed in section 4.3, that the relationship between static compression (expansion ratio) and power output is positive and linear. At the extreme 9.5:1 ratio brake power increases by 9.2%.

However, as also discussed in section 4.3, Sir Riccardo (1931) explains that practical historic and mechanical constraints necessitate a strict upper value. This is because combining a high expansion ratio with forced induction exponentially increases the risk of destructive engine auto-ignition. Anticipating the use of modern higher-octane fuels than in era, the final configuration selected is 7.5:1 as the maximum safe operating ceiling to prevent catastrophic mechanical failure.

8.5.2 Brake Power Result

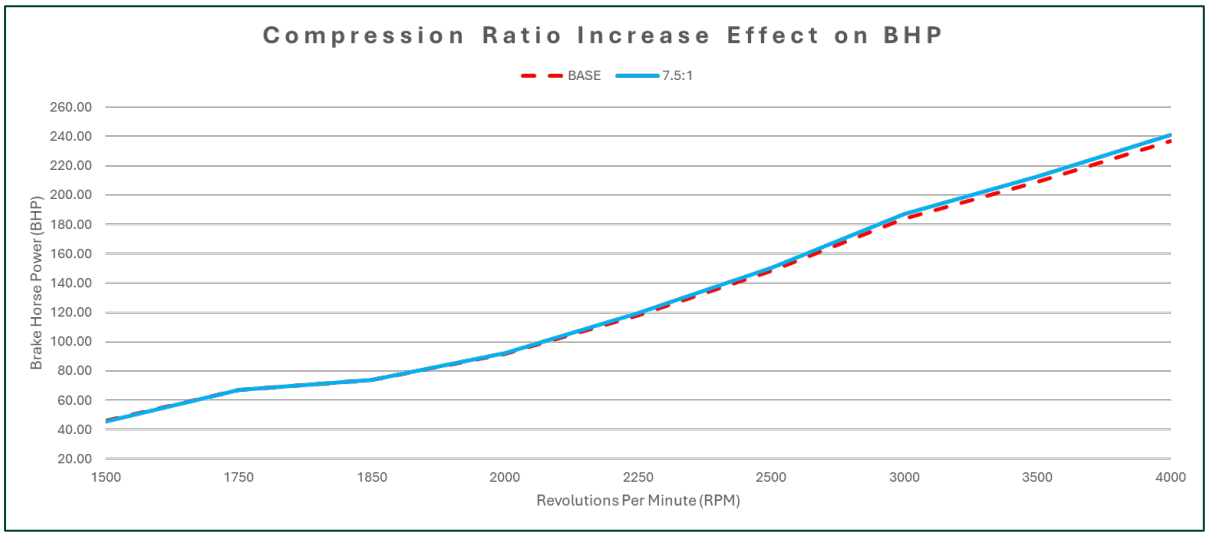

Figure 51 - Line Graph Showing Effect of Increasing Compression Ratio to 7.5:1 Against Brake Power

The full transient sweep analysis demonstrates that the new 7:5:1 compression ratio consistently slightly outperforms the baseline model from 1900 RPM onwards. As engine speed climbs, the gap widens culminating in a peak power of 241 BHP – a modest 2.1% gain. This gain is a direct result of extracting more mechanical work from the same inducted air/fuel charge.

8.5.3 Torque Result

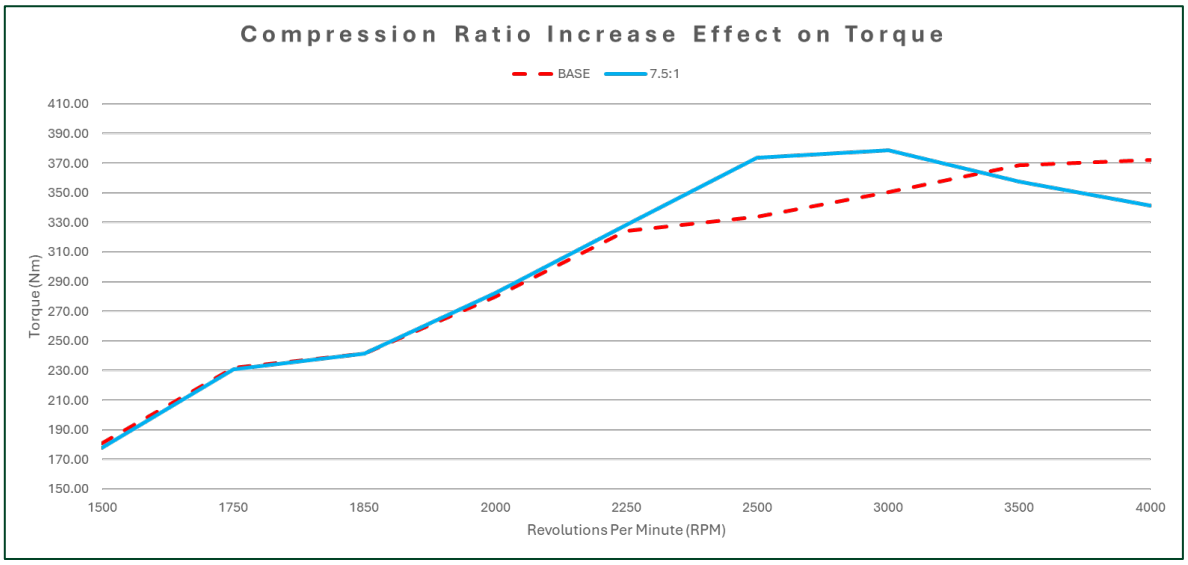

Figure 52 - Line Graph Showing Effect on Changing Compression Ratio to7.5:1 on Torque vs Baseline

Conversely, the full RPM torque sweep exhibits a more dramatic and highly advantageous change. While the baseline engine model climbs relatively linearly up to 4000 RPM, the new 7.5:1 ratio inflates mid-range torque to create a new plateau effect peaking at 3000 RPM at a level 8.3% higher than before. Beyond 3250 RPM, the new torque curve drops below the baseline. According to Zheng *et al*. (2010), this may be attributed to the fact that an increase in compression ratio can negatively impact trapped mass of the air-fuel mixture due to a physical reduction of the clearance volume at peak flow rates. However, for real-world drivability, the sizable gain in mid-range tractive effort is a highly favourable outcome.

8.5.4 Brake Specific Fuel Consumption

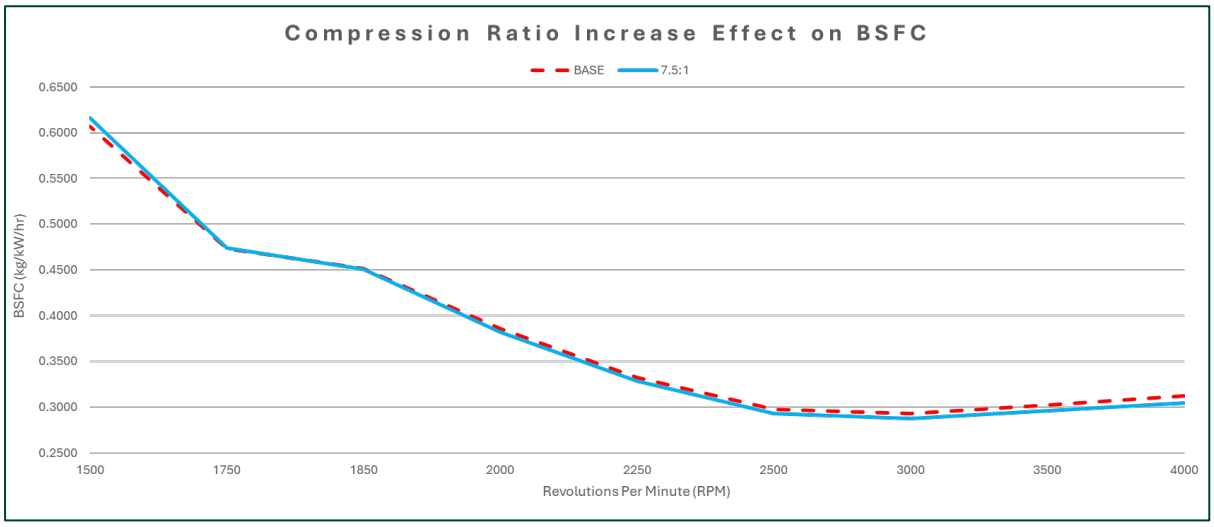

Figure 53 - Line Graph Analysing Effect of BSFC on Compression Ratio Increase vs Baseline

Validating the theoretical benefits of the Otto cycle efficiency, the above BSFC graph illustrates that the new 7.5:1 configuration is measurably more efficient from 1750 RPM onwards as compared to the baseline model. This means that the engine is not only burning more fuel to increase performance; it is converting the available fuel into mechanical energy more efficiently.

8.6 Pareto Optimal Engine

"The synthesis of optimisation"

The culmination of the results section for the parametric study is to synthesise all individually optimised parameters into a singular Pareto optimal engine model. This final configuration represents the maximum achievable performance within the Riccardo WAVE environment. All whilst maintaining important factors such as historical integrity, engine drivability, and thermodynamic efficiency.

Modifications implemented to this final model include:

Bore Increase	A 5% bore increase resulting in a new engine capacity of 4.849L – up 450 cc from previous
Intake Geometry	Reducing the main runner length by 66mm and increasing its diameter to 135mm
Camshaft Tuning	Intake advanced by -6 degrees, exhaust retarded by +7 degrees, and exhaust lift multiplied by a factor of 1.28
Engine Porting	A 0.4 global multiplier to simulate the synergised effects of internal surface smoothing
Compression Ratio	Increased from the historical 6.5:1 to a new safe maximum of 7.5:1

Table 3 - Summary of Pareto Optimal Modifications

Further, a final constants table of the Pareto optimal engine model is incorporated into appendix section E along with a full schematic of the final WAVE Canvas provided in appendix section F.

8.6.1 Final Brake Power Result

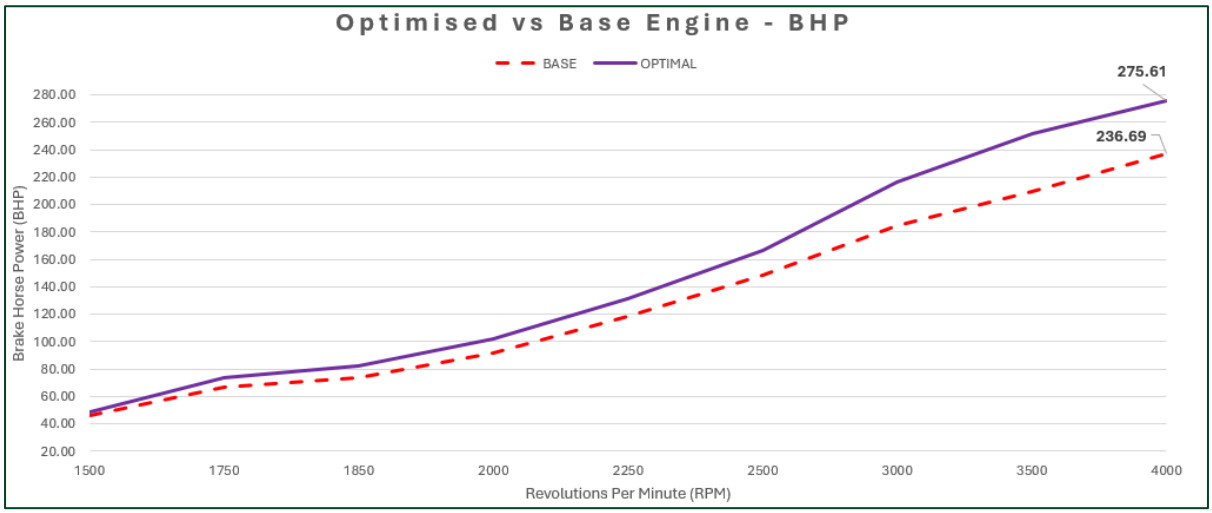

Figure 54 - Line Graph Showing Pareto Optimal BHP Increase vs Baseline Model

A final full RPM range sweep has been conducted to capture the compounding effects of the performance upgrades. The resultant above graph visually demonstrates a significant divergence between the baseline and Pareto optimal engine configuration. The synergy of increased displacement, optimised camshaft, and much less restrictive breathing yields a new peak of 275.61 BHP at 4000 RPM – up 16.8% from the validated base model.

8.6.2 Final Torque Result

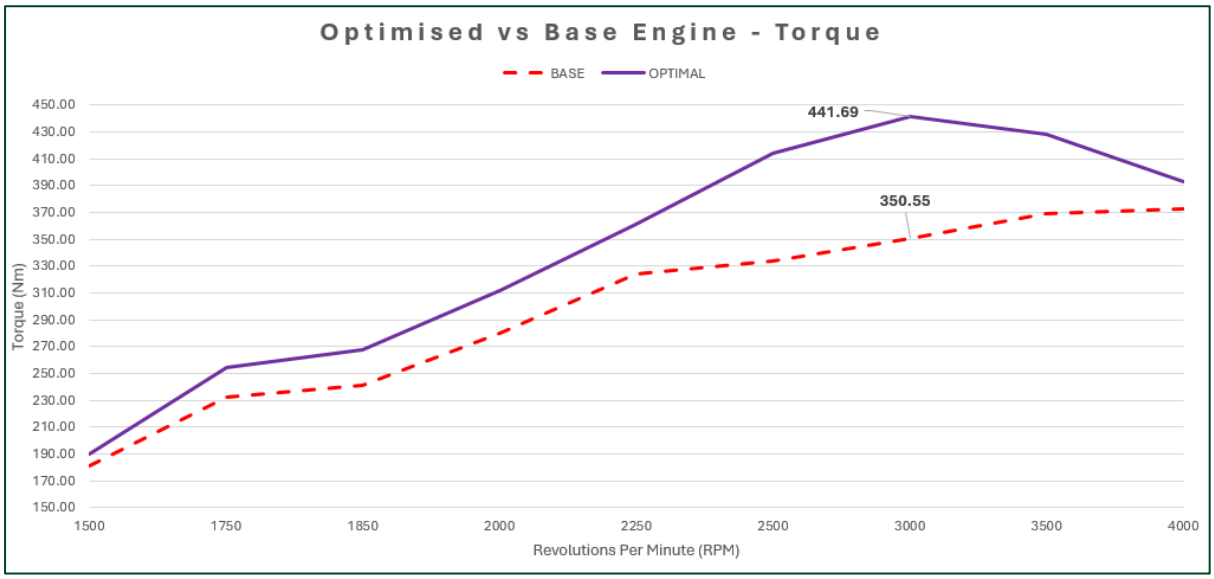

Figure 55 - Line Graph Analysing Pareto Optimal Torque vs Baseline Model

The above graph visually illustrates the significant engineering achievements garnered through a transformation of torque delivery. The final torque sweep reveals a significantly inflated mid-range surge – with a new peak of 441.7Nm occurring at 3000 RPM. This represents a seismic gain of 26.2% in mid-range tractive effort. Furthermore, the peak torque threshold remains elevated critically shifting the new peak to lower in the engines operating range (3000 - 3500 RPM). This means that the new engines' torque output is suitably matched to the Bentley Blowers' gearing, providing maximum tractive effort precisely where the vehicle drops in engine speed after an upshift (refer to appendix section C).

8.6.3 Final Brake Specific Fuel Consumption Result

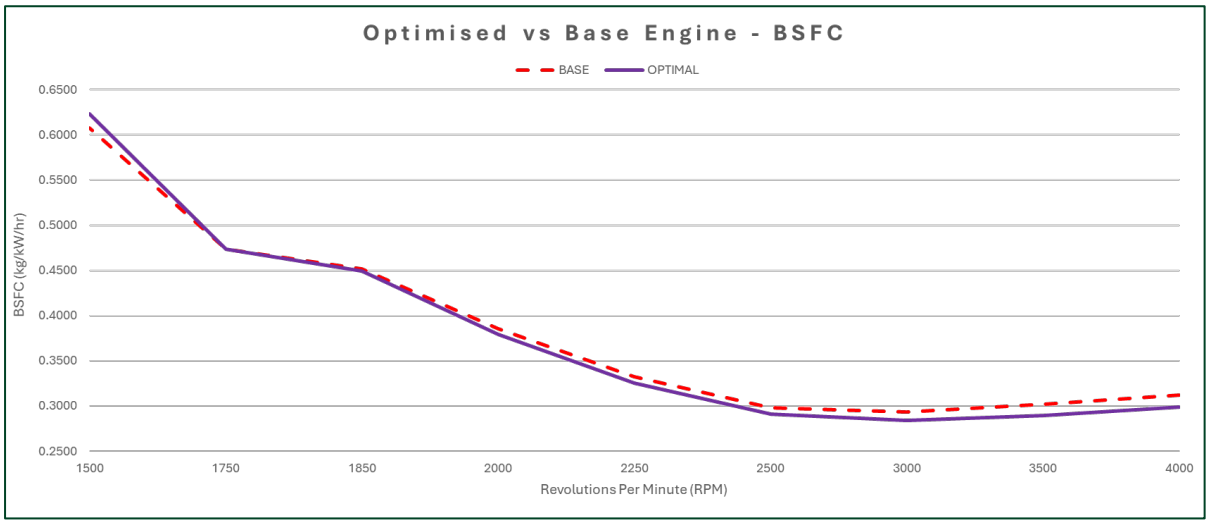

Figure 56 - Line Graph Analysing Pareto Optimal BSFC vs Baseline Model

Finally, the above BSFC graph provides conclusive validation to the engine upgrades. Despite generating 16.8% more brake power and 26.2% more mid-range torque, the Pareto optimal engine operates with superior thermodynamic efficiency across almost all the engines operational range. The optimised engine sits firmly below the baseline curve beyond 1750 RPM, with the gap increasing even further throughout. This indicates that it requires less fuel/air mass per unit of energy produced. This final analysis definitively confirms that the achieved performance gains are a result of superior fluid dynamics, improved volumetric efficiency, and an optimised expansion ratio – rather than only just enriching the fuel mixture.

8.6.4 Weighted Analysis of Modifications

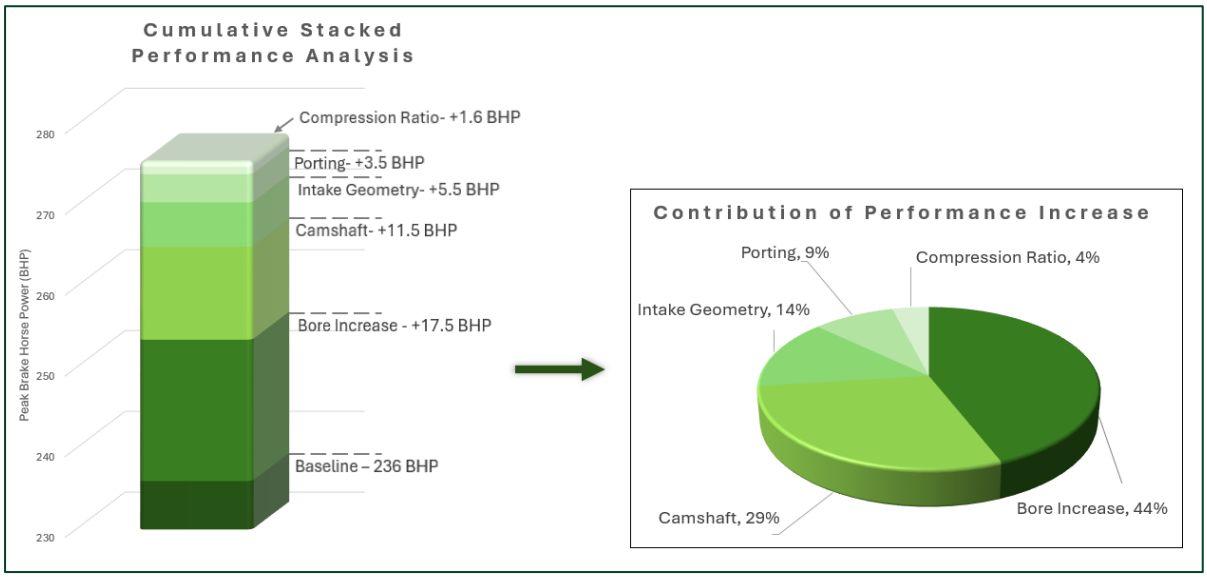

Figure 57 - Weighted Analysis of Modifications Stacked Bar Chart and Pie Chart

The above charts objectively evaluate the anticipated return on investment for each modification by breaking down the total performance gains into weighted percentages. The data shown provides empirical evidence that primarily physical expansion of the engine and refinement of flow (through optimising camshaft kinematics, intake geometry and porting) are overwhelmingly dominant factors of the overall Pareto optimal configuration. A 5% bore increase yields the greatest contribution with a 44% share of peak break power gains; closely followed by camshaft optimisation which represents 29%. It is crucial to note that the, already outlined as risky, increase in static compression ratio yields the lowest return contributing only 4% to total brake power gain.

This empirical weighting therefore firmly supports the projects earlier theoretical assumption that when optimising historic, particularly forced-induction, powertrains, pushing static compression ratio presents a disproportionate high-risk for a relative low reward. As such the safer volumetric and kinematic modifications to the bore and gas exchange system should indeed dictate the primary tuning strategy.

9.0 Discussions

"Interpreting the effectiveness of the mechanical changes"

Systematic optimisation of the Bentley Blower engine through the crucible of 1D CFD has yielded substantial performance gains – quantified with a 16.8% increase in brake power and a 26.2% increase in mid-range torque. It is now important to understand why the specific mechanical changes were effective; how they interact with the historical nature of the constraints, and what is revealed about the advantages of digital tuning methods.

9.1 Primary Intake Runner Length Optimisation

"Uncovering the hidden benefits garnered from quarter-wave resonance tuning"

Among the most revealing aspects of this study was optimisation of the primary intake runner length. Utilising the quarter-wave resonance theory, preliminary mathematical calculations predicted that a 79mm length reduction would optimally time the arrival of high-pressure waves with the IVC event at 3500 RPM. The high-resolution Riccardo WAVE sweep confirmed that the theory was leading the study down the right path, finally identifying the absolute optimum for the engine system was a 66mm reduction.

The 13mm discrepancy here demonstrates a fundamental limitation of isolated mechanical formulae and critically highlights the distinct advantage of 1D CFD. As explained by Smith and Morrison (1971), the standard quarter-wave formula assumes idealised and frictionless flow within a vacuum. This differs significantly to reality where the Bentely Blower intake system is subjected to complex boundary layer friction, thermal density shifts, and localised pressure disruptions throughout the system as it makes its way to the engine block. Ricardo WAVE can compute Navier-Stokes equations, taking account for all these variables simultaneously. This allows the simulation to accurately model the precise characteristics of the pressure wave, leading to the conclusion that the duct needs to be slightly longer than theoretically calculated to achieve optimal Helmholtz resonance in this case.

9.2 Camshaft Optimisation

"Adjusting camshaft kinematics to unlock historic bottlenecks"

The camshaft optimisation section of this project provided fascinating insights into the original historic engineering of the 1920s Bentley Blower. The parametric study revealed that the existing intake and exhaust valve durations, as well as intake lift, were already operating at an optimal level. As such any dimensional or mechanical change to alter these variables resulted in adverse power gains. This confirms that the original camshaft architecture, in some respects, already maximised the engines breathing performance.

However, where a sizable bottleneck was exposed was the exhaust valve lift – requiring a multiplier of 1.28 to achieve Pareto optimality. It is likely that in the 1920s, engineers were restricted to select high valve lift profiles due to primitive valve and spring technology which could lead to valve-float causing potentially catastrophic failure (Irving and Clymer, 2015). Today's modern CNC-machined billet camshafts and high-tensile alloy valve springs can accommodate the new, more aggressive lift profile (Joe, 2025). By increasing exhaust lift, the optimised engine can expel the combusted gasses with greater efficiency. Applying this change, along with timing adjustment, contributed an increase of 16% of mid-range torque and a 6.8% increase in brake power – rendering it as a non-destructive, fully reversable change with high impact.

9.3 Increased Compression Ratio

"Limitations of increasing static compression in forced induction"

Even though modern, naturally aspirated engines routinely use static compression ratios exceeding 12:1, the Bentley Blower simulation required a cap of 7.5:1 – despite Ricardo WAVE analysis predicting linear power gains up to 9.5:1. The contrast between what is possible in theory and the physical reality of this historical context forces the question, 'is pursuit of higher compression worth the risk?'

Ultimately, the answer is no; the Amherst Villiers Roots-Type supercharger is a positive-displacement pump with poor adiabatic efficiency, meaning it generates significant heat while compressing the intake charge (Sir Riccardo, 1931). The risk of auto-ignition becomes increasingly severe when this heated, pressurised charge is then forced into the fixed-head monobloc engine. Even with the assumption of modern, higher-octane fuels explained by Heywood (2018), the cylinder pressures at increased static compression ratios would likely exceed the structural limits of what is an irreplaceable, 1920s casting.

With the 7.5:1 cap placed upon static compression, a modest 1.7% gain in peak brake power provides further to the cumulating evidence that tuning historic, forced-induction powertrains should be approached with extreme caution. Also, it must be noted that the broader parametric study proves non-destructive, mechanical modifications, such as camshaft kinematics and pressure wave manifold tuning, yield vastly superior performance gains. As such, these safer alternatives should take priority in the tuning hierarchy.

9.4 Shift in Torque Delivery

"Realising improved vehicle dynamics and the 'Sawtooth' advantage"

An outcome of high importance from this project is a deliberate shift in the optimised engine's torque delivery. While the final Pareto optimal engine gained 16.8% in peak brake power, a significant and transformative result is the 26.2% increase in mid-range torque delivery. Rather than chasing peak RPM performance, the project outcome demonstrates a successfully optimised engine for real-world driveability and track performance.

Verified by the tractive effort Sawtooth Analysis (available in appendix section C), an upshift at the 3500 RPM target drops engine speed to approximately 2500 RPM – well within the torque surge stage of the engine. This was primarily achieved through the utilisation of intake geometry changes which forcefully shift the engines peak volumetric efficiency to lower within the RPM range; thus ensuring that the modified engine drops directly into an inflated torque band immediately after a gear change (Gillespie, 1992). As a result, the Bentley driver has idealised longitudinal force available at the tyre contact patch precisely at the point it is needed, drastically improving acceleration performance out of corners such as Tetre Rouge at Le Mans Circuit de la Sarthe.

9.5 Virtual Prototyping Advantage

"Validating the value virtual prototyping provides to heritage preservation"

An ultimate outcome of this project is successful validation of the engineering methodology of applying modern, industry standard techniques within a historical context – a sentiment advocated by the FIA (2023). Achieving the performance gains garnered within this project using traditional 1920s methods would have required machining several experimental camshafts, casting multiple custom intake ducts, and generally causing irreversible changes – with catastrophic engine failure being risked at every dyno run (NASA, 2005; Wang, 2002).

Hundreds of high-risk physical permutations were evaluated safely, cost effectively, and with zero waste by performing the process entirely within the Ricardo WAVE 1D CFD environment. A fitting final point of discussion then is that this project bridges successfully the gap between historic vehicle engineering and modern, sustainable development practices. This algins with the UN's SDG 9 and 12 (UN, 2015), definitively proving that the performance limits of these artifacts of history can be pushed without putting the physical artifact at risk.

10.0 Conclusion

"The past refined through the tools of the present"

10.1 Project Summary

This project aimed to answer if a 1D CFD systematic optimisation methodology could be employed to quantify and extract performance gains from the vintage, mechanically supercharged Bentley Blower engine. Through the comprehensive literature review, technical specification sheet, methodical development of a Ricardo WAVE digital-twin, validation, systematic optimisation, and detailed description of the Pareto optimal approach, all six project objectives were successfully met.

The final Pareto optimal configuration, which incorporated a change to the primary intake duct geometry, optimised camshaft kinematics, increased cylinder bore, porting, and a conservative compression ratio increase, combined to achieve a profound result. This is quantified by a 16.8% increase in peak brake power (275.61 BHP at 4000 RPM) and a transformative 26.2% increase in the all-important mid-range torque (441.69 Nm at 3000 RPM) compared to the validated baseline model.

10.2 Study Implications

Implications garnered from this study have the potential to be highly significant for the £7.3 billon historic motorsport sector (Federation of British Historic Vehicle Clubs, 2025). Shifting peak volumetric efficiency to a lower RPM improves tractive effort without subjecting vintage components to excessive rotational speeds. Crucially, the maintained, and indeed slightly improved, BSFC curve confirms that these gains are not simply fuel enrichment but a result of increased thermodynamic efficiency. It can therefore be concluded that virtual prototyping, in the form of Ricardo WAVE 1D CFD simulation, is validated as a valuable, non-destructive tool for historic motorsport engineering – allowing engineers to seek additional performance while safeguarding the irreplaceable, culturally significant artefacts of history.

10.3 Future Research Directions

While at a system-level the 1D CFD methodology remains highly robust for evaluating gas dynamics, it does inherently rely on spatial averaging and empirical sub-models (Realis, 2025). This means the primary limitation of this study is the approximation of highly turbulent, complex 3D in-cylinder flows (tumble and swirl) as well as the generalisation of the Bentley's cast-iron monobloc thermal properties. Future research is therefore recommended to build upon this foundation by translating the Pareto optimal manifold and combustion chamber geometries into a 3D analysis environment. This will facilitate analysis of high-resolution flow characteristics to further validate the changes. Further, physical manufacture of the new camshaft geometry to validate its kinematic stability on a test flow bench would bridge the final gap between digital optimisation and real-world application.

10.4 Closing Statement

Ultimately, this project has gone to prove the powerful synergy between 1920s historic engineering and modern 21st century computational fluid dynamics. The application of digital engineering to one of the most significant British engines in history, ensures that the legendary Bentley Blower continues to dominate the world of historic racing series, such as Le Mans Classic and Donnington Historic, for years to come.

11.0 Limitations

"Understanding where a model fails is just as important as where it succeeds."

The implementation of 1D CFD via Riccardo WAVE has proven to be a highly effective tool for conducting efficient, system-level parametric optimisation. However, inherent engineering and computational limitations possessed by this methodology must be acknowledged:

- **Computational Limitations of 1D vs 3D**

The fundamental limitation possessed by 1D CFD is its inability to capture and resolve complex, three-dimensional spatial phenomena. As discussed in section 4.5.1, Ricardo WAVE relies on spatial averaging and empirical sub-models, such as the Weibe function, to simulate the combustion process (Schoegl *et al.,* 2010). Consequently, this means the simulation cannot accurately predict localised fluid behaviours. This includes the specifics of flame-front propagation, formation of localised thermal hotspots, and the intricacies of tumble and swirl mechanics which occur within the Bentley's pent-roof combustion chamber (Martins *et al.*, 2018).

Further, the computational model used within this project utilises a simplified Woschini correlation heat-transfer sub-model. This means that highly complex thermal properties of the Bentley's cast-iron monobloc architecture is difficult to map definitively (Heywood, 2018).

- **Mechanical Stress Factors**

It is crucial to note that this project focuses exclusively on optimising gas exchange and enhancing thermodynamic performance. This means that hypothetically, within the Ricardo WAVE simulation, the engine can flow enough air/fuel mixture to generate 275.61 BHP and 441.69 Nm of torque. However, mechanical integrity of the physical engine hardware is not evaluated by 1D CFD. As researched by Pastewka *et al.* (2025), because finite element analysis (FEA) and tribological wear models, are not incorporated into this study, it cannot be verified that the century-old components, such as the crankshaft, connecting-rods, or bearings, could withstand the increase in peak cylinder pressures without suffering mechanical failure.

- **Data Validity and Manufacturing Tolerances**

Of course, as previously discussed in section 5.1, accuracy of the digital-twin is dictated exclusively by the fidelity of its input data. An opportunity for limitation here is established as a result of the context of 1920s historic engineering. As cited by Bentley Motors (2020), officially in a press release for the Continuation Series of twelve modern Bentley Blower replicas, the company stated that each of the original Blowers are, “unique,” and “one-of-a-kind,” due to the hand-built nature of the vehicles. Piston Heads also noted that there are tangible differences in handing and gearshift feel between models (Duff, 2021). Therefore, the precise geometric dimensions and flow characteristics of the tested engine, used to produce the dyno data profile within this project, almost certainly exhibits marginal differences as compared to other heritage or indeed Continuation model Bentley Blowers. As a result of the historical ambiguity, an inevitable margin of error is introduced into the baseline calibration.

- **Reliance on Historical Texts and Potentially Dated Literature**

Within standard academic research, reliance on sources published decades ago is generally considered as a limitation to accuracy of the literature due to rapid evolution of technology – especially within the automotive engineering industry. While modern literature provides extensive data around electronic fuel injection, variable geometry systems, and ECU calibration, it offers limited relevance in respect to mechanical tuning principles of the 1920s magneto controlled, carburetted, and Root-type supercharged powertrains. As such this projects bibliography incorporates multiple mid-20th-century publications, including texts such as Motor Sport Magazine of 1927, Pomeroy of 1955, Professor Low of 1930, and Sir Ricardo of 1931. This apparent limitation is indeed a methodological necessity to accurately understand the mechanical bottlenecks and period-correct thermodynamic constraints unique to the Bentley Blower. Therefore, even though the computational tools used within this project represents today’s industry standard methodology, the foundational tuning practices and fundamental principles are justifiably derived from period-correct historical engineering literature.

12.0 Recommendations

"Key avenues for future engineering research"

To advance the findings of this study, which will facilitate the transition from a theoretical Pareto optimal configuration to a race-event ready powertrain, several research recommendations are made:

- **Stepping Up to a 3D CFD Co-Simulation**

An immediate next research step to be recommended is to transition from a 1D to a 3D computational fluid dynamics analysis method. Future research could utilise software such as ANSYS Fluent to construct detailed 3D representations of the newly optimised intake and the engine's combustion chamber. By running an efficient co-simulation methodology, the 1D WAVE model provides accurate approximations for boundary conditions and early predictions of transient pressure waves. The 3D solver then goes further to visualise and optimise complex, in-cylinder tumble and swirl characteristics as well as flame front propagation mechanics – metrics that the current study could only approximate.

- **Mechanical Validation through Finite Element Analysis (FEA)**

Before the attempt of physical modification, it is recommended to prove the mechanical viability of the engine. This could be computationally researched through the crucible of a comprehensive FEA study – utilising software such as ANSYS Mechanical or SolidWorks Simulation. By extracting the peak cylinder pressure traces from the optimised WAVE model and applying them as load cases to a digital CAD model of the Bentley's primary rotating assembly and cylinder casing, engineers can calculate the updated stress concentrations and fatigue limits. This nature of future study would act to further safeguard the historically significant engine by providing accurate predictions for component safety and risk factors.

- **Test Flow Bench Physical Validation**

To provide ultimate physical validation of the simulation's accuracy, it should be recommended to prototype specific optimal modifications identified within the study. For example, if a single cylinder's worth of newly optimised camshaft kinematics was to be CNC-machined (including the -6 degree intake advance, -7 degree exhaust retardation, and 1.28× lift multiplier) and tested on a physical gas flow bench, discharge coefficients generated could be compared against values predicated by the WAVE model. As explained by Winklhofer and Hopfner (2012) and advocated by the Southwest Research Institute (SwRI) (Hennessy, 2020), this next step bridges the gap between virtual simulation and physical reality.

- **Full Dynamic Vehicle Simulation**

As one last concluding piece of research study, a Pareto Optimal engine map could be integrated into a full vehicle-level dynamic simulation. Tools such as IPG CarMaker or an Excel-based longitudinal vehicle dynamics model can be used to extrapolate key vehicle performance metrics such as acceleration curves, gearing, and V-max predictions (IPG Automotive, 2025). The importance of this nature of simulation work before manufacture is advocated by Bentley Mulliner in the Official Documentary – Return to Le Mans: Unfinished Business (The JBS Collection, 2025). This would not only fully quantify the sawtooth advantage, as theorised in discussion section 9.4, but also demonstrate how the Pareto optimal engine reduces actual lap time around specific target circuits such as Le Mans Circuit de la Sarthe – therefore providing an ultimate guiding metric of success for the historic motorsports industry.

13.0 References

Aaron (2026). *Cylinder Head Porting Explained: Process, Benefits & Cost*. [Online]. 2025. Woda Auto Parts.
Available from: https://autopartswd.com/cylinder-head-porting-explained. [Accessed: 5 March 2026].

Acosta, G. (2020). *Bentley Is Recreating It's Historic 4-1/2 Litre Blower Engine*. [Online]. 15 September 2020. EngineLabs.
Available from: https://www.enginelabs.com/news/bentley-is-recreating-its-historic-4-1-2-litre-blower-engine/. [Accessed: 20 March 2026].

Apsley, D. (2020). *Computational Fluid Dynamics: the Finite-Volume Method*. [Online]. Manchester: The University of Manchester.
Available from:
https://personalpages.manchester.ac.uk/staff/david.d.apsley/lectures/comphydr/p1.pdf. [Accessed: 11 December 2025].

Baughan, A. (2025). *The Science behind Engine Tuning: Insights from West Sussex Professionals*. [Online]. 2 February 2025. Rpmsussex.com.
Available from: https://www.rpmsussex.com/blog/the-science-behind-engine-tuning--insights-from-west-sussex-professionals. [Accessed: 11 November 2025].

Bentley Motors (2019). *1929 4½ Litre Supercharged Team Car #2 – UU 5872*. [Online]. 2019. Bentleymedia.com.
Available from: https://www.bentleymedia.com/en/heritage-collection/1929-team-blower-uu5872. [Accessed: 12 February 2026].

Bentley Motors (2025). *1930 Demonstrator Blower – GH 6951*. [Online]. 2025. Bentleymedia.com.
Available from: https://www.bentleymedia.com/en/heritage-collection/1930-demonstrator-blower-gh6951. [Accessed: 12 February 2026].

Bentley Motors (2020). *The First New Bentley Blower for 90 Years*. [Online]. 2020. Bentleymedia.com.
Available from: https://www.bentleymedia.com/en/models/blower. [Accessed: 17 April 2026].

Blair, G.P. (1999). *Design and Simulation of four-stroke Engines*. Warrendale, Pa: Society of Automotive Engineers.

Bosch, R. (2011). *Bosch Automotive Handbook*. 8th Ed. Erscheinungsort Nicht Ermittelbar: Robert Bosch.

Brown, A. & Wagstaff, I. (2017). *Bentley 4 1/2 Litre Owners Workshop Manual*. Haynes Publishing.

Cope, L. (2025). *What Is a Pareto-Optimal State in Decision Making?* [Online]. 5 November 2025. Engineer Fix.
Available from: https://engineerfix.com/what-is-a-pareto-optimal-state-in-decision-making/. [Accessed: 14 November 2025].

Dahham, R.Y., Wei, H. & Pan, J. (2022). Improving Thermal Efficiency of Internal Combustion Engines: Recent Progress and Remaining Challenges. *Energies*. [Online]. 15 (17). p. 6222.
Available from: https://www.mdpi.com/1996-1073/15/17/6222. [Accessed: 11 March 2026].

Duff, M. (2021). *Bentley Blower Continuation | PH Review*. [Online]. 21 April 2021. Pistonheads.com.
Available from: https://www.pistonheads.com/news/ph-driven/bentley-blower-continuation--ph-review/44048. [Accessed: 17 April 2026].

Esposito, S., Mally, M., Cai, L., Pitsch, H. & Pischinger, S. (2020). Validation of a RANS 3D-CFD Gaseous Emission Model with Space-, Species-, and Cycle-Resolved Measurements from an SI DI Engine. *Energies*. [Online]. 13 (17). pp. 4287–4287.
Available from: https://www.mdpi.com/1996-1073/13/17/4287. [Accessed: 6 March 2026].

Fayette Taylor, C. (1985). *The Internal-combustion Engine in Theory and Practice*. Massachusetts: The M.I.T. Press.

Federation of British Historic Vehicle Clubs (2025). *Britain's Love of Historic Vehicles Powers £7.3bn Boost to the UK Economy*. [Online]. 20 October 2025. Fbhvc.co.uk.
Available from: https://www.fbhvc.co.uk/news/article/britains-love-of-historic-vehicles-powers-73-billion-boost-to-the-uk-economy. [Accessed: 21 April 2026].

FIA (2023). *SECURING THE FUTURE OF OUR MOTORING HERITAGE PRESERVING HISTORIC VEHICLES' PLACE ON THE ROADS OF TOMORROW*. [Online].
Available from: https://www.fia.com/sites/default/files/chi_brochure_pages_0.pdf. [Accessed: 12 November 2025].

Frankel, A. (2021). *Driving a new Blower Bentley | Thank Frankel it's Friday*. [Online]. 23 April 2021. Goodwood.com.
Available from: https://www.goodwood.com/grr/race/historic/driving-a-new-blower-bentley--thank-frankel-its-friday/. [Accessed: 20 February 2026].

Gillespie, T.D. (1992). *Fundamentals of Vehicle Dynamics*. SAE International.

Gillogly, B. (2020). *How Bore vs. Stroke Can Affect Horsepower - Hagerty Media*. [Online]. 8 January 2020. Hagerty Media.
Available from: https://www.hagerty.com/media/maintenance-and-tech/how-bore-vs-stroke-can-affect-horsepower. [Accessed: 4 March 2026].

Gruav, S. (2021). *Sequential vs. Parallel Approval Workflows: Which Suits Your Artwork Approval Project?* [Online]. 25 June 2021. www.artworkflowhq.com.
Available from: https://www.artworkflowhq.com/resources/sequential-vs-parallel-workflows-for-artwork-management. [Accessed: 5 November 2025].

Gumbie, S. (2024). *The Acceptable Margin of Error in Resource Estimation Can Vary Depending on the Context and the Level of Precision required. Generally, a Margin of Error between 5% and 10% Is Considered Acceptable for Many Projects [1].* [Online]. 18 September 2024. Linkedin.com.
Available from: https://www.linkedin.com/pulse/what-margin-error-acceptable-resource-estimation-solomon-ma53f/. [Accessed: 15 April 2026].

Hay, M. (1990). *Bentley 4 1/2 Litre*. Haynes Publications.

Hennessy, C. (2020). *Single-Cylinder Research Engine*. [Online]. San Antonio, Texas: Southwest Research Institute.
Available from: https://www.swri.org/sites/default/files/brochures/single-cylinder-research-engine.pdf. [Accessed: 21 April 2026].

Heywood, J. (1988). *Internal Combustion Engine Fundamentals*. McGraw-Hill.

Heywood & John, B. (2018). *Internal Combustion Engine Fundamentals*. 2nd Ed. New York : McGraw-Hill Education.

Hubmann, C., Schöffmann, W., Friedl, H. & Howlett, M. (2012). *Compact Engine Architecture for Best Fuel Efficiency and High Performance – Challenge or Contradiction*. SAE International Journal of Engines.

Hucknall, S. (2024). *Bentley 4½ Litre: History Repeating | Classic & Sports Car*. [Online]. 2024. Classicandsportscar.com.
Available from: https://www.classicandsportscar.com/features/bentley-4-12-litre-history-repeating/. [Accessed: 20 February 2026].

IPG Automotive (2025). *Model-based Development and Validation of suspension, Steering and Chassis Control Systems*. [Online]. 2025. Ipg-automotive.com.
Available from: https://www.ipg-automotive.com/solutions/areas-of-application/vehicle-dynamics. [Accessed: 21 April 2026].

Irving, P.E. & Clymer, F. (2015). *Tuning for Speed*. Veloce Enterprises, Incorporated.

ISO (2017). *ISO/IEC 17025 Testing and Calibration Laboratories*. [Online]. 2017. ISO.
Available from: https://www.iso.org/ISO-IEC-17025-testing-and-calibration-laboratories.html.

Jan Siczek, K. (2016). *Tribological Processes in the Valve Train Systems with Lightweight Valves*. Amsterdam Elsevier, Butterworth-Heinemann.

Joe (2025). *STK Performance Camshafts: Materials, Types, and Engineering Excellence*. [Online]. 12 August 2025. STK Performance.
Available from: https://stk.co.za/stk-performance-camshafts-materials-types-and-engineering-excellence. [Accessed: 14 April 2026].

Kaufman, D. (2012). *Camshaft Selection - Engine Builder Magazine*. [Online]. 14 November 2012. Engine Builder Magazine.
Available from: https://www.enginebuildermag.com/2012/11/camshaft-selection/. [Accessed: 24 January 2026].

Kurczewski, N. (2007). *One for the Boys; 1930s Blower Bentley*. 12 February. p. 39.

Lawson, J. (2021). *Modern Engineering Improving Historic Motorsport | Engineer Live*. [Online]. 14 January 2021. Engineerlive.com.
Available from: https://www.engineerlive.com/content/modern-engineering-improving-historic-motorsport. [Accessed: 9 March 2026].

Le Mans Classic (2025). *Previous Editions*. [Online]. 2025. Le Mans Classic.
Available from: https://www.lemansclassic.com/en/previous-editions. [Accessed: 9 March 2026].

LeBarron, B. (2025). *Boosted Bumpsticks: Understanding Forced Induction Camshafts*. [Online]. 2025. Dragzine.com.
Available from: https://www.dragzine.com/tech-stories/boosted-bumpsticks-understanding-forced-induction-camshafts/. [Accessed: 5 March 2026].

Lopez, E., Jaione Etxebarria-Elezgarai, Jose Manuel Amigo & Seifert, A. (2023). The Importance of Choosing a Proper Validation Strategy in Predictive models. a Tutorial with Real Examples. *Analytica chimica acta*. 1275 (341532). pp. 341532–341532.
Available from: https://www.sciencedirect.com/science/article/pii/S0003267023007535 [Accessed: 14 November 2025].

Martins, J., Brito, F.P., Costa, T. & Costa, J. da (2018). *The Quest for Improving Efficiency in Internal Combustion Engines*. [Online]. 17 September 2018. ResearchGate.
Available from:
https://www.researchgate.net/publication/329091874_The_Quest_for_Improving_Efficiency_in_Internal_Combustion_Engines. [Accessed: 24 October 2025].

Millo, F., Piano, A., Peiretti Paradisi, B., Marzano, M.R., Bianco, A. & Pesce, F.C. (2020). Development and Assessment of an Integrated 1D-3D CFD Codes Coupling Methodology for Diesel Engine Combustion Simulation and Optimization. *Energies*. 13 (7). p. 1612.

Motor Sport (1927). 1927 Le Mans 24 Hours Race Report. *Motor Sport Magazine*.

NASA (2004). *Reducing the Time and Cost of Testing Engines*. [Online]. 2004. Spinoff.
Available from: https://ntrs.nasa.gov/citations/20050031186. [Accessed: 24 October 2025].

Nathan (2026). *Mercedes-Benz Celebrates 140 Years of Innovation, Kicks Off Biggest Product Offensive in Brand History*. [Online]. 29 January 2026. YS Khong Driving.
Available from: https://www.yskhongdriving.com/2026/01/29/mercedes-benz-celebrates-140-years-of-innovation-kicks-off-biggest-product-offensive-in-brand-history/. [Accessed: 24 February 2026].

P.G.G Knight (2020). *The S.U. Carburetter*. [Online]. 26 April 2020. Sucarb.co.uk.
Available from: https://sucarb.co.uk/technical/technical-su-carburetters. [Accessed: 25 February 2026].

Pastewka, L., Vakis, A.I., Aghababaei, R., Almqvist, A., Carbone, G., Chandross, M., Dini, D., Eder, S.J., Ehrich, H.J., Ewen, J.P., Menga, N., Molinari, J.-F., Moras, G., Nicola, L., Paggi, M., Putignano, C., Scaraggi, M., Yastrebov, V.A. & Müser, M.H. (2025). Modeling in tribology: Recent advances, applications, and Open Questions. *Tribology International*. [Online]. 218 (111326).
Available from: https://www.sciencedirect.com/science/article/pii/S0301679X25008217. [Accessed: 17 April 2026].

Pomeroy, L. (1955). *The Grand Prix Car Volume One*. Temple Press: Motor Racing Publications.

Professor Low, A.M. (1930). The Supercharged 4 1/2 Litre Bentley. *The Motor*. [Online]. 22 April. p. 554.
Available from: https://craigmcateer.co.uk/wp-content/uploads/2021/08/Bentley-Supercharged-Touring-4-12-1930.pdf. [Accessed: 25 February 2026].

RAC (2025). *Euro 1 to Euro 6 – Find out Your vehicle's Emissions Standard | RAC Drive*. [Online]. 5 March 2025. Rac.co.uk.
Available from: https://www.rac.co.uk/drive/advice/emissions/euro-emissions-standards/. [Accessed: 24 February 2026].

Realis (2025). *Combustion | Capabilities | Realis Simulation*. [Online]. 2025. Realis-simulation.com Available from: https://www.realis-simulation.com/capabilities/combustion/. [Accessed: 24 October 2025].

Schoegl, O., Schmidt, S., Abart, M., Zinner, C., Kirchberger, R., Fitl, M., Glinsner, K. & Leiber, S. (2010). Possibilities and Limits of 1D CFD Simulation Methodology for the Layout of 2-Stroke GDI Combustion System. *SAE Technical Paper Series*. 1 (2010-32-0017).

Schwer, L. (2009). *An Overview of the ASME V&V-10 Guide for Verification and Validation in Computational Solid Mechanics*. [Online]. Windsor, CA USA: The American Society of Mechanical Engineers.
Available from: https://repository.lib.ncsu.edu/server/api/core/bitstreams/a45e16f4-5cce-44f4-b2bd-fa760019c8aa/content. [Accessed: 15 April 2026].

Sharma, V., Hittalamane, S. & Gunjal, P. (2017). Exhaust Header Designing for Formula SAE Car. *International Journal of Innovative Research in Science, Engineering and Technology (An ISO*. [Online]. 3297 (9).
Available from: http://www.ijirset.com/upload/2017/september/191_69_Exhaust_2HARD.pdf. [Accessed: 5 March 2026].

Shaun (2025). *Back to Basics with Camshafts in Vehicle Performance*. [Online]. 14 January 2025. Vanderlindedevelopments.co.za.
Available from: https://www.vanderlindedevelopments.co.za/2025/01/14/camshafts/. [Accessed: 5 March 2026].

Sir Ricardo, H. (1931). *The High-speed Internal-combustion Engine*. [Online]. London and Glasgow: Blackie & Son Limited.
Available from: https://www.scribd.com/doc/40610101/The-High-Speed-Internal-Combustion-Engine-by-Sir-Harry-Ricardo. [Accessed: 4 March 2026].

Smith, P.H. & Morrison, J.C. (1971). *The Scientific Design of Exhaust and Intake Systems*. Engineering and Performance.

Stone, R. (2012). *Introduction to Internal Combustion Engines*. 4th Ed. London: Macmillan International Higher Education.

Tadros, M. (2025). Engine Optimization Model for Accurate Prediction of Friction Model in Marine Dual-Fuel Engine. *Algorithms*. 18 (7). pp. 415–415.

The JBS Collection (2025). *Return to Le Mans: Unfinished Business | Bentley Blower | Official Documentary*. [Online]. 22 December 2025. YouTube.
Available from: https://www.youtube.com/watch?v=thfrzm2lOYY. [Accessed: 21 April 2026].

United Nations (2015). *The 17 Sustainable Development Goals*. [Online]. 2015. United Nations.
Available from: https://sdgs.un.org/goals. [Accessed: 12 November 2025].

Wang, G.G. (2002). Definition and Review of Virtual Prototyping. *Journal of Computing and Information Science in Engineering*. [Online]. 2 (3). p. 232.
Available from: http://www.sfu.ca/~gwa5/index_files/Jcise-2001-76.PDF. [Accessed: 5 November 2025].

Winklhofer, E. & Hopfner, W. (2012). *Optical Single Cylinder Engines in Engine Research and Development*. [Online]. Poznan, Poland: AVL List GmbH.
Available from:
https://www.researchgate.net/publication/328722884_Optical_single_cylinder_engines_in_engine_research_and_development. [Accessed: 21 April 2026].

Yu, X., Zhu, L., Wang, Y., Filev, D. & Yao, X. (2022). *Internal Combustion Engine Calibration Using Optimization Algorithms*. [Online].
Available from: https://www-sciencedirect-com.ezproxy.staffs.ac.uk/science/article/pii/S0306261921012071. [Accessed: 14 November 2025].

Zheng, J.-J., Wang, J.-H., Wang, B., Huang, Z.-H. & Zhang, Y.-J. (2010). Effect of Compression Ratio on Combustion and Emission Characteristics of a direct-injection Natural Gas Engine. *Neiranji Xuebao/Transactions of CSICE (Chinese Society for Internal Combustion Engines)*. [Online]. 28 (1). pp. 20–25.
Available from:
https://www.researchgate.net/publication/286038495_Effect_of_compression_ratio_on_combustion_and_emission_characteristics_of_a_direct-injection_natural_gas_engine. [Accessed: 27 March 2026].

Appendix A: Bentley Blower Engine Technical Specification Sheet

Engine Technical Data Sheet

Category	Essential Data Point	
General	Make	Bentley
	Model	Blower (Race Trim)
	Type	4.398L SOHC 16V I4
	Power Output	244.4 hp @ 4,000 RPM
	Cooling	Water Cooled
Core Geometry/Info	Bore and Stroke	100 x 140mm
	Connecting Rod Length	285mm
	Air/ Fuel Ratio	12.5: 1
	Compression Ratio	6.5:1
	Number of Cylinders & Firing Order	4 Cylinders (1,3,4,2)
Valves	Configuration	4 Valves per Cylinder, (16 Total)
	Valve Lift Profiles (Cam Profiles)	See table 1, graph 1 and graph 2
	Valve Event Timings	See table 1
	Valve Diameters	Intake 50mm, Exhaust 30mm
Fueling	Type	2 × SU HVG5 Carburettors
	Bore Flow	1⅜ Inch
	Fuel Flow Rate	See graph 3
Intake/ Exhaust	Supercharger Type	Amherst Villiers Mk IV Roots-type
	Supercharger Flow Charactistics	14.7 + 12 psi
	Supercharger Drive Ratio	1: 1
	Intake Duct Length/ Diameters	See diagram 1
	Exhaust Duct Length/ Diameters	See diagram 1
	Ambient Conditions	25° C

Page 1 of 3

Figure 58 - Bentley Blower Engine Technical Specification Sheet 1 of 3

Engine Technical Data Sheet

Measured Cam Profiles			
Bank	Duration (Exh/Int)	Exhaust Lobe Max (mm)	Intake Lobe Max (mm)
1	157	8.56	8.57
	162	8.54	
2	157	8.56	8.58
	162	8.57	
3	157	8.56	8.55
	162	8.56	
4	157	8.56	8.59
	162	8.55	

Table 1 - Valve Lift Profiles and Valve Event Timings

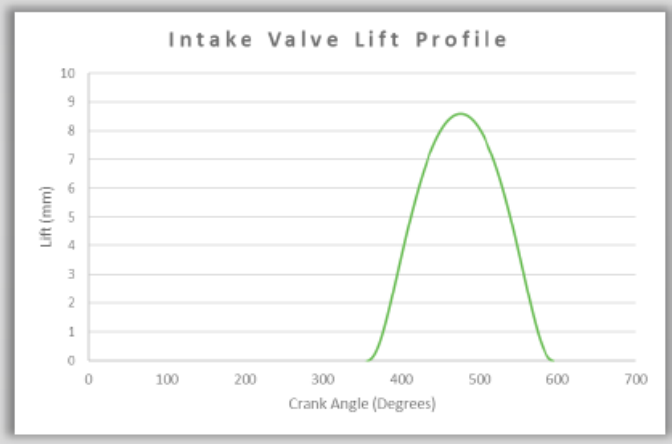

Graph 1 – Intake Valve Lift Profile

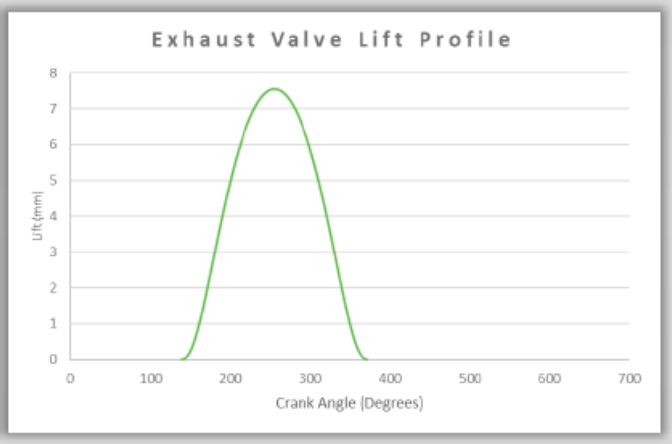

Graph 2 – Exhaust Valve Lift Profile

Page 2 of 3

Figure 59 - Bentley Blower Engine Technical Specification Sheet 2 of 3

Engine Technical Data Sheet

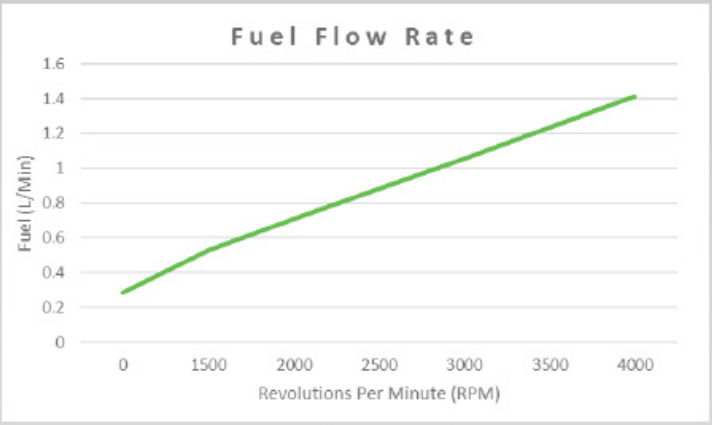

Graph 3 - Valve Lift Profiles and Valve Event Timings

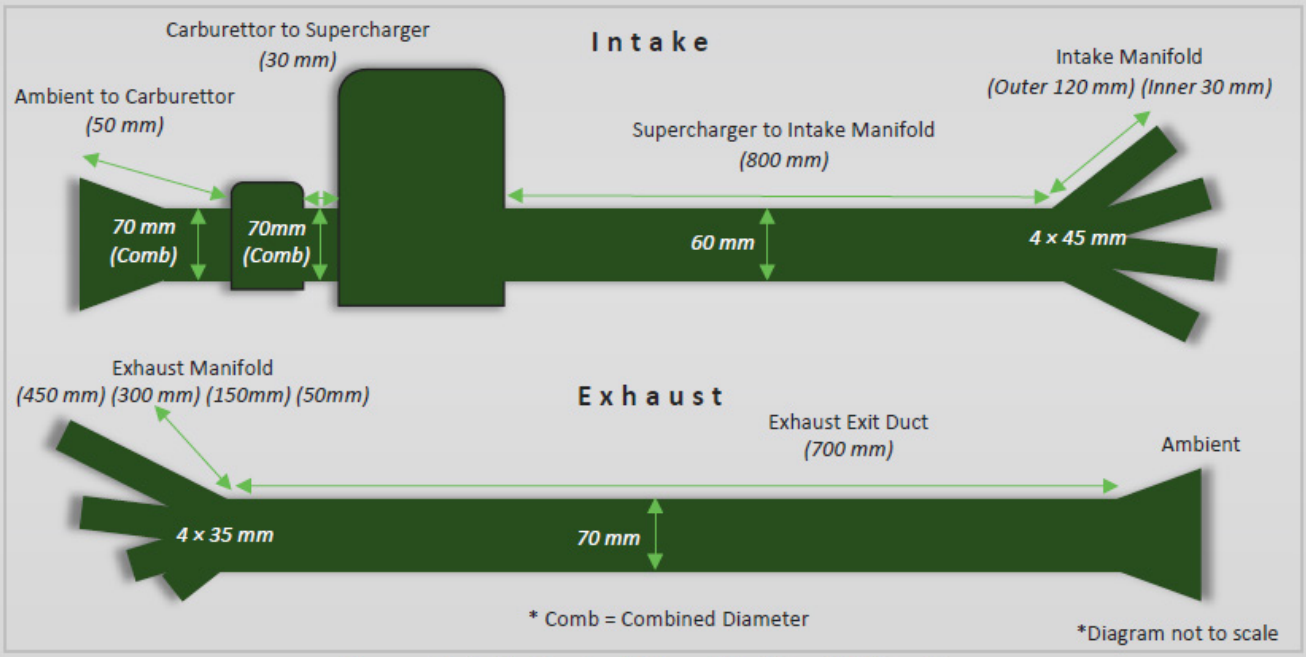

Diagram 1 - Intake Duct and Exhaust Duct Length/ Diameters

Page 3 of 3

Figure 60 - Bentley Blower Engine Technical Specification Sheet 3 of 3

Appendix B: Comparative Performance and Absolute Volumetric Efficiency with Sample Formulae

The below calculations determine absolute volumetric efficiency $\eta_{v(abs)}$ using the ratio which accounts for the thermal density penalty as outlined by Heywood (1988):

$$P_{(ratio)} = \frac{P_{(man)}}{P_{(amb)}} \qquad T_{(ratio)} = \frac{T_{(man)}}{T_{(amb)}} \qquad \eta_{v(abs)} = \eta_{v(base)} \times P_{(ratio)} \times T_{(ratio)}$$

Figure 61 - Absolute Volumetric Efficiency Equations

1. Defined Parameters

- Ambient Pressure ($P_{(amb)}$) = 14.7 psi
- Boost Pressure ($P_{(boost)}$) = 12.0 psi
- Manifold Absolute Pressure ($P_{(man)}$): 14.7 + 12.0 = 26.7 psi
- Ambient Temperature ($T_{(amb)}$) = 298.15 Kelvin (K) (25°C)
- Estimated Manifold Temperature ($T_{(man)}$) = 383.15 K (110°C)
  **Note: Derived from adiabatic compression with an assumed blower efficiency of 60%.*

2. Pressure Ratio

Firstly, the increase in volume because of the pressure increase alone is calculated:

$$P_{(ratio)} = \frac{P_{(man)}}{P_{(amb)}} = \frac{26.7}{14.7} = 1.816$$

3. Temperature Ratio

Because the air is heated during compression, it becomes less dense. This results in an inverse pressure ratio:

$$T_{(ratio)} = \frac{T_{(man)}}{T_{(amb)}} = \frac{298.15}{383.15} = 0.778$$

4. Final Absolute Volumetric Efficiency

Taking the assumption that the engine has a natural mechanical filling efficiency of 85% (typical for a period engine of this type) the final efficiency is a product of the three factors:

$$\eta_{v(abs)} = \eta_{v(base)} \times P_{(ratio)} \times T_{(ratio)} = 0.85 \times 1.816 \times 0.778 = 1.200$$

5. Result

This formulae confirms that despite the thermal efficiency loss, the force of the 12-psi boost from the constant-displacement supercharger successfully pushes the engines volumetric efficiency to 120%, a predicted 41% increase over its NA state. Find below a comparative performance table for all engine configurations:

Engine Configuration	RPM	Boost (psi)	Manifold Temperature	Power (bhp)	Absolute Volumetric Efficiency
Naturally Aspirated (Base)	3,500	0	25°C	110	85.00%
Blower (Road Specification)	3,500	9.5	88°C	175	115.60%
Blower (Racing Team Car)	4,200	12	110°C	240	123.40%

Table 4 - Absolute Volumetric Efficiency for a range of Bentley Configurations

The refinement from a theoretical 120% to 123.4% accounts also for the evaporative cooling effect because of the high volume of fuel within the charge as well as the positive scavenging pressure inherent the Bentley's valve overlap profile (Ricardo, 1931).

Appendix C: Tractive Effort Sawtooth Analysis

1. Defined Parameters

Using the gearing ratios along with some other vital drivetrain specifications, such as tyre radius and drivetrain efficiency, and tractive effort (TE), a sawtooth analysis can be derived. This validates the aim to target 3500 RPM as the occurrence of the peak torque and power figures for this report:

Drivetrain Specifications	
Peak Torque	370 Nm
Drivetrain Efficiency	89.18%
Tyre Radius	0.4537 m
Shift Target	3500 RPM
Gear	Ratio
1	9.91
2	5.84
3	4.25
4	3.06

Table 5 - Bentley Blower Driveline Specifications

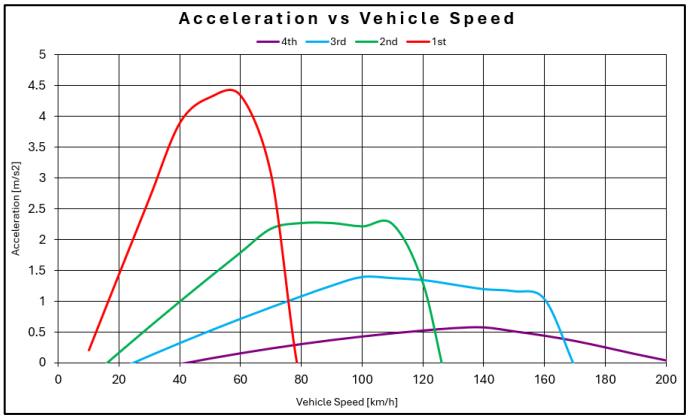

Figure 62 - Acceleration vs Vehicle Speed Gearing Data

To achieve maximum performance the objective is to maximise the area under the acceleration curve to maintain the highest possible acceleration. Having the shift point at 3500 RPM ensures that the drop in tractive force is minimised and therefore making the most efficient utilisation of the Bentley's 4.399L engine torque curve.

2. Tractive Effort Calculation

Tractive Effort (TE) representants the longitudinal force available at the tyres contact patch to effectively overcome aerodynamic drag factors and accelerate the vehicles' mass forwards:

$$TE = \frac{T \times G \times \eta}{r}$$

Where:

- T = Peak torque (Nm)
- G = Gear ratio
- η = Drivetrain efficiency
- r = Tyre radius

Equation 8 - Tractive Effort Gearing Formula

Shift Recovery and Tractive Effort Results Table				
Gear	Shift Speed (km/h)	Shift RPM	Recovery RPM	Tractive Effort (N)
1st - 2nd	60.4	3,500	2,062	4,248
2nd - 3rd	102.5	3,500	2,547	3,091
3rd - 4th	140.9	3,500	2,520	2,226

Table 6 - Results Table for Shift Recovery and Tractive Effort

3. Sawtooth Analysis

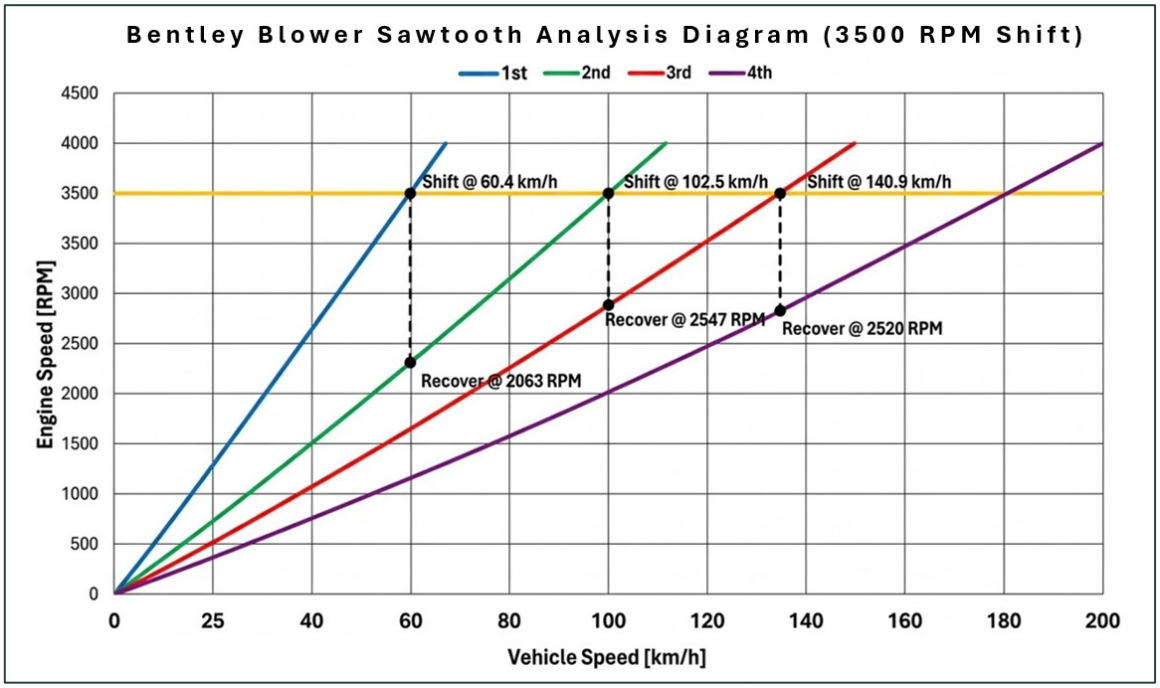

Figure 63 - Sawtooth Shift Analysis Diagram

The above Sawtooth diagram correlates the engines torque band with the vehicle velocity. It shows that shifting at 3500 PRM ensures the engine recovers at approximately 2000 – 2500 RPM which sits comfortably within the surge phase of the engines torque profile. Shifting later would yield diminishing returns as previously discussed issues of the era's mechanical limits and risk due to high mean piston speeds (>16m/s).

Appendix D: Calibration Process Table

RPM	Dyno Range	First Run	Error %	Combustion Sub-Model Adjustment	Error %	Heat Transfer Sub-Model Adjustment	Error %
1500	45.4	69.0	52.02%	47.9	5.41%	46.0	1.24%
1750	65.2	80.5	23.41%	67.2	3.01%	67.2	3.01%
1850	74.1	84.5	14.05%	78.6	6.06%	73.9	-0.25%
2000	88.5	94.5	6.82%	94.5	6.82%	91.5	3.35%
2250	115.2	120.6	4.66%	120.6	4.66%	118.2	2.57%
2500	145.5	150.8	3.65%	150.8	3.65%	148.5	2.03%
3000	183.1	185.9	1.55%	185.9	1.55%	184.1	0.57%
3500	214.3	207.4	-3.21%	207.4	-3.21%	209.2	-2.37%
Mean Absolute Error (MAE)			12.32%		4.21%		2.06%

Table 7 - Engine Calibration Figures

Appendix E: Constants Table Progression

Pareto Optimal Engine												
Name	Units	Run Case 1	Run Case 2	Run Case 3	Run Case 4	Run Case 5	Run Case 6	Run Case 7	Run Case 8	Run Case 9	Skip Case 10	Skip Case 11
AFR		12.5	12.5	12.5	12.5	12.5	12.5	12.5	12.5	12.5	12.5	12.5
BDUR	deg	10	20	20	40	70	100	110	110	110	110	100
Bore	mm	105	105	105	105	105	105	105	105	105	105	105
C_R		7.5	7.5	7.5	7.5	7.5	7.5	7.5	7.5	7.5	7.5	7.5
EVDIA	mm	30	30	30	30	30	30	30	30	30	30	30
EXHD	cm	5	5	5	5	5	5	5	5	5	5	5
HT		0.4	0.8	1.2	1.3	1.3	1.4	2.5	3	5.5	5.5	5.5
IVDIA	mm	50	50	50	50	50	50	50	50	50	50	50
LR	cm	7	7	7	7	7	7	7	7	7	7	7
NCYC		20	20	20	20	20	20	20	20	20	20	20
PA	cm^2	197.92	197.92	197.92	197.92	197.92	197.92	197.92	197.92	197.92	197.92	197.92
PD	cm	7	7	7	7	7	7	7	7	7	7	7
PL		9	9	9	9	9	9	9	9	9	9	9
PV	cm^3	346.36	346.36	346.36	346.36	346.36	346.36	346.36	346.36	346.36	346.36	346.36
RANG	deg	0	0	0	0	0	0	0	0	0	0	0
RDI	cm	4.5	4.5	4.5	4.5	4.5	4.5	4.5	4.5	4.5	4.5	4.5
RDO	cm	4.5	4.5	4.5	4.5	4.5	4.5	4.5	4.5	4.5	4.5	4.5
speed	rpm	4000	3500	3000	2500	2250	2000	1850	1750	1500	1000	500
Stroke	mm	140	140	140	140	140	140	140	140	140	140	140
THB50	deg	10	10	10	10	10	10	10	10	10	10	10
THROTTLE	deg	90	90	90	90	90	90	90	90	90	90	90
WAL_FRI		0.4	0.4	0.4	0.4	0.4	0.4	0.4	0.4	0.4	0.4	0.4
ZD	cm	13.5	13.5	13.5	13.5	13.5	13.5	13.5	13.5	13.5	13.5	13.5

- Changed/ New Variable

Table 8 - Contants Table for Pareto Optimal Engine

Base Engine												
Name	Units	Run Case 1	Run Case 2	Run Case 3	Run Case 4	Run Case 5	Run Case 6	Run Case 7	Run Case 8	Run Case 9	Skip Case 10	Skip Case 11
AFR		12.5	12.5	12.5	12.5	12.5	12.5	12.5	12.5	12.5	12.5	12.5
BDUR	deg	10	20	20	40	70	100	110	110	110	110	100
Bore	mm	100	100	100	100	100	100	100	100	100	100	100
C_R		6.5	6.5	6.5	6.5	6.5	6.5	6.5	6.5	6.5	6.5	6.5
EVDIA	mm	30	30	30	30	30	30	30	30	30	30	30
EXHD	cm	5	5	5	5	5	5	5	5	5	5	5
HT		0.4	0.8	1.2	1.3	1.3	1.4	2.5	3	5.5	5.5	5.5
IVDIA	mm	50	50	50	50	50	50	50	50	50	50	50
LR	cm	7	7	7	7	7	7	7	7	7	7	7
NCYC		20	20	20	20	20	20	20	20	20	20	20
PA	cm^2	197.92	197.92	197.92	197.92	197.92	197.92	197.92	197.92	197.92	197.92	197.92
PD	cm	7	7	7	7	7	7	7	7	7	7	7
PL		9	9	9	9	9	9	9	9	9	9	9
PV	cm^3	346.36	346.36	346.36	346.36	346.36	346.36	346.36	346.36	346.36	346.36	346.36
RANG	deg	0	0	0	0	0	0	0	0	0	0	0
RDI	cm	4.5	4.5	4.5	4.5	4.5	4.5	4.5	4.5	4.5	4.5	4.5
RDO	cm	4.5	4.5	4.5	4.5	4.5	4.5	4.5	4.5	4.5	4.5	4.5
speed	rpm	4000	3500	3000	2500	2250	2000	1850	1750	1500	1000	500
Stroke	mm	140	140	140	140	140	140	140	140	140	140	140
THB50	deg	10	10	10	10	10	10	10	10	10	10	10
THROTTLE	deg	90	90	90	90	90	90	90	90	90	90	90
ZD	cm	7	7	7	7	7	7	7	7	7	7	7

- Changed/ New Variable

Table 9 - Constants Table for Base Engine

Pre- Calibrated Engine												
Name	Units	Run Case 1	Run Case 2	Run Case 3	Run Case 4	Run Case 5	Run Case 6	Run Case 7	Run Case 8	Run Case 9	Run Case 10	Run Case 11
AFR		12.5	12.5	12.5	12.5	12.5	12.5	12.5	12.5	12.5	12.5	12.5
BDUR	deg	22.5	22.45	22.4	22.3	22.1	22	21.9	21.9	21.8	21.5	21.2
Bore	mm	100	100	100	100	100	100	100	100	100	100	100
C_R		6.5	6.5	6.5	6.5	6.5	6.5	6.5	6.5	6.5	6.5	6.5
EVDIA	mm	30	30	30	30	30	30	30	30	30	30	30
EXHD	cm	5	5	5	5	5	5	5	5	5	5	5
IVDIA	mm	50	50	50	50	50	50	50	50	50	50	50
LR	cm	45	45	45	45	45	45	45	45	45	45	45
NCYC		20	20	20	20	20	20	20	20	20	20	20
PA	cm^2	197.92	197.92	197.92	197.92	197.92	197.92	197.92	197.92	197.92	197.92	197.92
PD	cm	7	7	7	7	7	7	7	7	7	7	7
PL		9	9	9	9	9	9	9	9	9	9	9
PV	cm^3	346.36	346.36	346.36	346.36	346.36	346.36	346.36	346.36	346.36	346.36	346.36
RANG	deg	0	0	0	0	0	0	0	0	0	0	0
RDI	cm	4.5	4.5	4.5	4.5	4.5	4.5	4.5	4.5	4.5	4.5	4.5
RDO	cm	4.5	4.5	4.5	4.5	4.5	4.5	4.5	4.5	4.5	4.5	4.5
speed	rpm	4000	3500	3000	2500	2250	2000	1850	1750	1500	1000	500
Stroke	mm	140	140	140	140	140	140	140	140	140	140	140
THB50	deg	10	10	10	10	10	10	10	10	10	10	10
THROTTLE	deg	90	90	90	90	90	90	90	90	90	90	90
ZD	cm	7	7	7	7	7	7	7	7	7	7	7

Table 10 - Pre-Calibration Phase Contants Table

Appendix F: Pareto Optimal Engine WAVE Canvas

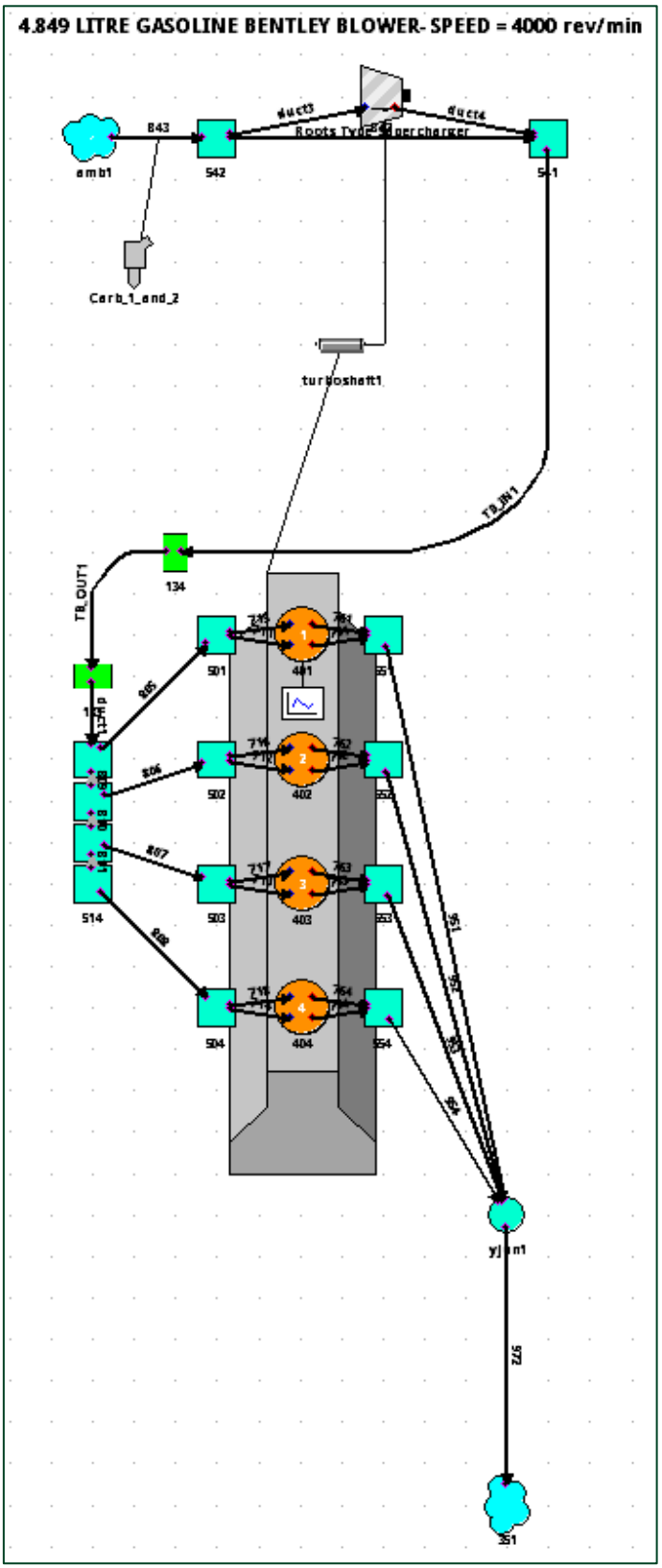

Figure 64 - Pareto Optimal Engine WAVE Canvas